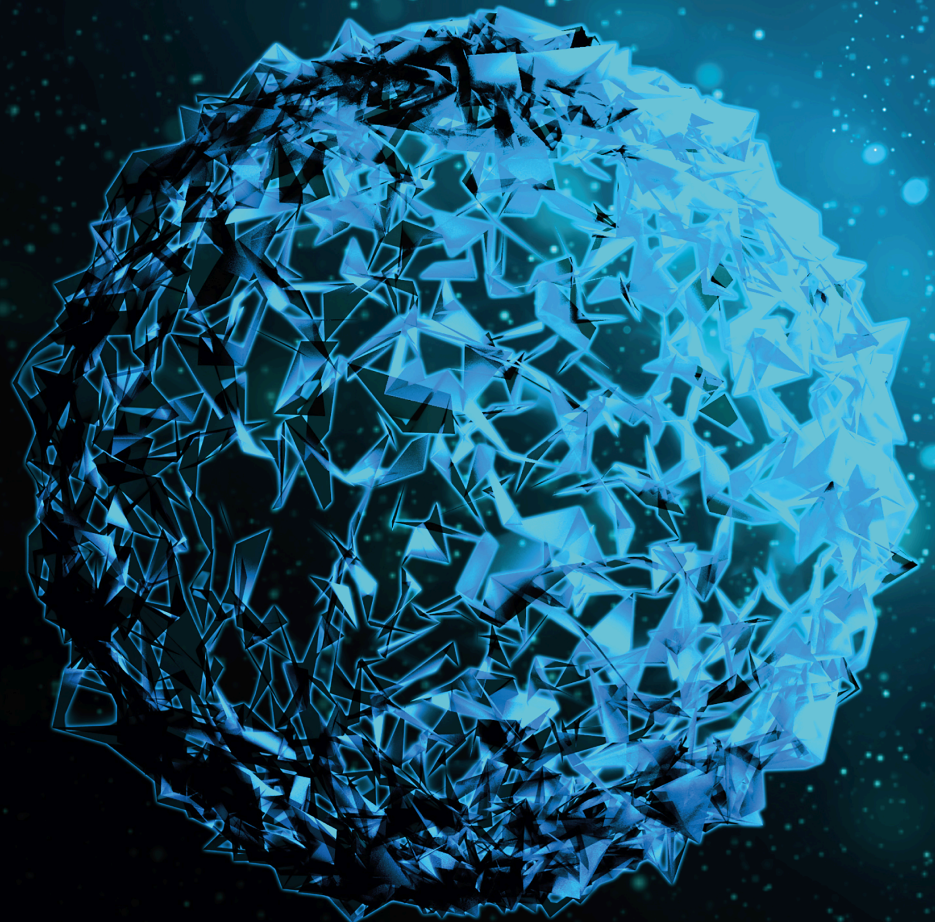


# Propelling Healthcare with Advanced Therapy: The Future of Medicine

Lead Guest Editor: Haixu Chen

Guest Editors: Zheng Zhang, Xiaoyan Xie, Qiang Zeng, Peiliang Geng, and  
Jinfeng Zhang





---

# **Propelling Healthcare with Advanced Therapy: The Future of Medicine**

BioMed Research International

---

## **Propelling Healthcare with Advanced Therapy: The Future of Medicine**

Lead Guest Editor: Haixu Chen

Guest Editors: Zheng Zhang, Xiaoyan Xie, Qiang  
Zeng, Peiliang Geng, and Jinfeng Zhang



---

Copyright © 2024 Hindawi Limited. All rights reserved.












This is a special issue published in "BioMed Research International." All articles are open access articles distributed under the Creative Commons Attribution License, which permits unrestricted use, distribution, and reproduction in any medium, provided the original work is properly cited.

## Section Editors

Penny A. Asbell, USA  
David Bernardo , Spain  
Gerald Brandacher, USA  
Kim Bridle , Australia  
Laura Chronopoulou , Italy  
Gerald A. Colvin , USA  
Aaron S. Dumont, USA  
Pierfrancesco Franco , Italy  
Raj P. Kandpal , USA  
Fabrizio Montecucco , Italy  
Mangesh S. Pednekar , India  
Letterio S. Politi , USA  
Jinsong Ren , China  
William B. Rodgers, USA  
Harry W. Schroeder , USA  
Andrea Scribante , Italy  
Germán Vicente-Rodríguez , Spain  
Momiao Xiong , USA  
Hui Zhang , China

## Academic Editors

### Stem Cells and Tissue Engineering

Mohammad Amin Abdollahifar, Iran  
Tarun Agarwal , India  
François Berthiaume , USA  
Jose' Luis Calvo-Guirado, Spain  
Malay Chaklader , USA  
Magali Cucchiaroni , Germany  
Willeke F. Daamen , The Netherlands  
Costantino Del Gaudio , Italy  
Li Duan , China  
Francesco Fascetti Leon, Italy  
Venkata N. S. Garikipati , USA  
Kirsten Haastert-Talini , Germany  
Esmail Jabbari, USA  
Jangho Kim, Republic of Korea  
Annunziata Mauro , Italy  
Kibret Mequanint , Canada

Vitale Miceli , Italy  
Bruna Sinjari , Italy  
María Troya , Spain  
Przemko Tylzanowski , Belgium  
Imran Ullah, Pakistan  
Junji Xu , China  
Kai-Chiang Yang , Taiwan

# Contents

## **Retracted: Cell-in-Cell: From Cell Biology to Translational Medicine**

BioMed Research International

Retraction (1 page), Article ID 9852141, Volume 2024 (2024)

## **Retracted: Using Haemocoagulase Agkistrodon in Patients Undergoing Transurethral Plasmakinetic Resection of the Prostate: A Pilot, Real-World, and Propensity Score-Matched Study**

BioMed Research International

Retraction (1 page), Article ID 9825156, Volume 2024 (2024)

## **Retracted: A Novel Missense Mutation of Arginine Vasopressin Receptor 2 in a Chinese Family with Congenital Nephrogenic Diabetes Insipidus: X-Chromosome Inactivation in Female CNDI Patients with Heterozygote 814A>G Mutation**

BioMed Research International

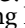

Retraction (1 page), Article ID 9753837, Volume 2024 (2024)

## **Advances in Cuffless Continuous Blood Pressure Monitoring Technology Based on PPG Signals**

Caijie Qin , Xiaohua Wang , Guangjun Xu , and Xibo Ma 



Review Article (16 pages), Article ID 8094351, Volume 2022 (2022)

## **[Retracted] Cell-in-Cell: From Cell Biology to Translational Medicine**

Qiao Chen, Xiaoning Wang , and Meifang He 

Review Article (7 pages), Article ID 7608521, Volume 2022 (2022)

## **[Retracted] A Novel Missense Mutation of Arginine Vasopressin Receptor 2 in a Chinese Family with Congenital Nephrogenic Diabetes Insipidus: X-Chromosome Inactivation in Female CNDI Patients with Heterozygote 814A>G Mutation**

Li Zang, Yuping Gong, Yijun Li, Jingtao Dou, Zhaohui Lyu, Xiaoqing Su, Yawei Zhang , and Yiming Mu 





Research Article (7 pages), Article ID 7073158, Volume 2022 (2022)

## **Association between Mesenchymal Stem Cells and COVID-19 Therapy: Systematic Review and Current Trends**

Amaan Javed , Saurab Karki , Zeba Sami , Zuha Khan , Anagha Shree , Biki Kumar Sah , Shankhaneel Ghosh , and Sara Saxena 

Review Article (17 pages), Article ID 9346939, Volume 2022 (2022)

## **[Retracted] Using Haemocoagulase Agkistrodon in Patients Undergoing Transurethral Plasmakinetic Resection of the Prostate: A Pilot, Real-World, and Propensity Score-Matched Study**

Cong Zhu, Lan Yang, Hao Zi, Bing-Hui Li, Qiao Huang , Meng-Xin Lu, Xiao-Dong Li, Xuan-Yi Ren, Hua Tao , Hankun Hu , and Xian-Tao Zeng 

Research Article (9 pages), Article ID 9200854, Volume 2022 (2022)

## *Retraction*

# **Retracted: Cell-in-Cell: From Cell Biology to Translational Medicine**

### **BioMed Research International**

Received 12 March 2024; Accepted 12 March 2024; Published 20 March 2024

Copyright © 2024 BioMed Research International. This is an open access article distributed under the Creative Commons Attribution License, which permits unrestricted use, distribution, and reproduction in any medium, provided the original work is properly cited.

This article has been retracted by Hindawi following an investigation undertaken by the publisher [1]. This investigation has uncovered evidence of one or more of the following indicators of systematic manipulation of the publication process:

- (1) Discrepancies in scope
- (2) Discrepancies in the description of the research reported
- (3) Discrepancies between the availability of data and the research described
- (4) Inappropriate citations
- (5) Incoherent, meaningless and/or irrelevant content included in the article
- (6) Manipulated or compromised peer review

The presence of these indicators undermines our confidence in the integrity of the article's content and we cannot, therefore, vouch for its reliability. Please note that this notice is intended solely to alert readers that the content of this article is unreliable. We have not investigated whether authors were aware of or involved in the systematic manipulation of the publication process.

Wiley and Hindawi regrets that the usual quality checks did not identify these issues before publication and have since put additional measures in place to safeguard research integrity.

We wish to credit our own Research Integrity and Research Publishing teams and anonymous and named external researchers and research integrity experts for contributing to this investigation.

The corresponding author, as the representative of all authors, has been given the opportunity to register their agreement or disagreement to this retraction. We have kept a record of any response received.

### **References**

- [1] Q. Chen, X. Wang, and M. He, "Cell-in-Cell: From Cell Biology to Translational Medicine," *BioMed Research International*, vol. 2022, Article ID 7608521, 7 pages, 2022.

## Retraction

# Retracted: Using Haemocoagulase Agkistrodon in Patients Undergoing Transurethral Plasmakinetic Resection of the Prostate: A Pilot, Real-World, and Propensity Score-Matched Study

### BioMed Research International

Received 12 March 2024; Accepted 12 March 2024; Published 20 March 2024

Copyright © 2024 BioMed Research International. This is an open access article distributed under the Creative Commons Attribution License, which permits unrestricted use, distribution, and reproduction in any medium, provided the original work is properly cited.

This article has been retracted by Hindawi following an investigation undertaken by the publisher [1]. This investigation has uncovered evidence of one or more of the following indicators of systematic manipulation of the publication process:

- (1) Discrepancies in scope
- (2) Discrepancies in the description of the research reported
- (3) Discrepancies between the availability of data and the research described
- (4) Inappropriate citations
- (5) Incoherent, meaningless and/or irrelevant content included in the article
- (6) Manipulated or compromised peer review

The presence of these indicators undermines our confidence in the integrity of the article's content and we cannot, therefore, vouch for its reliability. Please note that this notice is intended solely to alert readers that the content of this article is unreliable. We have not investigated whether authors were aware of or involved in the systematic manipulation of the publication process.

Wiley and Hindawi regrets that the usual quality checks did not identify these issues before publication and have since put additional measures in place to safeguard research integrity.

We wish to credit our own Research Integrity and Research Publishing teams and anonymous and named external researchers and research integrity experts for contributing to this investigation.

The corresponding author, as the representative of all authors, has been given the opportunity to register their agreement or disagreement to this retraction. We have kept a record of any response received.

### References

- [1] C. Zhu, L. Yang, H. Zi et al., "Using Haemocoagulase Agkistrodon in Patients Undergoing Transurethral Plasmakinetic Resection of the Prostate: A Pilot, Real-World, and Propensity Score-Matched Study," *BioMed Research International*, vol. 2022, Article ID 9200854, 9 pages, 2022.



## Retraction

# Retracted: A Novel Missense Mutation of Arginine Vasopressin Receptor 2 in a Chinese Family with Congenital Nephrogenic Diabetes Insipidus: X-Chromosome Inactivation in Female CNDI Patients with Heterozygote 814A>G Mutation

### BioMed Research International

Received 12 March 2024; Accepted 12 March 2024; Published 20 March 2024

Copyright © 2024 BioMed Research International. This is an open access article distributed under the Creative Commons Attribution License, which permits unrestricted use, distribution, and reproduction in any medium, provided the original work is properly cited.

This article has been retracted by Hindawi following an investigation undertaken by the publisher [1]. This investigation has uncovered evidence of one or more of the following indicators of systematic manipulation of the publication process:

- (1) Discrepancies in scope
- (2) Discrepancies in the description of the research reported
- (3) Discrepancies between the availability of data and the research described
- (4) Inappropriate citations
- (5) Incoherent, meaningless and/or irrelevant content included in the article
- (6) Manipulated or compromised peer review

The presence of these indicators undermines our confidence in the integrity of the article's content and we cannot, therefore, vouch for its reliability. Please note that this notice is intended solely to alert readers that the content of this article is unreliable. We have not investigated whether authors were aware of or involved in the systematic manipulation of the publication process.

Wiley and Hindawi regrets that the usual quality checks did not identify these issues before publication and have since put additional measures in place to safeguard research integrity.

We wish to credit our own Research Integrity and Research Publishing teams and anonymous and named external researchers and research integrity experts for contributing to this investigation.





The corresponding author, as the representative of all authors, has been given the opportunity to register their agreement or disagreement to this retraction. We have kept a record of any response received.

### References

- [1] L. Zang, Y. Gong, Y. Li et al., "A Novel Missense Mutation of Arginine Vasopressin Receptor 2 in a Chinese Family with Congenital Nephrogenic Diabetes Insipidus: X-Chromosome Inactivation in Female CNDI Patients with Heterozygote 814A>G Mutation," *BioMed Research International*, vol. 2022, Article ID 7073158, 7 pages, 2022.

## Review Article

# Advances in Cuffless Continuous Blood Pressure Monitoring Technology Based on PPG Signals

Caijie Qin <sup>1,2</sup>, Xiaohua Wang <sup>3</sup>, Guangjun Xu <sup>4</sup>, and Xibo Ma <sup>2,5</sup>

<sup>1</sup>Institute of Information Engineering, Sanming University, Sanming, China

<sup>2</sup>CBSR&NLPR, Institute of Automation, Chinese Academy of Sciences, Beijing, China

<sup>3</sup>Department of Nephrology, The Second Medical Center, Chinese PLA General Hospital, Beijing, China

<sup>4</sup>Data Center, Agricultural Bank of China, Beijing 100049, China

<sup>5</sup>School of Artificial Intelligence, University of Chinese Academy of Sciences, Beijing 100049, China

Correspondence should be addressed to Xibo Ma; [xibo.ma@ia.ac.cn](mailto:xibo.ma@ia.ac.cn)

Received 29 May 2022; Accepted 30 July 2022; Published 1 October 2022

Academic Editor: Fu-Ming Tsai

Copyright © 2022 Caijie Qin et al. This is an open access article distributed under the Creative Commons Attribution License, which permits unrestricted use, distribution, and reproduction in any medium, provided the original work is properly cited.

**Objective.** To review the progress of research on photoplethysmography- (PPG-) based cuffless continuous blood pressure monitoring technologies and prospect the challenges that need to be addressed in the future. **Methods.** Using Web of Science and PubMed as search engines, the literature on cuffless continuous blood pressure studies using PPG signals in the recent five years were searched. **Results.** Based on the retrieved literature, this paper describes the available open datasets, commonly used signal preprocessing methods, and model evaluation criteria. Early researches employed multisite PPG signals to calculate pulse wave velocity or time and predicted blood pressure by a simple linear equation. Later, extensive researches were dedicated to mine the features of PPG signals related to blood pressure and regressed blood pressure by machine learning models. Most recently, many researches have emerged to experiment with complex deep learning models for blood pressure prediction with the raw PPG signal as input. **Conclusion.** This paper summarized the methods in the retrieved literature, provided insight into the artificial intelligence algorithms employed in the literature, and concluded with a discussion of the challenges and opportunities for the development of cuffless continuous blood pressure monitoring technologies.

## 1. Introduction

Cardiovascular diseases (CVD) have become the number one threat to human health, claiming 10.4 million lives worldwide each year [1]. Of all its causes, hypertension is the most dangerous one, because abnormal blood pressure (BP) can cause damage to vital organs such as the heart, brain, kidneys, and retina and even lead to myocardial infarction, cerebral hemorrhage, kidney failure, and other critical symptoms [2]. In recent years, with the aging population, the prevalence of obesity, and other factors, the prevalence of hypertension is on the rise around the world. According to the report of World Health Organization (WHO), the number of hypertension patients has doubled in the past 30 years and now exceeds 1.2 billion [3]. Moreover, some studies have shown that an increasing number

of children and adolescents have abnormal blood pressure which causes negative effects on their health. Therefore, with its high morbidity, disability, and mortality rates, cardiovascular disease caused by blood pressure abnormalities has imposed a heavy burden on humans worldwide and became a major public health problem.

**1.1. Introduction to Conventional Technologies.** Prevention is the main way to control the prevalence of hypertension. Through the real-time detection of blood pressure and timely intervention of blood pressure, the risk of cardiovascular complications and death can be greatly reduced. Blood pressure measurement methods are divided into invasive measurement and noninvasive measurement methods. Therein, the former method implants a pressure sensor catheter into the aorta to detect pressure changes [4]. This

method produces accurate results but is expensive, painful, and not suitable for routine measurement. At present, the commonly used noninvasive blood pressure measurement methods include the Korotkoff sound, oscillometric, arterial tension, and volume compensation methods.

- (1) Korotkoff sound method blocks arterial blood flow by inflating cuff and then uses a stethoscope to identify the percussive sound of blood flow reopening the vessel, while measuring the external pressure values detected by a manometer [5]. The Korotkoff sound method is the reference standard for cuff intermittent blood pressure measurements, but it is easily disturbed by external interference and relies on measuring physician's proficiency
- (2) The oscillometric method is similar to the Korotkoff sound method in that the arterial vessel is blocked by cuff inflation, and subsequent deflation of the cuff allows the vessel to flow again. Instead of detecting the sound, a pressure sensor on the air band detects the arterial pressure superimposed on the cuff [6]. The main disadvantages of oscillometric method are that it is sensitive to motion and needs the subject to remain stationary during measurement. Therefore, both the oscillometric method and the Korotkoff sound method need the subjects to wear a cuff, and thus, only intermittent single-point blood pressure measurements can be performed
- (3) Arterial tension method applies a certain pressure to the arterial vessel near the skin surface of the human body to cause a deformation of the vessel wall [7]. When the external pressure reaches a fixed value, the pressure inside the arterial vessel will be equal to the pressure on the skin surface, and the external pressure value can be considered the blood pressure. However, this method should ensure that the pressure transducer is placed directly above the artery and remains relatively stationary, which restricts its development
- (4) Volume compensation method detects vascular blood volume by a finger cuff with a photoelectric volume sensor [8]. With the constant change of external pressure acting on the blood vessel wall by the cuff, the regulating system makes the blood vessel blood volume constant. Therewith, the external pressure of the cuff is equal to the intravascular pressure, and blood pressure can be measured indirectly through the external pressure detection. However, this method needs to apply pressure to the measurement site of the human body, which may cause venous congestion during prolonged measurement, so it is not suitable for continuous measurement

Blood pressure is a dynamic physiological parameter, which has a diel rhythm [9] and is easy to fluctuate greatly with emotional changes or external stimuli [10]. A single intermittent blood pressure measurement usually cannot

reflect the individual's physiological or pathological conditions. As such, continuous monitoring of blood pressure is of great significance. Otherwise, the cuff measurement methods usually cause discomfort to the user, so they are not suitable for infants, patients with open wounds (skin burns or ulcers, etc.), and people with large arm circumferences. Consequently, the research on cuffless continuous blood pressure monitoring is an urgent and significant task.

*1.2. Photoplethysmography.* Photoplethysmography (PPG) is a noninvasive method to detect the blood volume changes in tissues by photoelectric means. This method is based on the Lambert-Beer law [11], which indicates that the light passing through the blood tissue will be attenuated by the length of the propagation path, the density of the tissue, the absorbance, and other factors. The blood volume varies periodically with the blood ejection of the heart, as does the light intensity through the skin [12]. PPG waveform reflects abundant information about the cardiovascular function of the subject, and its formation is closely related to blood pressure as theoretically proven [13]. Moreover, since PPG signal can be easily collected with a photoelectric sensor, the prediction of blood pressure by PPG signal is an attractive and promising research direction.

As shown in Figure 1, the common PPG pulse waveform comprises an ascending branch and a descending branch. The ascending branch reflects the process of arterial expansion during ventricular ejection, while the descending branch reflects the vascular retraction during late ejection. As the ventricles diastole, the intraventricular pressure becomes lower than the blood pressure in the aorta, whereupon the blood flows back, followed by the closure of the aortic valve and a forward flow of blood. Therefrom, a smaller rise is formed in the descending branch, exhibiting a diastolic peak on the waveform.

PPG signals are cheap to acquire, easy to build into wearable devices (phones, smartwatches, etc.), and free of cuff limitations. Because of the urgent need for continuous cuffless blood pressure monitoring, PPG has attracted numerous attentions of the medical community all over the world, and a large number of researchers have conducted in-depth researches in recent years. Using Web of Science and PubMed as search engines, this paper reviewed PPG-based continuous cuffless blood pressure monitoring technologies over the past five years, focused on artificial intelligence-based solutions, and summarized specific implementations that could be used for reference.

## 2. Materials

*2.1. Datasets.* In the field of blood pressure prediction, researchers have released some open datasets that provide a data basis for fair comparison of different algorithms. Medical Information Mart for Intensive Care (MIMIC) is the most frequently used public dataset, which is a collaborative effort of physicians and computer science experts from Beth Israel Deaconess Medical Center (BIDMC), Massachusetts Institute of Technology (MIT), Oxford University, Massachusetts General Hospital (MGH), and others [14].

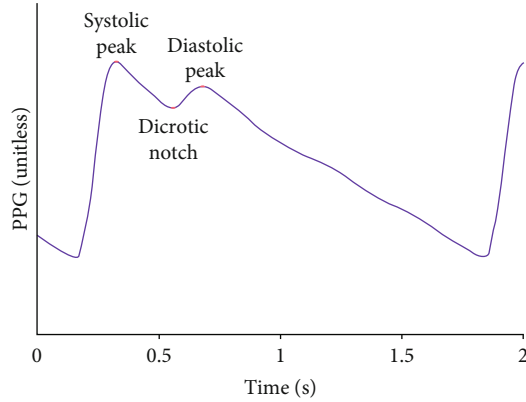


FIGURE 1: A common PPG pulse waveform.

The MIMIC dataset provides physiological data such as electrocardiogram (ECG), photoplethysmography (PPG), arterial blood pressure (ABP), and respiration signals (RESP) collected from intensive care unit (ICU) wards. MIMIC III V1.4, as the most commonly used dataset version, contains data on 53,423 adult patients admitted to ICU between 2001 and 2012 and 7,870 neonates admitted between 2001 and 2008. All data in MIMIC are freely available to researchers worldwide and can be accessed through PhysiоNet (<http://physionet.org/>).

The BP dataset in the University of California Irvine machine learning repository (UCI\_BP) is derived from MIMIC II, and the data is stored in the v7.3 mat format of MATLAB [15]. This version of the dataset is also widely used because it has undergone some preprocessing and validation.

Some studies are based on the Queensland Vital Signs dataset [16], a monitoring dataset from 32 patients, all of whom used arterial blood pressure monitoring lasting from 13 minutes to 5 hours. The dataset also saves the corresponding data signal visualization results for easy viewing and use.

Another dataset used for blood pressure prediction is clinical data from patients admitted to Guilin People's Hospital in Guilin, China, and can be downloaded through the Figshare repository [17]. This dataset (PPG\_BP, Figshare) contains statistics on 657 PPG segments of 219 subjects with a sampling frequency of 1000 Hz, which can be used for in-depth study of the relationship between PPG signals and blood pressure.

There are also some researches based on self-collected datasets, which explored the relationship between PPG signals and physiological parameters to some extent, but most of these datasets are small due to the acquisition device and cost. Table 1 illustrates the datasets commonly used in the retrieved literature. As the collection time of each subject in the dataset is long, these long-time signals are usually segmented according to the needs of algorithm processing, and the resulting short duration sequence is called the sample herein.

**2.2. Evaluation Metrics.** Blood pressure prediction is a regression analysis and can be evaluated by mean error (ME), mean absolute error (MAE), standard deviation

(STD), and root mean square error (RSME). The calculation criterion of ME is shown in formula (1), which represents the arithmetic mean of the error between the predicted value ( $\hat{y}_i$ ) and true blood pressure ( $y_i$ ). The calculation criteria of the MAE and STD are shown in formulas (2) and (3). The MAE is the average of the absolute values of the errors between the predicted value ( $\hat{y}_i$ ) and true blood pressure ( $y_i$ ). The calculation criterion of the RMSE as shown in formula (4) is obtained by calculating the square root of the mean of the square of the difference between the predicted value ( $\hat{y}_i$ ) and true blood pressure ( $y_i$ ).

$$ME = \frac{1}{n} \sum_{i=1}^n \hat{y}_i y_i, \quad (1)$$

$$MAE = \frac{1}{n} \sum_{i=1}^n |\hat{y}_i y_i|, \quad (2)$$

$$STD = \sqrt{\frac{1}{n-1} \sum_{i=1}^n (e_i \bar{e}_i)}, \quad e_i = \hat{y}_i y_i, \quad (3)$$

$$RMSE = \sqrt{\frac{1}{n} \sum_{i=1}^n (\hat{y}_i y_i)^2} \quad (4)$$

Compared with ME, the MAE indicator eliminates positive and negative offsets, and the STD reflects the dispersion of errors. Hence, MAE and STD are a pair of commonly used evaluation metrics in blood pressure estimation. The American Association for the Advancement of Medical Instrumentation (AAMI) stipulates that the MAE of blood pressure measuring devices should be less than 5 mmHg and the STD should be less than 8 mmHg. Alternatively, the grading criteria established by the British Hypertension Society (BHS) are shown in Table 2, which specifies the percentages of cumulative frequency with errors less than 3 thresholds, respectively, and achieving grade A or grade B is in line with the conditions for clinical use.

### 3. Methods

**3.1. Preprocessing.** Whether from public datasets or self-collected datasets, the PPG signals obtained are complex and easy to overlap with noise. Taking the frequently used MIMIC as an example, the subjects are patients in ICU, and their physical conditions have complex impacts on the PPG signals. Therefore, preprocessing the PPG signals to obtain high-quality signals is an important link affecting the accuracy of both subsequent feature analysis and artificial intelligence models.

- (1) Filtering: PPG signal is a very weak signal with a frequency range of 0-25 Hz and easy to be disturbed by external factors as well as its collection device during the acquisition process. The noises mainly include baseline drift caused by body motion and breathing and industrial frequency disturbance caused by electromagnetic wave radiation. These noises have a

TABLE 1: Summary of the database retrieved.

Authors	Dataset	Subjects	Samples	Signals
Slapničar et al. [21]	MIMIC III	510	—	PPG
Aguirre et al. [18]	MIMIC III	1131	6478	PPG
Leitner et al. [31]	MIMIC III	100	—	PPG
Baek et al. [92]	MIMIC II	942	1912	PPG, ECG
Schlesinger et al. [93]	MIMIC II	329	136459	PPG
Wang et al. [94]	MIMIC II	72	58795	PPG
Yen et al. [87]	UCI_BP	1551	—	PPG
Panwar et al. [86]	UCI_BP	1557	—	PPG
Khalid et al. [58]	Queensland, MIMIC II	—	8133, 9877	PPG
Han et al. [33]	PPG_BP Figshare	—	116	PPG

TABLE 2: The standards of BHS.

		Cumulative error percentage		
		5 mmHg	10 mmHg	15 mmHg
BHS	Grade A	60%	85%	95%
	Grade B	50%	75%	90%
	Grade C	40%	65%	85%

serious impact on the analysis of the PPG signal; therefore, filtering operations are required. Many researchers adopted Butterworth filter, which allows signals within a specific frequency range to pass and suppresses signals outside the given frequency range. For instance, Aguirre et al. [18] used a Butterworth filter with the cut-off frequency set to 0.5-8 Hz. Ghosh et al. [19] used a third-order Butterworth bandpass IIR filter with the cut-off frequency set to 1.5-20 Hz. Tiloca et al. [20] adopted a Butterworth FIR filter to limit the PPG signal to the frequency band range of [0.5-6] Hz. Likewise, Slapničar et al. [21] employed a fourth-order Butterworth filter with the cut-off frequency of [0.5-8] Hz to eliminate baseline drift and high-frequency noise. Furthermore in the research by Slapničar et al. [22], a fourth-order Butterworth bandpass filter with the cut-off frequency of 0.5-4 Hz was adopted. Other studies such as El-Hajj et al. [23] chose discrete wavelet decomposition to set the decomposition coefficients of the low-frequency and high-frequency components to 0 and performed soft threshold denoising on the remaining decomposition coefficients. In the study by Li et al. [24], the discrete Fourier transform was used to convert the temporal signal to the frequency domain and filter out the low-frequency components by setting the cut-off frequency. Besides, the Chebyshev filter with the cut-off frequency of 10 Hz was adopted for PPG signal filtering in the research by Hasanzadeh et al. [25]

- (2) Segmentation: the duration of the collected PPG signals is different. For instance, many PPG signals in the MIMIC dataset last up to tens of hours. Thus,

PPG signals are usually divided into windows, referred to herein as segments. The length of the split windows can be set according to the needs of the subsequent AI algorithm, ranging from a single cycle to tens of seconds

- (3) Signal quality assessment: the PPG signals are still complex and variable after denoising; hence, thorough criteria need to be established to remove signals with poor quality, thereby reducing the negative impacts of anomalous signals on subsequent AI algorithms. This task is challenging, and no consistent criteria have been established yet, which often needs to be determined empirically or experimentally. First, the poor signals can be removed by some empirical values, such as limiting systolic blood pressure (SBP) and diastolic blood pressure (DBP) to 80-180 mmHg and 60-130 mmHg, respectively [26, 27], deleting the PPG signals with heart rate below 60 beats per minute [28], and rejecting outliers by using quartile [29] or 3-sigma criterion [30]. Moreover, considering the periodicity of PPG, some researches adopted autocorrelation between PPG periodic signals [31], dynamic time warping [32], or high-order statistics, such as skewness and kurtosis [33, 34], to further standardize the quality of PPG signals
- (4) Normalization: converting the amplitude of the PPG signal to the range of [0-1] can simplify and enhance the analysis process of the PPG signal and ensure that the extracted values are meaningful and fair to the subsequent characterization process. The normalization methods of these studies are relatively uniform, with some using the method in formula (5) to convert the amplitude of the PPG signal to 0-1 [35] and others normalizing the PPG signal to have a mean of 0 and a variance of 1 [21]:

$$x'_i = \frac{x_i - \min(x)}{\max(x) - \min(x)}, \quad (5)$$

where  $x'_i$  refers to the amplitude of the sample after conversion,  $x_i$  refers to the original amplitude of the sample, and  $\min(x)$  and  $\max(x)$  are the minimum and the maximum amplitude in the set of samples, respectively

**3.2. Methods.** A dataset consisting of a large number of PPG segments (here also called samples) belonging to different subjects is obtained after preprocessing. Next, the dataset is divided into training and test sets (deep learning models may include training, validation, and test sets) according to proportion or other means and are fed into models for subsequent study. Most researches divided the training and test sets randomly by sample, while only a few researches divided the training and test sets strictly by subjects. The latter method is more recommended. Two factors are considered in the case: primarily, PPG segments belonging to the same subject are correlated [32]; thus, dividing the dataset only by samples may bring out impure results due to the fact that there are segments of the same subject in both the training and test sets. Secondly, considering that we need to deploy the algorithm on mobile phones or wearable devices in the future, the users to be tested must be the unseen subjects in the training set. For the above reasons, it is more robust to divide the training and test sets by subjects.

**3.2.1. Blood Pressure Estimation Method Based on Pulse Wave Velocity or Transit Time.** The propagation speed of pulse wave is mainly influenced by the compliance of the arterial vessels. When the blood pressure is high, the arterial compliance becomes worse, and the propagation speed of pulse wave becomes faster. Conversely, when the blood pressure is low, then the artery compliance increases, and the transmission speed of the pulse wave slows down. The equation for the propagation velocity of waves in an elastic tube of an ideal type is

$$c_0 = \sqrt{\frac{Eh}{\rho D}} \quad (6)$$

Here,  $E$  is the elastic modulus of the artery,  $h$  is the thickness of the artery wall,  $D$  is the inner diameter of the artery, and  $\rho$  is the blood density [36]. Pulse wave velocity (PWV) or pulse transit time (PTT) is an attractive index for blood pressure estimation. PTT can be considered the interval of pulse wave transmission time at different sites of arteries, which is inversely proportional to PWV. Besides, the pulse arrival time (PAT) has resemblance to PTT, which can be calculated by the time interval between the R peak of ECG and the peak of PPG. There are two common measurement methods for PTT/PAT. One is to synchronously measure the ECG and PPG signals. Alternatively, multiple sensors can be deployed at the proximal and distal ends, thereby calculating the time interval between the PPG signals at the difference sites of the human body.

Once the PTT/PAT/PWV is calculated, blood pressure can be estimated with a simple formula, which is a common method in early researches. Viunyttskyi et al. [37] recorded both single-channel ECG and PPG signals through a self-

designed device. The adopted dataset included a total of 30 records consisting of the records collected by the self-designed hardware and extracted from the MIMIC database. Blood pressure was estimated by a simple linear equation with an RMSE of 5.71 for SBP and 5.13 for DBP. Lazazzera et al. [38] collected PPG signals from the wrist and fingertips through two sensors placed on the back and the front of the smartwatch. The time intervals of the two sites PPG were fed into a linear model to estimate blood pressure. The model was validated on 44 subjects, and the results almost satisfied the standard of AAMI. Kim et al. [39] employed two sensors to collect PPG signals at different locations of the same finger and estimated blood pressure by a simple model with the time difference between the two sites PPG. The error rate was stable at about 5% in a small experimental cohort, and the error rate referred to the ratio of the prediction error to the true BP value. The signal acquirement by Byfield et al. [40] is similar to that designed by Kim et al., and the time interval of the two sites PPG was subjected to a Gaussian regression model for blood pressure prediction. Otherwise, Tabei et al. [41] synchronously acquired the PPG signals at the index of the left and right hand through the cameras of two mobile phones and sequentially calculated the PTT to estimate blood pressure.

Some other studies combined phonocardiogram (PCG) [42], impedance plethysmography (IPG) [43], and ballistocardiogram (BCG) [44] to obtain two sites signals, thereby estimating blood pressure by PTT/PAT/PWV. However, both ECG signals and multisite PPG signals require additional sensors. Hardware consumption increases the difficulty of deployment of wearable devices, and it is particularly hard to build into mobile phones because of the difficulty of hardware changes to widely used phones. Table 3 summarizes BP estimation methods based on PTT/PAT/PWV presented in the paper.

**3.2.2. Blood Pressure Estimation Method Based on Pulse Wave Analysis (PWA).** The morphology of PPG waveform contains a wealth of physiological and pathological information and has a close relationship with the cardiovascular system. Pulse wave analysis (PWA) aims at expiring the physiological significance of the pulse wave by extracting rich features from PPG and its derivatives and combines with powerful artificial intelligence algorithms to estimate blood pressure. The paper [45, 46] provided prospective studies on the feasibility of using a single PPG signal to estimate blood pressure. Inspired by these researches, extensive studies are dedicated to mining BP-related features and combine traditional machine learning for blood pressure estimation. Researches of blood pressure estimation methods based on PWV focus on two aspects: One is mining features with strong correlation to blood pressure, and the other is the optimization of artificial intelligence algorithms. Many features of PPG waveform have been experimentally proven to be related to blood pressure, including the aforementioned PTT. The features adopted in the existing studies can be classified into time domain features, frequency domain features, demographic information, etc. As typical one among them, the peak of PPG waveform is considered

TABLE 3: Summary of BP estimation methods based on PTT/PAT/PWV.

Authors	Signals	Position of sensors	Subjects	Results (mmHg)	
				SBP	DBP
Viunytyskiy et al. [37]	PPG, ECG	Finger, chest	30 records	RMSE: 5.71	RMSE: 5.13
Lazazzera et al. [38]	PPG, PPG	Wrist, finger	5 + 44 subjects	ME: -1.52 STD: 9.45	ME: 0.39 STD: 4.93
Kim et al. [39]	PPG, PPG	Finger, finger	21 subjects	Error rate $\approx$ 5%	
Byfield et al. [40]	PPG, PPG	Finger, finger	26 subjects	MAE: 2.117 STD: 0.257	MAE: 2.935 STD: 0.721
Tabei et al. [41]	PPG, PPG	Finger, finger	6 subjects	MAE: 2.07 STD: 2.06	MAE: 2.12 STD: 1.85
Marzorati et al. [42]	PPG, PCG	Finger, chest	20 subjects	MAE: 3.06	MAE: 1.83
Huynh et al. [43]	PPG, IPG	Finger, wrist	15 subjects	RMSE: 8.47 STD: 0.91	RMSE: 5.02 STD: 0.73
Yousefian et al. [44]	PCD, BCG	Wrist, wrist	22 subjects	MAE: 7.6	MAE: 5.1

related to stroke volume [47], while the pulse width at 50% and pulse area ratio are indicators related to total peripheral resistance [48]. In addition, the photoplethysmographic intensity ratio (PIR) can reflect variations in the internal diameter of the artery and correlates with changes in blood pressure [49], and the artery stiffness index (ASI) presents arterial stiffness [50]. Moreover, the  $K$  value can reflect the changes in peripheral resistance of blood vessels, elasticity of arterial walls, and blood viscosity [51]. The first derivative (VPG) and second derivative (APG) of PPG play an important role in detecting the fiducial points of PPG and analyzing the physiological significance of PPG waveform [52]. Therefore, abundant features can be extracted from the PPG derivatives for analysis. Furthermore, Fourier transform, singular value decomposition, wavelet transform, and other techniques can be adopted to map the time domain signal to the frequency domain, to perform spectral analysis of the PPG signal. Besides, entropy is a measure of signal uncertainty [53], so extracting the entropy of the PPG signal facilitates the analysis of complex blood pressure signals. Some of the typical features are listed in Table 4, and some of them are depicted in Figures 2 and 3.

In the existing studies, the maximum feature dimension extracted from PPG waveform reaches up to more than 200, among which redundant features will reduce the accuracy of the model and increase the complexity of the model. Hence, the feature selection method is advised to reduce the dimension of features, screen out the most relevant feature subset, and enhance the accuracy of the algorithm. Correlation analysis, multicollinearity analysis, recursive elimination, minimum redundancy maximum correlation, and intelligent optimization strategies such as genetic algorithm (GA) are all extensively used feature selection methods.

Machine learning algorithms can identify and analyze the complex mapping between PPG signals and blood pressure, thereby establishing an effective blood pressure prediction model. A large number of researches have applied different regression models to estimate blood pressure, such as multiple linear regression (MLR), regression tree (RT), random forest regression (RFR), support vector machine

regression (SVR), Adaboosting regression, and artificial neural network (ANN). In particular, some researches have proved that random forest regression is a more robust algorithm because it can evaluate the importance of features and is not sensitive to outliers [54]. The BP estimation methods base on PWA retrieved in this paper are listed in Table 5.

Thambiraj et al. [55] extracted 43 features from ECG and PPG signals, employed a genetic algorithm to search for the optimal feature subset, and used a random forest model to estimate blood pressure. The MAEs of this method were 9.54 and 5.48 mmHg for SBP and DBP, respectively. Tiloca et al. [20] extracted 11 features including PTT, PIR, and heart rate from PPG and ECG signals in the MIMIC II dataset and employed a random forest regression model to predict blood pressure, which obtained a RMSE of 13.01 and 12.89 mmHg for SBP and DBP. The two aforementioned experimental datasets were not large and the experimental results did not meet the requirements of the BHS or AAMI standards. Hasanzadeh et al. [25] modified an algorithm for detecting the fiducial points of PPG signal, which helped to improve the accuracy of feature extraction. Based on 19 features such as heart rate, pulse width, and reflex index extracted from PPG signals, the blood pressure was estimated by linear regression, decision tree, random forest, and Adaboosting regression models. The validation results on the UCI dataset dedicated that Adaboosting and random forest regression outperformed other models. However, compared with the AAMI and BHS standards, the result of SBP could not satisfy the standards. Liu et al. [56] collected PPG and ECG signals from 35 clinical patients and extracted 15 relevant features to compare the performance of four regression models: decision tree, support vector machine, Adaboosting, and random forest. The results demonstrated that random forest regression outperformed the other models, with  $ME \pm STD$  of SBP and DBP were  $0.04 \pm 6.11$ , and  $0.11 \pm 3.62$  mmHg, respectively. Since the study only enrolled 35 subjects, the performance of the method needs to be verified on a large experimental cohort. Khalid et al. [57] extracted 5 features including area, time, and pulse width on PPG segments refined from the Queensland

TABLE 4: A list of typical feature extracted from the PPG and its derivatives.

Feature	Description
Amplitude	Amplitude of the fiducial points in Figure 2 (e.g., systolic peak, diastolic peak, and dicotic notch)
Time	Time interval between the fiducial points in Figure 2 (e.g., systolic peak, diastolic peak, dicotic notch, and onset)
Time domain	Systolic width at 10%, 25%, 33%, 50%, 66%, and 75% and diastolic width at 10%, 25%, 33%, 50%, 66%, and 75%, as shown in Figure 3
Area	Systolic area, diastolic area, and their ratios
Derivatives	Ratio of amplitude of fiducial points on first-order derivative and second-order derivative in Figure 2
Frequency domain	Amplitude and frequency of the first, second, and third peaks of the frequency domain signal
Demographic information	Age, gender, height, weight, body mass index (BMI), etc.
Entropy	Shannon entropy, spectral entropy, approximate entropy, sample entropy, etc.
Statistical characteristics	Mean, standard deviation, skewness, kurtosis, etc.
Others	$K$ value, PIR, ASI, etc.

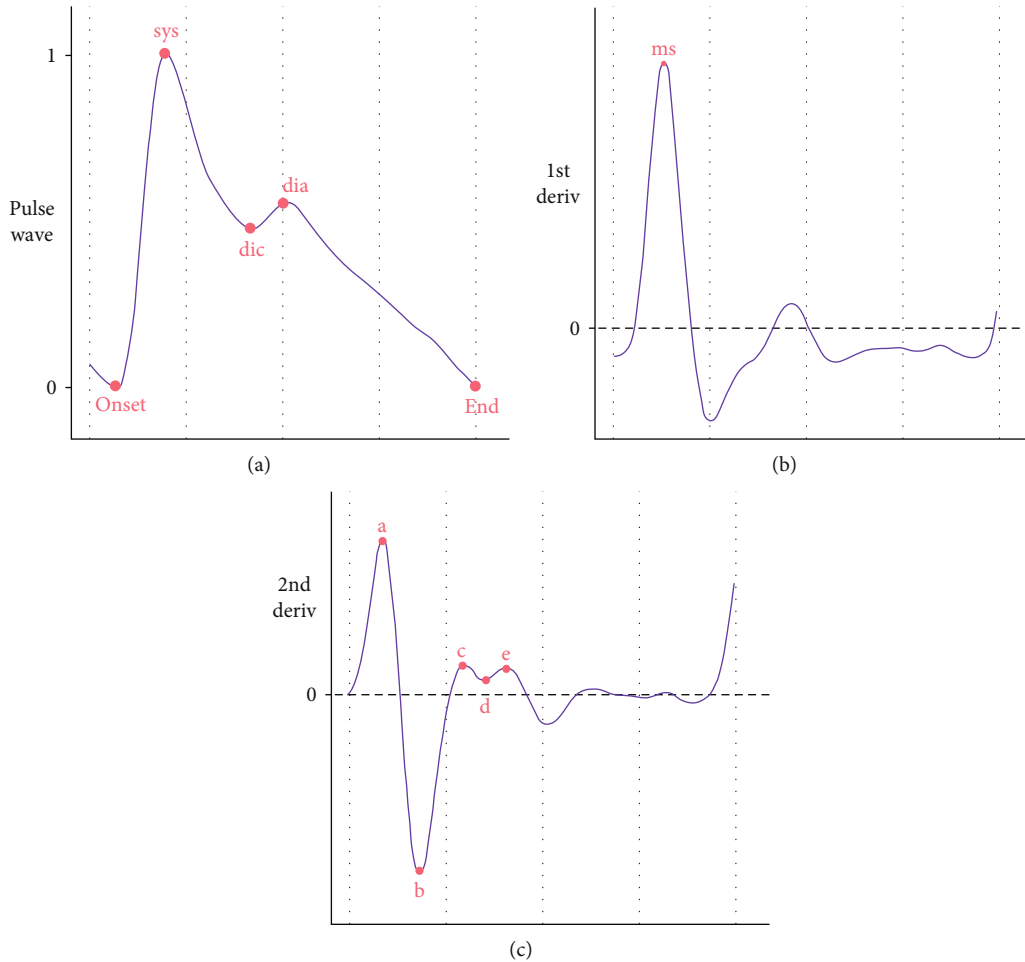


FIGURE 2: Fiducial points of PPG wave and its derivatives: The three subplots from top to bottom are (a) PPG pulse wave, (b) first-order derivative, and (c) second-order derivative. In (a), “onset” and “end” denote the beginning and the end of the waveform, respectively, “sys” and “dia” represent the systolic and diastolic peaks, and “dic” represents the dicotic notch. In (b), “ms” denotes the maximum slope point. In (c), “a,” “b,” “c,” “d,” and “e” are five key fiducial points of the second derivative.



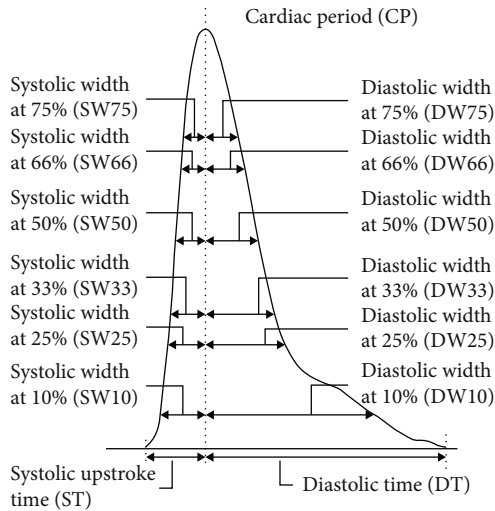


FIGURE 3: Pulse width feature of the PPG waveform.

dataset, followed by a variance inflation factor (VIF) to perform a multicollinearity test on the features, and eliminated two redundant features. In this study, MLR, SVR, and RT were used to estimate blood pressure, and the results revealed that regression tree model achieved the best performance. A subsequent study by Khalid et al. [58] refined a comprehensive dataset of 18,010 PPG segments from Queensland and MIMIC datasets and extracted 16 time domain features from these PPG segments. The multicollinearity test was performed on the features by variance inflation factor (VIF), and the most significant 3 features were screened out. Subsequently, the  $k$ -nearest neighbor model was first adopted to cluster hypotension, hypertension, and normotensive and then combined with the regression tree algorithm to estimate blood pressure. The results obtained in this study were in line with AAMI standards. The two studies both used manual check to determine the quality of the signal, which needs to be improved in the future. Similarly, after  $k$  means clustering with three features extracted from ECG and PPG signals, Farki et al. [59] employed gradient boosting, random forest, and multilayer perceptron regression methods to regress the blood pressure for each cluster. The method was validated on the MIMIC dataset and yielded an MAE of 2.56 for SBP and 2.23 for DBP, but the details of the dataset were not clearly disclosed. Haddad et al. [60] extracted 27 features from PPG and its derivatives based on the 30-second PPG segments of 28 subjects in the MIMIC dataset. The study constructed the MLR model for blood pressure prediction and resulted in an error of  $6.10 \pm 8.01$  mmHg for SBP and  $4.65 \pm .22$  mmHg for DBP. Manamperi et al. [61] extracted 53 features from PPG and its derivatives and predicted blood pressure through a 6-layer ANN model. The experimental results on the MIMIC II dataset showed that both SBP and DBP achieved the grade A of the BHS standard. Subsequent trials with 50 voluntary subjects achieved the grade A of the BHS standard for DBP and grade B for SBP. Attarpour et al. [62] collected the wrist and fingertip PPG signals from 111 volunteers and then extracted a total of 34 features from PPG signal

and its second derivative, height, weight, etc. Subsequently, the optimal feature subset was selected by using the moving backward algorithm and genetic algorithm, and finally, the blood pressure was predicted by a multilayer neural network. By comparison, a genetic algorithm-based feature selection algorithm improved the performance of blood pressure estimation, with an accuracy (MAE  $\pm$  STD) of SBP as  $5.59 \pm 0.30$  mmHg and DBP as  $4.45 \pm 0.16$  mmHg. Chakraborty et al. [63] collected 670 records from 50 patients in the open dataset and extracted 15 time domain features. The study adopted neighborhood component analysis (NCA) and relief (RLF), respectively, to finally select the optimal feature subset consisting of four features. Based on the modified ANN model, the proposed algorithm obtained an error of  $0.461 \pm 2.62$  mmHg for SBP and  $0.15 \pm 4.482$  mmHg for DBP, whereas the first minute initial calibration and the four-minute blood pressure estimation made the method not very real-time, and the fiducial detection technique adopted in the study was sensitive to noise. Yang et al. [64] extracted 90 features including PAT, heart rate, and complexity features of PPG and ECG signals and employed support vector machine, Lasso, and artificial neural network models to predict blood pressure. This study validated on 14 male volunteers, and the optimal result (MAE  $\pm$  STD) of SBP was  $7.33 \pm 9.53$  mmHg obtained by the support vector machine model, while the optimal result of DBP was  $5.15 \pm 6.46$  mmHg obtained by the ANN model. Otherwise, Chen et al. [65] extracted 14 features of ECG and PPG from the open dataset, selected features by the mean impact value (MIV) index, and finally predicted blood pressure using SVR model optimized by a genetic algorithm. The proposed algorithm yielded an error (MAE  $\pm$  STD) of  $3.27 \pm 5.52$  mmHg for SBP and  $1.16 \pm 1.97$  mmHg for DBP. Similarly, Tan et al. [66] synchronously collected PPG and ECG from 10 healthy volunteers, extracted 17 time domain features, and retained features with the cumulative contribution rate more than 85% by MIV. The study used a GA-based BP network to model SBP and DBP separately, and the proposed algorithm outperformed the traditional regression model and ANN. Since the data size in the previous three studies was not big enough, the generalization ability and confidence of the model would be affected to some extent.

The following two researches dedicated efforts to explore the features related to blood pressure estimation. Chowdhury et al. [67] adopted the public dataset consisting of 657 PPG samples from 219 subjects and extracted 107 features including time domain, frequency domain, time-frequency domain, and demographic information. In this study, correlation evaluation, ReliefF, and minimum redundant maximum correlation were adopted for feature selection, and five machine learning methods, linear regression, regression tree, Gaussian process regression (GPR), support vector machine regression, and ensemble tree regression, were used for blood pressure estimation. The ReliefF method combined with GPR outperformed other algorithms, with a RMSE of 6.74 and 3.59 mmHg for SBP and DBP, respectively. Dey et al. [68] collected PPG signals from 206 volunteers using Samsung Galaxy S6 mobile phones and extracted 233 features in the time and frequency domain from PPG

TABLE 5: The summary of BP estimation methods based on PWA.

Authors	Dataset	Signals	Features	Feature selection	AI algorithm	Result (mmHg)	
						SBP	DBP
Haddad et al. [60]	MIMIC I 28 subjects	PPG	27	—	MLR	MAE: 6.10 STD: 8.01	MAE: 4.65 STD: 6.22
El-Hajj et al. [23]	MIMIC II 942 subjects	PPG	52	Pearson's coefficient, mutual information, recursive elimination	Deep learning recurrent model	MAE: 4.51 STD: 7.81	MAE: 2.6 STD: 4.41
Li et al. [24]	MIMIC 50 subjects	PPG, ECG	7	—	Deep LSTM	MAE: 6.726 STD: 14.505	MAE: 2.516 STD: 6.442
Farki et al. [59]	MIMIC II	PPG, ECG	3	—	$k$ means+ (RFR, gradient boosting regression, multilayer perceptron)	MAE: 2.56	MAE: 2.23
Senturk et al. [70]	MIMIC II	PPG, ECG	19	—	RNN, NARX-NN, LSTM	ME: 0.0224 STD: 2.211	ME: 0.0417 STD: 1.2193
Thambiraj et al. [55]	UCL_BP 3801 records	PPG, ECG	43	GA	RFR	MAE: 9.54	MAE: 5.48
Tiloca et al. [20]	MIMIC II	PPG, ECG	11	—	RFR	RMSE: 13.01	RMSE: 12.89
Manamperi et al. [61]	MIMIC II, self-collected 50 subjects	PPG	53	—	ANN	MAE: 4.8	MAE: 2.5
Hasanzadeh et al. [25]	UCL_BP	PPG	19	—	LR, decision tree, RFR, Adaboosting	MAE: 8.22 STD: 10.38	MAE: 4.17 STD: 4.22
El-Hajj et al. [69]	MIMIC II	PPG	22	Pearson's correlation, random forest feature importance, RFE, sequential forward search	Feedforward neural networks, LSTM, GRU	MAE: 3.23 STD: 4.74	MAE: 1.59 STD: 1.77
Khalid et al. [58]	Queensland, MIMIC 18010segments	PPG	16	VIF	KNN+RT	ME: 0.07 STD: 7.1	ME: -0.08 STD: 6.0
Yang et al. [64]	Self-collected 14 subjects	PPG, ECG	90	—	SVR, Lasso, ANN	MAE: 7.33 STD: 9.53	MAE: 5.15 STD: 6.46
Attarpour et al. [62]	Self-collect 111 subjects	PPG	34	Moving backward algorithm, GA	Multilayer neural network	MAE: 5.59 STD: 0.30	MAE: 4.45 STD: 0.16
Liu et al. [56]	Self-collected 35 subjects	PPG, ECG	15	—	DTR, SVR, Adaboosting, RFR	ME: 0.04 STD: 6.11	ME: 0.11 STD: 3.62
Chakraborty et al. [63]	MIMIC II 50 subjects	PPG	15	NCA, RLF	Modified ANN	ME: 0.461 STD: 2.62	ME: 0.15 STD: 4.482
Chen et al. [65]	MIMIC III	PPG, ECG	14	MIV	GA-SVR	MAE: 3.27 STD: 5.52	MAE: 1.16 STD: 1.97
Chowdhury et al. [67]	Figshare_BP 219 subjects	PPG	107	Correlation, RLF, minimum redundancy maximum correlation	LR, RT, Gaussian process regression, SVR, integration tree regression	RSME: 6.74	RSME: 3.59
Khalid et al. [57]	Queensland 8133 segments	PPG	5	VIF	MLR, SVR, RT	ME: -0.1 STD: 6.5	ME: -0.6 STD: 5.2
Dey et al. [68]	Self-collected 206 subjects	PPG	233	—	Lasso	MAE: 6.9	MAE: 5
Tan et al. [66]	Self-collect 10 subjects	PPG, ECG	17	MIV	GA-BP	RMSE: 2.114	RMSE: 1.30

and its derivatives, which is the study with the highest number of feature dimensions in the retrieved literature. The study employed a Lasso regression model and categorical modeling based on demographic information, which improved the accuracy of blood pressure predictions. However, the performance of the model does not satisfy the AAMI standard.

In addition to traditional machine learning models, some studies have used more complex deep learning networks for blood pressure estimation after extracting the relevant features of PPG signals. El-Hajj et al. [69] extracted a total of 22 time domain features from the PPG signals and their derivatives, combined Pearson's correlation, random forest feature importance, recursive feature elimination, and sequential forward selection methods, to finally select seven consistently accepted features that have the greatest impact on blood pressure estimation. The validation results on the UCI dataset pointed out that LSTM and GRU outperformed other models, which were promising and both met the AAMI criteria. In a subsequent study, El-Hajj et al. [23] refined 942 subjects from the MIMIC II dataset and extracted 52 features from PPG and its derivatives. Combined with Pearson's correlation, mutual information, and recursive elimination method, the optimal feature subset consisting of 24 features were selected. The research designed a complex deep learning model that involved a bidirectional RNN layer, a series of conventional recurrent layers, and an attention layer, which resulted in an error (MAE  $\pm$  STD) of  $4.51 \pm 7.81$  mmHg for SBP and  $2.6 \pm 4.41$  mmHg for DBP. Li et al. [24] extracted seven features (including PTT) from PPG and ECG signals, combined with a deep learning model for blood pressure estimation. The first layer of the deep learning model is a bidirectional long short-term memory layer, followed by a multilayer LSTM with a residual module. The validation results of this method on the MIMIC II dataset showed that SBP and DBP met grades B and A of BHS standard, respectively. Senturk et al. [70] extracted time domain and frequent domain features from signals in the MIMIC II dataset, combined with chaotic features such as the Shannon entropy, sample entropy, and fuzzy entropy and then compared the performance of three machine learning algorithms in blood pressure estimation. The results demonstrated that the nonlinear autoregressive with exogenous input neural network (NARX-NN) was superior to other algorithms, with an ME  $\pm$  STD of  $0.0224 \pm 2.211$  mmHg for SBP and  $0.0417 \pm 1.2193$  mmHg for DBP. However, the size of the dataset used was not clearly disclosed in the study, so there might be barriers to comparing results across studies.

*3.2.3. Blood Pressure Estimation Method Based on Deep Learning with Raw PPG.* The methods of blood pressure estimation based on PWA may incorporate irrelevant features or not fully mine the information contained in the PPG waveform, and their results highly depend on the accuracy of fiducial point detection of the PPG waveform. In recent years, with the rapid development of deep learning, many researches tend to use the raw PPG signals as input and utilize the advantages of deep learning in extracting complex high-dimensional fea-

tures and advanced convolution computing capabilities for continuous blood pressure monitoring.

Blood pressure estimation methods based on deep learning network use the raw PPG waveform as input, and since the derivatives of PPG also contain features related to blood pressure [71], many studies take the PPG derivatives as input of the model. Researches on deep learning-based blood pressure monitoring methods mainly focus on the optimization of deep learning models and variants. One of the most classic models is the CNN-LSTM model, which is also the most widely used in literature. The hybrid model uses the convolutional neural network (CNN) layer to extract the complex features of the PPG signals and model them in time series with the help of the long short-term memory (LSTM) layer. For instance, in the research by Tazarv et al. [72], CNN was used as a feature extraction module, and LSTM was responsible for modeling over the time series. The CNN-LSTM model was validated on 20 randomly selected subjects from MIMIC II, resulting in an error of  $3.70 \pm 3.07$  and  $2.02 \pm 1.76$  mmHg for SBP and DBP, while the validation results on the Queensland dataset also reached the grade A of the BHS standard and complied with the AAMI standard. Similarly, Mou et al. [73] employed a CNN-LSTM model for blood pressure estimation and validated on three subjects of the MIMIC dataset. The results showed that, compared with the traditional models, the proposed model had a significant improvement in both training time and prediction accuracy. Otherwise, Esmaelpoor et al. [74] employed a CNN-LSTM two-stage model, with the CNN structure for extracting the features of PPG in the first stage and the LSTM structure for modeling the sequence signal in the second stage. Considering the correlation between SBP and DBP, the SBP prediction was applied to the next stage of DBP prediction, and vice versa. The model was tested on 200 subjects in the MIMIC II dataset and resulted in an error (MAE  $\pm$  STD) of  $3.97 \pm 5.55$  and  $2.10 \pm 2.84$  mmHg for SBP and DBP, respectively, which complied with the AAMI standard and reached the grade A of the BHS standard. Nevertheless, the dataset was not strictly divided by subjects, which affected the confidence of the experimental results. Baker et al. [75] utilized a CNN-LSTM model that combined the feature extraction capability of the convolutional layer and the temporal data modeling capability of the LSTM layer, with PPG and ECG signals from the open dataset as input, resulting in an MAE of 4.41 and 2.91 mmHg for SBP and DBP, respectively. Tanveer et al. [76] proposed an ANN-LSTM network which consisted of an ANN for extracting features and two stacked LSTM layers for modeling sequence signals. The proposed model was tested on 39 subjects in MIMIC I and achieved an MAE of 1.10 mmHg for SBP and 0.58 mmHg for DBP. Besides, the network proposed by Leitner et al. [31] adopted a gated recurrent unit (GRU) instead of the LSTM on the basis of the CNN-LSTM framework, because GRU has similar functions and slightly different parameters with LSTM. The proposed model was validated on long-term data of 100 subjects in the MIMIC dataset, combined with transfer learning-based calibration techniques, and resulted in an MAE of 3.52 and 2.20 mmHg for SBP and DBP, respectively.

Some other researches have introduced an attention mechanism to assign appropriate weights between different input channels or input vectors; therefore, the deep learning model can focus on more meaningful information and then improve the prediction accuracy. Qiu et al. [77] incorporated the squeeze and excitation block (SE module) in a 25-layer ResNet, which assigned weights to channel dimensions and improved channel attention. The hybrid model took PPG and ECG signals as input and predicted blood pressure on two datasets that included 1216 and 40 subjects from the MIMIC dataset, respectively. The prediction results of the model on the two datasets both achieved the grade A of the BHS standard and satisfied the AAMI standard. Chuang et al. [78] screened 11,000 PPG and ECG segments from 45 subjects in the MIMIC dataset and introduced an attention mechanism to the CNN-LSTM model to identify meaningful features. The results showed that combining the time and frequency domain signals of PPG and ECG could fully obtain the intrinsic characteristics of the signals, which resulted in an error (MAE  $\pm$  STD) of  $2.94 \pm 4.65$  mmHg for SBP and  $2.02 \pm 3.81$  mmHg for DBP. The two aforementioned studies used a combination input of PPG and ECG to predict blood pressure, which necessarily increased hardware consumption. Aguirre et al. [18] proposed a recurrent neural network (RNN) encoder-decoder structure with an attention module and integrated demographic information such as age and gender to improve the prediction of mean ABP pulse. Under the condition that the training set and test set were strictly divided according to subjects, the MAE of SBP and DBP reached  $6.57 \pm 0.20$  and  $14.39 \pm 0.42$  mmHg, respectively.

The residual network (ResNet) [79] proposed by Microsoft Labs in 2015 can well solve the problems of gradient disappearance and gradient explosion brought by the deepening of layers through the residual structure. Schrumppf et al. [80] compared the performance of AlexNet, ResNet, LSTM, and the model proposed by Slapničar et al. [21]. With PPG signals and their derivatives as input, ResNet outperformed other models under the condition of strictly differentiated subjects in training and test sets, with an MAE of 16.4 and 8.5 mmHg for SBP and DBP, respectively. However, the associated SDs are not presented. Furthermore, MAEs of 16.4 and 8.5 mmHg are relatively large, meeting neither AAMI nor BHS standards. After transfer learning-based calibration, the prediction performance was significantly improved. Based on PPG and ECG signals of 40 subjects selected from the MIMIC dataset, Paviglianiti et al. [81] compared the performance of three deep learning models, ResNet, LSTM, and WaveNet. The results pointed out that ResNet combined with three LSTM layers achieved the best prediction performance, with an MAE of 4.118 and 2.228 mmHg for SBP and DBP, respectively.

The PPG signals are one-dimensional physiological signals, while some studies have transformed them into two-dimensional images, thereby performing transfer learning through a model pretrained on ImageNet. Wang et al. [82] converted one-dimensional PPG signals into images by using the visibility graph (VG) approach. This innovative approach preserved the time-frequency information in the

PPG signals and allowed transform learning using CNN models pretrained on the large database ImageNet. The proposed idea was validated on 348 records from UCI\_BP dataset, and the pretrained AlexNet model outperformed other models, leading to an MAE of 6.17 and 3.66 mmHg for SBP and DBP, respectively.

Other deep learning models and their variants include the following: Treebupachatsakul et al. [83] performed Fourier transform on PPG and ECG signals in open datasets and used the amplitude and phase of PPG and ECG signals as input to a context aggregation network (CAN). The network resulted in a RMSE of 7.1455 and 6.0862 mmHg for SBP and DBP, respectively. However, the associated MAEs or SDs are not presented. Sadrawi et al. [84] compared the performance of two deep convolutional autoencoders, LeNet-5 and U-Net, and employed a genetic algorithm to optimize the integration of encoders in the cross-validation process. The method was evaluated on 18 subjects in a single center and yielded an MAE of 2.54 mmHg for SBP and 1.48 mmHg for DBP. The network proposed by Brophy et al. [85] was based on the GAN framework, which mainly consists of a generator with two layers of LSTM and a discriminator with four layers of CNN. Notably, the model is different from previous models in its ability to generate continuous ABP based on the PPG signal, rather than directly producing two values of SBP and DBP. The proposed model was trained on the UCI dataset and tested on the Queensland dataset with long-time data selected from one subject, resulting in an ME of  $2.95 \pm 19.33$  mmHg in mean arterial pressure. However, the population considered was only one subjects, too few to reduce the confidence of the results. Otherwise, Slapničar et al. [21] took PPG alongside its derivatives as input and proposed a complex network model (spectrotemporal ResNet) combining the residual module with a spectrotemporal block, which could fully extract the temporal and frequency information of the signals. The proposed model was validated on over 700 hours of PPG signals from 510 subjects in the MIMIC III dataset, resulting in an MAE of 9.43 mmHg for SBP and 6.88 mmHg for DBP.

Furthermore, some researches have also experimented on the CNN with large convolutional kernels, which may enable the model to obtain larger effective receptive fields. Panwar et al. [86] proposed a deep learning framework consisting of CNN, LSTM, and fully connected layer, and adopted filters of size  $9 \times 1$  in the CNN layers. When evaluated on 1557 subjects from the open dataset, the MAE and STD of the proposed model were 2.30 and 0.196 mmHg for SBP, while 3.97 and 0.064 mmHg for DBP. The hybrid network structure proposed by Yen et al. [87] was composed of multiscale CNN, LSTM, and dense layers, in which the CNN structures adopted  $9 \times 1$  and  $25 \times 1$  kernel filters, respectively. The model was tested on 1551 subjects from the UCI\_BP dataset, resulting in an MAE of  $2.942 \pm 5.076$  and  $1.747 \pm 3.042$  mmHg for SBP and DBP, respectively.

Table 6 illustrates the BP estimation methods based on deep learning model presented in this paper.

TABLE 6: The summary of BP estimation methods based on deep learning.

Authors	Dataset	Signals	AI algorithm	Result (mmHg)	
				SBP	DBP
Tazarv et al. [72]	MIMIC II 20 subjects	PPG	CNN-LSTM	MAE: 3.70 STD: 3.07	MAE: 2.02 STD: 1.76
Chuang et al. [78]	MIMIC 45 subjects	PPG, ECG	CNN-LSTM+self-attention	MAE: 2.94 STD: 4.65	MAE: 2.02 STD: 3.81
Treebupachatsakul et al. [83]	UCI 812 samples	PPG, ECG	CAN	RMSE: 7.1455	RMSE: 6.0862
Mou et al. [73]	MIMIC 3 subjects	PPG	CNN-LSTM	MAE: 4.42 for ABP	
Paviglianiti et al. [81]	MIMIC 40 subjects	PPG, ECG	ResNet, LSTM, WaveNet, ResNet+LSTM	MAE: 4.118	MAE: 2.228
Slapničar et al. [21]	MIMIC III 510 subjects	PPG, derivatives	Spectrotemporal ResNet	MAE: 9.43	MAE: 6.88
Brophy et al. [85]	UCI_BP Queensland 6 subjects	PPG	GAN	MAE: 2.95 STD: 19.33 for MAP	
Aguirre et al. [18]	MIMIC 1131 subjects	PPG	RNN encoder-decoder + attention	MAE: 6.57 STD: 0.20	MAE: 14.39 STD: 0.42
Wang et al. [82]	UCI_BP 348 records	Image transformed from PPG	Pretrained AlexNet, Inception-V3, VGG-19	MAE: 6.17	MAE: 3.66
Esmalpoor et al. [74]	MIMICII 200 subjects	PPG	CNN-LSTM	MAE: 3.97 STD: 5.55	MAE: 2.10 STD: 2.84
Baker et al. [75]	MIMIC III 200000 segments	PPG, ECG	CNN-LSTM	MAE: 4.41 STD: 6.11	MAE: 2.91 STD: 4.23
Qiu et al. [77]	MIMIC 1216 subjects	PPG, ECG	ResNet + SE	MAE: 3.70	MAE: 2.81
Leitner et al. [31]	MIMIC 100 subjects	PPG	CNN-GRU	MAE: 3.52	MAE: 2.20
Schrumpf et al. [80]	MIMIC 3750 + 625 subjects	PPG	AlexNet, ResNet, LSTM, model of Slapničar et al.	MAE: 16.4	MAE: 8.5
Yen et al. [87]	UCI 1551 subjects	PPG	CNN-LSTM	MAE: 2.942 STD: 5.076	MAE: 1.747 STD: 3.042
Tanveer et al. [76]	MIMIC I 39 subjects	PPG, ECG	ANN-LSTM	MAE: 1.10	MAE: 0.58
Panwar et al. [86]	MIMIC II 1557 subjects	PPG	CNN-LSTM	MAE: 2.30 STD: 0.196	MAE: 3.97 STD: 0.064
Sadrawi et al. [84]	Self-collected 18 subjects	PPG	GA + Lenet5/U-net	MAE: 2.54	MAE: 1.48

#### 4. Future Research Directions

Continuous monitoring of blood pressure will be an urgent task in the future, therefore deploying the function on mobile phones or other portable wearable devices to realize daily BP monitoring will have a broad application prospect. From the early simple regression based on multiplexed signals, to PPG feature extraction combined with artificial intelligence algorithms, and then to deep learning models with raw PPG signal most recently, researches on continuous cuffless blood pressure estimation have made great progress over time. However, the current technology still cannot meet the standards of practical applications. The major challenges that need to be addressed urgently include the development of large-scale heterogeneous datasets, mining of strongly correlated feature sets, optimization of lightweight

efficient models, researches on personalized modeling technology, and rPPG-based blood pressure estimation technology.

- (1) Most of the retrieved studies are based on open datasets. For example, the MIMIC dataset is collected from patients in the ICU, whose complex physical conditions have various effects on blood pressure. However, there are differences in blood pressure changes between diverse groups, such as young people and those with cardiovascular disease. Some researches were based on self-collected datasets, but the small amount of data led to low confidence in the validation results. Therefore, it is urgent to establish large-scale heterogeneous datasets to improve the adaptability of the model to different

populations, verify the results of the algorithm, and promote the optimization of the algorithm

- (2) Due to the easy acquirement, low cost, and convenient deployment of PPG signals, PPG-based blood pressure estimation methods have gained a strong momentum in recent years, and many studies dedicated to explore the relationship between PPG features and the physiological significance of blood pressure. Considering the individual difference of PPG signals, there is no set of features directly related to blood pressure has been generally employed, so it is necessary to explore PPG features with explicit physiological significance in the future. Additionally, the existing offline training model should be deployed on mobile phones or other wearable devices, and the balance between the complexity and accuracy of the algorithm needs to be considered. Therefore, the development of lightweight and accurate models is also a very challenging task in the future
- (3) Because of the differences of blood pressure among individuals, even deep learning models trained on large-scale datasets cannot fully learn them. Thus, within the acceptable conditions for commercial deployment, the accuracy of the model can be improved through individual calibration. Haddad et al. [88] adopted a straightforward approach that calibrated estimation of the blood pressure with simple offsets from the same subject. Schrumppf et al. [80] adopted the idea of transfer learning to fine-tune the specific layer of the model with a small amount of template data of the target subject. These methods may mitigate the systematic error in blood pressure estimation, but the mapping relation between the input signal and the estimation of blood pressure still relies on the performance of AI model
- (4) Remote photoplethysmography (rPPG) can be used to extract the PPG signal by using a camera to capture the periodic signal of skin color caused by the cardiac cycle. As smartphones become common devices, rPPG technology can be easily deployed on mobile phones for home-style daily blood pressure monitoring. In recent years, some prospective researches [89–91] have made some progress. Affected by the influence of video quality, subjects' head movement, illumination, and other factors, rPPG-based blood pressure monitoring technology faces great challenges in front-end data collection and processing. However, as rPPG technology is simple, feasible, and easy to deploy, it is still an appealing direction in the future

## 5. Conclusion

This paper retrieved the progress of research in the past five years on the PPG signal-based cuffless continuous blood pressure prediction technology. In conclusion, PPG is a

promising and appealing technology with great potential for application in cuffless continuous blood pressure monitoring. Although diverse BP estimation methods such as that based on PTT/PAT/PWV, PWA, and deep learning have emerged and achieved some results, to reach the standard of commercial application, the continuous blood pressure monitoring technology based on PPG needs in-depth researches in the following aspects: the construction of heterogeneous large datasets, feature mining and optimization of lightweight model, personalized calibration technology, and rPPG technology.

## Data Availability

No data were used to support this study.

## Conflicts of Interest

All authors have declared no conflict of interest.

## Authors' Contributions

Caijie Qin and Xiaohua Wang contributed equally to this work.

## Acknowledgments

This work has been partially supported by the National Key Research Programs of China (2016YFA0100900, 2016YFA0100902), the Chinese National Natural Science Foundation Projects (#82090051 #81871442), and in part by the Youth Innovation Promotion Association CAS (#Y201930), the Educational Research Project for Young and Middle-aged Teachers in Fujian Province (JT180513), and the Scientific Research and Development Fund project of Sanming University (B201824). This work has been partially supported by Fujian Key Lab of Agriculture IOT Application, IOT Application Engineering Research Center of Fujian Province Colleges and Universities, Digital Fujian Research Institute for Industrial Energy Big Data, and Laboratory for the Analysis and Application of Industry Big Data.

## References

- [1] B. Zhou, P. Perel, G. A. Mensah, and M. Ezzati, "Global epidemiology, health burden and effective interventions for elevated blood pressure and hypertension," *Nature Reviews Cardiology*, vol. 18, no. 11, pp. 785–802, 2021.
- [2] K. Suvila and T. J. Niiranen, "Interrelations between high blood pressure, organ damage, and cardiovascular disease: no more room for doubt," *Hypertension*, vol. 79, no. 3, pp. 516–517, 2022.
- [3] NCD Risk Factor Collaboration (NCD-RisC), "Worldwide trends in hypertension prevalence and progress in treatment and control from 1990 to 2019: a pooled analysis of 1201 population-representative studies with 104 million participants," *The Lancet*, vol. 398, no. 10304, pp. 957–980, 2021.
- [4] M. P. Fundora, A. G. Beshish, N. Rao et al., "Comparison of invasive and oscillometric blood pressure measurement in obese and nonobese children," *American Journal of Hypertension*, vol. 34, no. 6, pp. 619–625, 2021.

- [5] G. G. Arabidze, V. V. Petrov, and J. A. Staessen, "Blood pressure by Korotkoff's auscultatory method: end of an era or bright future?," *Blood Pressure Monitoring*, vol. 1, no. 4, pp. 321–327, 1996.
- [6] A. Sapiński, S. Swidzińska, and F. Sapiński, "Theoretic principles of arterial blood pressure determination using the sphygmo-oscillography method," *Kardiologia Polska*, vol. 29, no. 8, pp. 576–582, 1986.
- [7] R. Rubinshtein, J. T. Kuvin, M. Soffler et al., "Assessment of endothelial function by non-invasive peripheral arterial tonometry predicts late cardiovascular adverse events," *European Heart Journal*, vol. 31, no. 9, pp. 1142–1148, 2010.
- [8] S. Tanaka, M. Nogawa, T. Yamakoshi, and K. Yamakoshi, "Accuracy assessment of a noninvasive device for monitoring beat-by-beat blood pressure in the radial artery using the volume-compensation method," *IEEE Transactions on Bio-Medical Engineering*, vol. 54, no. 10, pp. 1892–1895, 2007.
- [9] K. Asayama, M. Satoh, and M. Kikuya, "Diurnal blood pressure changes," *Hypertension Research Official Journal of the Japanese Society of Hypertension*, vol. 41, no. 9, pp. 669–678, 2018.
- [10] M. Shukla, R. Pandey, D. Jain, and J. Y. F. Lau, "Poor emotional responsiveness in clinical hypertension: reduced accuracy in the labelling and matching of emotional faces amongst individuals with hypertension and prehypertension," *Psychology & Health*, vol. 33, no. 6, pp. 765–782, 2018.
- [11] M. Cejnar, H. Kobler, and S. N. Hunyor, "Quantitative photoplethysmography: Lambert-Beer law or inverse function incorporating light scatter," *Journal of Biomedical Engineering*, vol. 15, no. 2, pp. 151–154, 1993.
- [12] J. Allen, "Photoplethysmography and its application in clinical physiological measurement," *Physiological Measurement*, vol. 28, no. 3, pp. R1–39, 2007.
- [13] M. Elgendi, "On the analysis of fingertip photoplethysmogram signals," *Current Cardiology Reviews*, vol. 8, no. 1, pp. 14–25, 2012.
- [14] A. E. Johnson, T. J. Pollard, L. Shen et al., "MIMIC-III, a freely accessible critical care database," *Scientific Data*, vol. 24, no. 3, article 160035, 2016.
- [15] M. Kachuee, M. M. Kiani, H. Mohammadzade, and M. Shabany, "Cuff-less high-accuracy calibration-free blood pressure estimation using pulse transit time," *Annals of Pure & Applied Logic*, vol. 63, no. 3, pp. 271–281, 2015.
- [16] D. Liu, M. Görges, and S. A. Jenkins, "University of Queensland vital signs dataset," *Anesthesia Analgesia*, vol. 114, no. 3, pp. 584–589, 2012.
- [17] Y. Liang, Z. Chen, G. Liu, and M. Elgendi, "A new, short-recorded photoplethysmogram dataset for blood pressure monitoring in China," *Scientific Data*, vol. 5, no. 1, pp. 180020–180027, 2018.
- [18] N. Aguirre, E. Grall-Maës, L. J. Cymberknop, and R. L. Armentano, "Blood pressure morphology assessment from photoplethysmogram and demographic information using deep learning with attention mechanism," *Sensors*, vol. 21, no. 6, p. 2167, 2021.
- [19] A. Ghosh, T. Chatterjee, and S. Sarkar, "Introduction of boosting algorithms in continuous non-invasive cuff-less blood pressure estimation using pulse arrival time," in *2021 43rd Annual International Conference of the IEEE Engineering in Medicine & Biology Society (EMBC)*, pp. 5429–5432, Mexico, 2021.
- [20] A. Tiloca, G. Pagana, and D. Demarchi, "A random tree based algorithm for blood pressure estimation," in *IEEE MTT-S International Microwave Biomedical Conference (IMBioC)*, Toulouse, France, 2020.
- [21] G. Slapničar, N. Mlakar, and M. Luštrek, "Blood pressure estimation from photoplethysmogram using a spectro-temporal deep neural network," *Sensors*, vol. 19, no. 15, p. 3420, 2019.
- [22] G. Slapničar and M. Luštrek, "Blood pressure estimation with a wristband optical sensor," in *ACM International Joint Conference on Pervasive and Ubiquitous Computing/ACM International Symposium on Wearable Computers (UbiComp/ISWC)*, pp. 758–761, Singapore, 2018.
- [23] C. El-Hajj and P. A. Kyriacou, "Cuffless blood pressure estimation from PPG signals and its derivatives using deep learning models," *Biomedical Signal Processing and Control*, vol. 70, no. 2021, article 102984, 2021.
- [24] Y. H. Li, L. N. Harfiya, K. Purwandari, and Y. D. Lin, "Real-time cuffless continuous blood pressure estimation using deep learning model," *Sensors*, vol. 20, no. 19, p. 5606, 2020.
- [25] N. Hasanzadeh, M. M. Ahmadi, and H. Mohammadzade, "Blood pressure estimation using photoplethysmogram signal and its morphological features," *IEEE Sensors Journal*, vol. 20, no. 8, pp. 4300–4310, 2020.
- [26] C. El-Hajj and P. A. Kyriacou, "Recurrent neural network models for blood pressure monitoring using PPG morphological features," in *2021 43rd Annual International Conference of the IEEE Engineering in Medicine & Biology Society (EMBC)*, pp. 1865–1868, Mexico, 2021.
- [27] Z. Li and W. He, "A continuous blood pressure estimation method using Photoplethysmography by GRNN-based model," *Sensors*, vol. 21, no. 21, p. 7207, 2021.
- [28] C. El-Hajj and P. A. Kyriacou, "Deep learning models for cuffless blood pressure monitoring from PPG signals using attention mechanism," *Biomedical Signal Processing and Control*, vol. 65, no. 9455, article 102301, 2021.
- [29] F. Shirbani, C. Blackmore, C. Kazzi, I. Tan, M. Butlin, and A. P. Avolio, "Sensitivity of video-based pulse arrival time to dynamic blood pressure changes," in *40th Annual International Conference of the IEEE Engineering in Medicine and Biology Society (EMBC)*, pp. 3639–3641, Hawaii, USA, 2018.
- [30] J. H. Moon, M. K. Kang, C. E. Choi, J. Min, H. Y. Lee, and S. Lim, "Validation of a wearable cuff-less wristwatch-type blood pressure monitoring device," *Scientific Reports*, vol. 10, no. 1, article 19015, 2020.
- [31] J. Leitner, P. H. Chian, and S. Dey, "Personalized blood pressure estimation using photoplethysmography: a transfer learning approach," *IEEE Journal of Biomedical Health Informatics*, vol. 26, no. 1, pp. 218–228, 2022.
- [32] G. Lovisotto, H. Turner, S. Eberz, and I. Martinovic, "Seeing Red: PPG Biometrics Using Smartphone Cameras," in *IEEE/CVF Conference on Computer Vision and Pattern Recognition (CVPR)*, pp. 3565–3574, Washington, USA, 2020.
- [33] C. Han, M. Gu, F. Yu, R. Huang, X. Huang, and L. Cui, "Calibration-free blood pressure assessment using an integrated deep learning method," in *International Conference on Bioinformatics and Biomedicine (Virtual Conference)*, pp. 1001–1005, Seoul, Korea (South), 2020.
- [34] H. Tjahjadi, K. Ramli, and H. Murfi, "Noninvasive classification of blood pressure based on photoplethysmography signals using bidirectional long short-term memory and time-

- frequency analysis," *IEEE Access*, vol. 8, pp. 20735–20748, 2020.
- [35] T. Athaya and S. Choi, "An estimation method of continuous non-invasive arterial blood pressure waveform using photoplethysmography: a u-net architecture-based approach," *Sensors*, vol. 21, no. 5, 2021.
- [36] T. Young, "III. An essay on the cohesion of fluids," *Proceedings of the Royal Society of London*, vol. 95, pp. 65–87, 1805.
- [37] O. Viunytyskiy, V. Shulgin, V. Sharonov, and A. Totsky, "Non-invasive cuffless measurement of blood pressure based on machine learning," in *International Conference on Advanced Trends in Radioelectronics, Telecommunications and Computer Engineering (TCSET)*, pp. 203–206, Lviv-Slavske, Ukraine, 2020.
- [38] R. Lazazzera, Y. Belhaj, and G. Carrault, "A new wearable device for blood pressure estimation using photoplethysmogram," *Sensors*, vol. 19, no. 11, 2019.
- [39] S. C. Kim and S. H. Cho, "Blood pressure estimation algorithm based on photoplethysmography pulse analyses," *Applied Sciences*, vol. 10, no. 12, 2020.
- [40] R. Byfield, M. Miller, J. Miles, G. Guidoboni, and J. Lin, "Towards robust blood pressure estimation from pulse wave velocity measured by photoplethysmography sensors," *IEEE Sensors Journal*, vol. 22, no. 3, pp. 2475–2483, 2022.
- [41] F. Tabei, J. M. Gresham, B. Askarian, K. Jung, and J. W. Chong, "Cuff-less blood pressure monitoring system using smartphones," *IEEE Access*, vol. 8, pp. 11534–11545, 2020.
- [42] D. Marzorati, D. Bovio, C. Salito, L. Mainardi, and P. Cerveri, "Chest wearable apparatus for cuffless continuous blood pressure measurements based on ppg and pcg signals," *IEEE Access*, vol. 8, pp. 55424–55437, 2020.
- [43] T. H. Huynh, R. Jafari, and W. Y. Chung, "Noninvasive cuffless blood pressure estimation using pulse transit time and impedance plethysmography," *IEEE Transactions on Biomedical Engineering*, vol. 66, no. 4, pp. 967–976, 2019.
- [44] P. Yousefian, S. Shin, A. Mousavi et al., "The potential of wearable limb ballistocardiogram in blood pressure monitoring via pulse transit time," *Scientific Reports*, vol. 9, no. 1, article 10666, 2019.
- [45] X. F. Teng and Y. T. Zhang, "Continuous and noninvasive estimation of arterial blood pressure using a photoplethysmographic approach," in *25th Annual Inter. Conf. of the IEEE Engineering in Medicine and Biology Society*, pp. 3153–3156, Cancun, Mexico, 2003.
- [46] Y. Yoon and G. Yoon, "Nonconstrained blood pressure measurement by photoplethysmography," *Journal of the Optical Society of Korea*, vol. 10, no. 2, pp. 91–95, 2006.
- [47] W. B. Murray and P. A. Foster, "The peripheral pulse wave: information overlooked," *Journal of Clinical Monitoring*, vol. 12, no. 5, pp. 365–377, 1996.
- [48] A. A. Awad, A. S. Haddadin, H. Tantawy et al., "The relationship between the photoplethysmographic waveform and systemic vascular resistance," *Journal of Clinical Monitoring & Computing*, vol. 21, no. 6, pp. 365–372, 2007.
- [49] I. Sharifi, S. Goudarzi, and M. B. Khodabakhshi, "A novel dynamical approach in continuous cuffless blood pressure estimation based on ECG and PPG signals," *Artificial Intelligence in Medicine*, vol. 97, pp. 143–151, 2019.
- [50] V. Ouyang, B. Ma, N. Pignatelli et al., "The use of multi-site photoplethysmography (PPG) as a screening tool for coronary arterial disease and atherosclerosis," *Physiological Measurement*, vol. 42, no. 6, article 064006, 2021.
- [51] W. Wu, L. Yang, S. Zhang et al., "Development of a new characteristic parameter - waveform index of finger blood volume pulse," *Computer Assisted Surgery*, vol. 21, no. sup1, pp. 6–10, 2016.
- [52] K. Takazawa, N. Tanaka, M. Fujita et al., "Assessment of vasoactive agents and vascular aging by the second derivative of photoplethysmogram waveform," *Hypertension*, vol. 32, no. 2, pp. 365–370, 1998.
- [53] D. C. K. Soh, E. Y. K. Ng, V. Jahmunah, S. L. Oh, T. R. San, and U. R. Acharya, "A computational intelligence tool for the detection of hypertension using empirical mode decomposition," *Computers in Biology and Medicine*, vol. 118, article 103630, 2020.
- [54] L. Breiman, "Random forests," *Machine Learning*, vol. 45, no. 1, pp. 5–32, 2001.
- [55] G. Thambiraj, U. Gandhi, U. Mangalanathan, V. J. M. Jose, and M. Anand, "Investigation on the effect of Womersley number, ECG and PPG features for cuff less blood pressure estimation using machine learning," *Biomedical Signal Processing and Control*, vol. 60, article 101942, 2020.
- [56] Z. Liu, B. Zhou, Y. Li, M. Tang, and F. Miao, "Continuous blood pressure estimation from electrocardiogram and photoplethysmogram during arrhythmias," *Frontiers in Physiology*, vol. 11, article 575407, 2020.
- [57] S. G. Khalid, J. Zhang, F. Chen, and D. Zheng, "Blood pressure estimation using photoplethysmography only: comparison between different machine learning approaches," *Journal of Healthcare Engineering*, vol. 2018, Article ID 1548647, 13 pages, 2018.
- [58] S. G. Khalid, H. Liu, T. Zia, J. Zhang, F. Chen, and D. Zheng, "Cuffless blood pressure estimation using single channel photoplethysmography: a two-step method," *IEEE Access*, vol. 8, pp. 58146–58154, 2020.
- [59] A. Farki, R. B. Kazemzadeh, and E. A. Noughabi, "A novel clustering-based algorithm for continuous and noninvasive cuff-less blood pressure estimation," *Journal of Healthcare Engineering*, vol. 2022, Article ID 3549238, 13 pages, 2022.
- [60] S. Haddad, A. Boukhayma, and A. Caizzone, "Continuous PPG-based blood pressure monitoring using multi-linear regression," *IEEE Journal of Biomedical Health Informatics*, vol. 26, no. 5, pp. 2096–2105, 2022.
- [61] B. Manamperi and C. Chitraranjan, "A robust neural network-based method to estimate arterial blood pressure using photoplethysmography," in *International Conference on Bioinformatics and Bioengineering (BIBE)*, pp. 681–685, Athens, Greece, 2019.
- [62] A. Attarpour, A. Mahnam, A. Aminitabar, and H. Samani, "Cuff-less continuous measurement of blood pressure using wrist and fingertip photo-plethysmograms: evaluation and feature analysis," *Biomedical Signal Processing and Control*, vol. 49, pp. 212–220, 2019.
- [63] A. Chakraborty, D. Sadhukhan, S. Pal, and M. Mitra, "PPG-BASED automated estimation of blood pressure using patient-specific neural network modeling," *Journal of Mechanics in Medicine and Biology*, vol. 20, no. 6, article 2050037, 2020.
- [64] S. Yang, W. S. W. Zaki, S. P. Morgan, S. Y. Cho, R. Correia, and Y. Zhang, "Blood pressure estimation with complexity features from electrocardiogram and photoplethysmogram signals," *Optical and Quantum Electronics*, vol. 52, no. 3, pp. 135–150, 2020.



- [65] S. Chen, Z. Ji, H. Wu, and Y. Xu, "A non-invasive continuous blood pressure estimation approach based on machine learning," *Sensors*, vol. 19, no. 11, 2019.
- [66] X. Tan, Z. Ji, and Y. Zhang, "Non-invasive continuous blood pressure measurement based on mean impact value method, BP neural network, and genetic algorithm," *Technology and Health Care*, vol. 26, Supplement1, pp. 87–101, 2018.
- [67] M. H. Chowdhury, M. N. I. Shuzan, M. E. H. Chowdhury et al., "Estimating blood pressure from the photoplethysmogram signal and demographic features using machine learning techniques," *Sensors*, vol. 20, no. 11, 2020.
- [68] J. Dey, A. Gaurav, and V. N. Tiwari, "InstaBP: cuff-less blood pressure monitoring on smartphone using single PPG sensor," in *Annu Int Conf IEEE Eng Med Biol Soc*, pp. 5002–5005, Hawaii, USA, 2018.
- [69] C. El-Hajj and P. A. Kyriacou, "Cuffless and continuous blood pressure estimation from ppg signals using recurrent neural networks," in *Annual International Conference of the IEEE Engineering in Medicine & Biology Society (EMBC)*, pp. 4269–4272, Montreal, Canada, 2020.
- [70] U. Senturk, K. Polat, and I. Yucedag, "A non-invasive continuous cuffless blood pressure estimation using dynamic recurrent neural networks," *Applied Acoustics*, vol. 170, article 107534, 2020.
- [71] Q. Yousef, M. B. I. Reaz, and M. A. M. Ali, "The analysis of PPG morphology: investigating the effects of aging on arterial compliance," *Measurement Science Review*, vol. 12, no. 6, pp. 266–271, 2012.
- [72] A. Tazarv and M. Levorato, "A deep learning approach to predict blood pressure from ppg signals," in *2021 43rd Annual International Conference of the IEEE Engineering in Medicine & Biology Society (EMBC)*, pp. 5658–5662, Mexico, 2021.
- [73] H. Mou and J. Yu, "CNN-LSTM prediction method for blood pressure based on pulse wave," *Electronics*, vol. 10, no. 14, 2021.
- [74] J. Esmalpoor, M. H. Moradi, and A. Kakhodamohammadi, "A multistage deep neural network model for blood pressure estimation using photoplethysmogram signals," *Computer in Biology and Medicine*, vol. 120, article 103719, 2020.
- [75] S. Baker, W. Xiang, and I. Atkinson, "A hybrid neural network for continuous and non-invasive estimation of blood pressure from raw electrocardiogram and photoplethysmogram waveforms," *Computer Methods and Programs in Biomedicine*, vol. 207, article 106191, 2021.
- [76] M. S. Tanveer and M. K. Hasan, "Cuffless blood pressure estimation from electrocardiogram and photoplethysmogram using waveform based ANN-LSTM network," *Biomedical Signal Processing and Control*, vol. 51, pp. 382–392, 2019.
- [77] Y. Qiu, D. D. Liu, G. Y. Yang et al., "Cuffless blood pressure estimation based on composite neural network and graphics information," *Biomedical Signal Processing and Control*, vol. 70, article 103001, 2021.
- [78] C. C. Chuang, C. C. Lee, C. H. Yeng, E. C. So, and Y. J. Chen, "Attention mechanism-based convolutional long short-term memory neural networks to electrocardiogram-based blood pressure estimation," *Applied Sciences*, vol. 11, no. 24, article 12019, 2021.
- [79] K. M. He, X. Y. Zhang, S. Q. Ren, and J. Sun, "Deep Residual Learning for Image Recognition," in *2016 IEEE Conference on Computer Vision and Pattern Recognition (CVPR)*, pp. 770–778, Las Vegas, NV, USA, 2016.
- [80] F. Schruppf, P. Frenzel, C. Aust, G. Osterhoff, and M. Fuchs, "Assessment of non-invasive blood pressure prediction from ppg and rPPG signals using deep learning," *Sensors*, vol. 21, no. 18, 2021.
- [81] A. Paviglianiti, V. Randazzo, S. Villata, G. Cirrincione, and E. Pasero, "A comparison of deep learning techniques for arterial blood pressure prediction," *Cognitive Computation*, vol. 27, pp. 1–22, 2021.
- [82] W. Wang, P. Mohseni, K. L. Kilgore, and L. Najafzadeh, "Cuffless blood pressure estimation from photoplethysmography via visibility graph and transfer learning," *IEEE Journal of Biomedical and Health Informatics*, vol. 26, no. 5, pp. 2075–2085, 2022.
- [83] T. Treebupachatsakul, A. Boosamalee, S. Shinnakerdchoke, S. Pechprasarn, and N. Thongpance, "Cuff-less blood pressure prediction from ecg and ppg signals using Fourier transformation and amplitude randomization preprocessing for context aggregation network training," *Biosensors*, vol. 12, no. 3, pp. 159–179, 2022.
- [84] M. Sadrawi, Y. T. Lin, C. H. Lin et al., "Genetic deep convolutional autoencoder applied for generative continuous arterial blood pressure via photoplethysmography," *Sensors*, vol. 20, no. 14, 2020.
- [85] E. Brophy, M. De Vos, G. Boylan, and T. Ward, "Estimation of continuous blood pressure from PPG via a federated learning approach," *Sensors*, vol. 21, no. 18, 2021.
- [86] M. Panwar, A. Gautam, D. Biswas, and A. Acharyya, "PP-Net: a deep learning framework for PPG-based blood pressure and heart rate estimation," *IEEE Sensors Journal*, vol. 20, no. 17, pp. 10000–10011, 2020.
- [87] C. T. Yen and C. H. Liao, "Blood pressure and heart rate measurements using photoplethysmography with modified LRCN," *CMC-Computers Materials & Continua*, vol. 71, no. 1, pp. 1973–1986, 2022.
- [88] S. Haddad, A. Boukhayma, G. Di Pietrantonio, A. Barison, G. de Preux, and A. Caizzone, "Photoplethysmography based blood pressure monitoring using the senbiosys ring," in *2021 43rd Annual International Conference of the IEEE Engineering in Medicine & Biology Society (EMBC)*, pp. 1609–1612, Mexico, 2021.
- [89] F. Bousefsaf, D. Djeldjli, Y. Ouzar, C. Maaoui, and A. Pruski, "iPPG 2 cPPG: reconstructing contact from imaging photoplethysmographic signals using U-Net architectures," *Computer in Biology Medicine*, vol. 138, article 104860, 2021.
- [90] D. Djeldjli, F. Bousefsaf, C. Maaoui, F. Bereksi-Reguig, and A. Pruski, "Remote estimation of pulse wave features related to arterial stiffness and blood pressure using a camera," *Biomedical Signal Processing and Control*, vol. 64, article 102242, 2021.
- [91] M. Rong and K. Li, "A blood pressure prediction method based on imaging photoplethysmography in combination with machine learning," *Biomedical Signal Processing and Control*, vol. 64, article 102328, 2021.
- [92] S. Baek, J. Jang, and S. Yoon, "End-to-end blood pressure prediction via fully convolutional networks," *IEEE Access*, vol. 7, pp. 185458–185468, 2019.
- [93] O. Schlesinger, N. Vigderhouse, Y. Moshe, and D. Eytan, "Estimation and tracking of blood pressure using routinely acquired photoplethysmographic signals and deep neural networks," *Critical Care Explorations*, vol. 2, no. 4, article e0095, 2020.
- [94] L. Wang, W. Zhou, Y. Xing, and X. Zhou, "A novel neural network model for blood pressure estimation using photoplethysmography without electrocardiogram," *Journal of Healthcare Engineering*, vol. 2018, Article ID 7804243, 9 pages, 2018.

## *Retraction*

# **Retracted: Cell-in-Cell: From Cell Biology to Translational Medicine**

### **BioMed Research International**

Received 12 March 2024; Accepted 12 March 2024; Published 20 March 2024

Copyright © 2024 BioMed Research International. This is an open access article distributed under the Creative Commons Attribution License, which permits unrestricted use, distribution, and reproduction in any medium, provided the original work is properly cited.

This article has been retracted by Hindawi following an investigation undertaken by the publisher [1]. This investigation has uncovered evidence of one or more of the following indicators of systematic manipulation of the publication process:

- (1) Discrepancies in scope
- (2) Discrepancies in the description of the research reported
- (3) Discrepancies between the availability of data and the research described
- (4) Inappropriate citations
- (5) Incoherent, meaningless and/or irrelevant content included in the article
- (6) Manipulated or compromised peer review

The presence of these indicators undermines our confidence in the integrity of the article's content and we cannot, therefore, vouch for its reliability. Please note that this notice is intended solely to alert readers that the content of this article is unreliable. We have not investigated whether authors were aware of or involved in the systematic manipulation of the publication process.

Wiley and Hindawi regrets that the usual quality checks did not identify these issues before publication and have since put additional measures in place to safeguard research integrity.

We wish to credit our own Research Integrity and Research Publishing teams and anonymous and named external researchers and research integrity experts for contributing to this investigation.

The corresponding author, as the representative of all authors, has been given the opportunity to register their agreement or disagreement to this retraction. We have kept a record of any response received.

### **References**

- [1] Q. Chen, X. Wang, and M. He, "Cell-in-Cell: From Cell Biology to Translational Medicine," *BioMed Research International*, vol. 2022, Article ID 7608521, 7 pages, 2022.

## Review Article

# Cell-in-Cell: From Cell Biology to Translational Medicine

Qiao Chen,<sup>1</sup> Xiaoning Wang<sup>2</sup>,<sup>3</sup> and Meifang He<sup>3</sup>

<sup>1</sup>Department of Nutrition, Third Medical Center of PLA General Hospital, Beijing, China

<sup>2</sup>National Clinic Center of Geriatric & the State Key Laboratory of Kidney, The Chinese PLA General Hospital, Beijing, China

<sup>3</sup>Department of General Surgery, The First Affiliated Hospital, Sun Yat-sen University, Guangzhou, China

Correspondence should be addressed to Xiaoning Wang; [xnwang88@163.com](mailto:xnwang88@163.com) and Meifang He; [hemeifang@mail.sysu.edu.cn](mailto:hemeifang@mail.sysu.edu.cn)

Received 23 May 2022; Revised 26 July 2022; Accepted 21 August 2022; Published 14 September 2022

Academic Editor: Nikhil Agrawal

Copyright © 2022 Qiao Chen et al. This is an open access article distributed under the Creative Commons Attribution License, which permits unrestricted use, distribution, and reproduction in any medium, provided the original work is properly cited.

Cell-in-cell structures (CICs) refer to cytoplasmic internalization of a cell by another cell, which are found throughout various biological systems and have been a part of scientific dogma for a long time. However, neither the mechanisms underlying this phenomenon nor their possible roles in disease development have resulted in major breakthroughs until recent years. In view of the ubiquity of CICs in inflammatory tissue and tumors, it is tempting to think that these specific structures could be associated with clinical diagnosis and treatment and thus would become a new hotspot for translational medicine. Translational medicine is a new concept in the field of international biomedical research that appeared in the last 20 years, which transforms basic research into clinical application. With the growing interest in this field, this review addresses recent research on CICs and their potential clinical implications in cytomorphological diagnosis and the pathology of human diseases, while discussing as yet unanswered questions. We also put forward future directions to reduce the gap in our knowledge caused by our currently limited understanding of CICs.

## 1. Introduction

Cell-in-cell structures (CICs), characterized by one or more live cells (referred to as effector cells) internalized into another cells (referred to as host cells), have been considered simple physiological or pathological phenomena without extensive biological significance. For decades, researchers mainly emphasized morphological descriptions and observed CICs by microscopy in a wide range of cell types and tissues, both *in vivo* and *in vitro*. In general, CICs commonly occur at a rate of 0.3–2.5% of the total sample population in a wide range of carcinomas, while surprisingly, in some cases, CIC formation is as high as ~6% in heterogeneous breast cancer tissue in a patient with poor prognosis [1, 2]. Currently, CICs are attracting increasing attention because of their correlation with various physiological and pathological conditions, their involvement in inflammation and carcinoma initiation and progression, and their potential implications in translational medicine. CICs occur universally in diverse tissues; therefore, establishing how the functional status of CICs influences diseases and

treatment response is important. Efforts to explore the clinicopathological correlates of CICs in patients will provide new approaches to disease treatment and prevention. For the purposes of discussion, CICs will be divided into two basic types: homotypic CICs, in which both of the effector and host cells are the same cell type, and heterotypic CICs, in which the effector cell is internalized into a host of a different cell type. Notably, important breakthroughs have been made the possible mechanisms and potential significance of CICs, including homotypic CICs, referred to as entosis, and heterotypic CICs, referred to as emperipolesis, which have clinical and potential therapeutic applications.

## 2. Homotypic CIC Formation and Its Biological Significance

The molecular mechanisms and core elements underlying the formation of homotypic CICs has been reviewed recently [3]. Homotypic CIC formation is induced in response to any of the following stimuli: low energy states by glucose withdrawal [4], aberrant shape regulation of invading cells in

mitosis [5, 6], and detachment of effector cells from the extracellular matrix [7]. Subsequently, CIC invasion is regulated genetically by three core machineries, including intact adherens junctions (AJs), imbalance of contractile actomyosin (CA) of invading cells, and the mechanical ring (MR) between the peripheries of invading and engulfing cells [3]. Cells activated the phosphorylation of myosin light chain (MLC2) and diaphanous-related formin1 (mDia1) with higher RhoA activity, thereby producing biophysical forces that drive penetration, representing an intriguing and distinctive form of phagocytosis [8, 9]. At the interface between the two cells, E-cadherin-mediated AJs interact with F-actin through  $\alpha$ -catenin,  $\beta$ -catenin, and vinculin and form a ring-like structure termed the mechanical ring, which is involved in homotypic CIC formation [10, 11] (Figure 1).

Following entry into the cytoplasm of the host cell, there are several possible fates for the internalized cell. It might persist as a live cell and even undergo cell division while still internalized [7, 12]. However, the most common fate for the internalized cells is lysosomal cell death. Recently, Overholzer et al. defined a nonapoptotic cell death program mediated by CIC process, entosis, in which suspended epithelial cells actively invasive and the cells die inside their neighboring host cell [7]. Entosis is involved in the linker cell clearance in *Caenorhabditis elegans* and in luminal epithelial cell elimination in embryo implantation, suggesting that entosis is an ancient process to regulate key events required for embryonic development [13, 14]. Entosis occurs from bacteria to mammals, it indicates that entotic process is conserved across evolution. Consistent with this model, entosis contributes to cell competition in *Drosophila* by controlling the process by which “fit” cells eliminate their less fit neighbors and can also mediate cell completion in tumor cells [15]. Cell competition mediated by entosis plays both promotive and suppressive roles in tumors. “Winner” cells (hosts) use entosis as a mechanism of cell competition to kill “loser” cells (engulfed cells) and become clonally dominant in a heterogeneous population, suggesting that entosis for cell competition contributes to clonal selection in tumor evolution [16, 17]. Moreover, nutrients, such as amino acid and glucose, are provided following engulfed cell death and degradation, which promotes the survival of the host cell under starvation conditions [18]. Strikingly, host cells not only benefit from the nutrients released by the engulfed cells but also experience multinucleation because of the steric interference by the engulfed cells, propagating genomic instability and thereby driving tumor progression [19]. In addition, host cells with mutated p53 often survive following abnormal mitotic events, which indicates that mutated p53 is associated with CIC’s contribution to genomic instability for tumor progression [20]. Nevertheless, entosis inhibits tumorigenesis by eliminating cells detached from the extracellular matrix [7]. Further research supports this view that host cells engulf cells with aberrant mitosis as a tumor-suppressive act of “assisted suicide,” indicating entosis as an antitumorigenic effect in cancer [5]. A recent study indicated that in a nontumor context, aneuploid daughter cells during the entotic process are engulfed and eliminated by host cells, thus playing a surveillance role in the mainte-

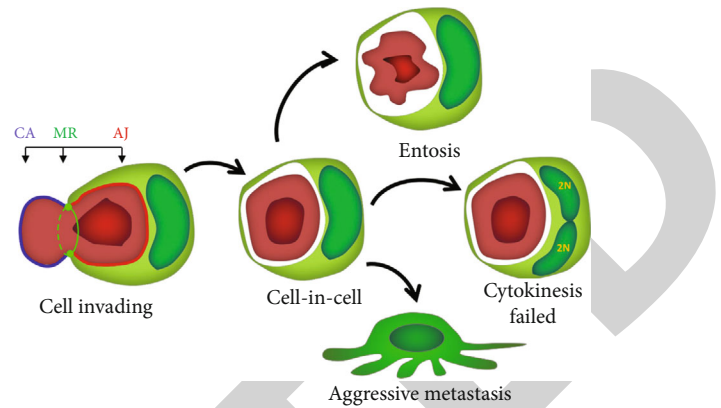


FIGURE 1: The mechanisms and its biological significance of homotypic CICs. Homotypic CICs are formed by three core machineries, including intact adherens junctions (AJs), imbalance of contractile actomyosin (CA) of invading cells, and the mechanical ring (MR). Homotypic CICs play important roles in tumor evolution, genomic instability, and tumor aggressive.

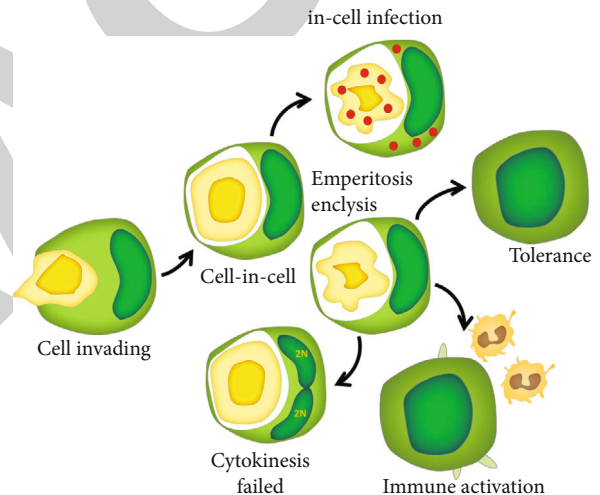


FIGURE 2: The role of heterotypic CICs in different aspects of biology. Heterotypic CICs are involved in physiological and pathological process such as virus infection, immune regulation, and tumor immune escape.

nance of genome integrity [6]. Therefore, identifying and characterizing the mechanisms of entosis in different cellular and molecular contexts would be helpful to further understand its biological effects in physiological and pathological processes.

### 3. Heterotypic CICs Correlate with Clinic Implications

The formation of heterotypic CICs, emperipolysis, refers to lymphocytes being internalized into tumor cells, which plays pivotal roles in multiple biological processes such as homeostasis and tumor immune escape. The concept of emperipolysis includes different CIC models, such as cannibalism [21], emperitosis [22], and enclysis [23] (Figure 2). Studies by Lugini et al.’s group observed that melanoma cell lines

derived from metastatic lesions, rather than primary tumors, hosted CICs via cannibalism. It has been shown that metastatic tumor cells cannibalize their siblings, and even immune cells, under starvation conditions [21, 24]. These cannibalistic properties provide them with a survival advantage via immune escape. Consistent with CICs contributing to tumor immune escape, research on emperitosis demonstrated that noncytotoxic effector cells exhibit entotic cell death as tumor cells die inside their neighbors, while only cytotoxic effector cells inside undergo apoptotic death because of the reuptake of their own secreted granzyme B. Granzyme B is the cytotoxic granule secreted by cytotoxic T lymphocytes (CTL) and natural killer cells (NK) during elimination of tumor cells and can induce apoptosis [25]. Further investigation showed that a rapid bubbling of the wrapped vacuole led to the reuptake of autologous granzyme B by effector cytotoxic cells rather than being released into the cytoplasm of the host cell to kill the engulfed effector cells. If vacuole formation was impaired, the host cells rather than engulfed cells can die [22, 26]. It was suggested that the vacuole might be a key point for biotherapy because inhibiting vacuole bubbling could induce suicide inside to kill the host cells as a Trojan horse effect, resulting in enhanced killing efficiency from both outside and inside [22]. In contrast, Su et al. reported that heterotypic CICs mediate in-cell killing by the penetration of NK cells into tumor cells, resulting in the death of the host tumor cells other than the NK cells [27]. Indeed, the well-known membrane protein, CD44, negatively regulates of CIC formation [27]. Therefore, considering that CD44 is associated with oncogenic phenotypes, targeting CD44 as a novel therapeutic strategy might be an effective way to enhance CIC formation, immune response, and tumor suppression [28]. In addition to the impact on tumor immunization, heterotypic CICs are also involved in the autoimmune response. Benseler et al. observed that after the adoptive transfer of naïve autoreactive CD8<sup>+</sup> T cells, these cells were rapidly eliminated in the liver rather than causing the development of immune-mediated pathology. Further investigation showed normal hepatocytes enclosing the CD8<sup>+</sup> T cells in their cytoplasm, which were degraded in lysosomes via suicidal emperipolesis, contributing to the maintenance of tolerance in mice [29]. CICs also have an important physiological function in regulating homeostasis in the liver. Recently, Li and Baker discovered that hepatocytes could engulf and degrade regulatory CD4<sup>+</sup> T cells (regulatory T cells, Tregs) but not CD8<sup>+</sup> T cells or B cells via enclysis [15]. Distinct from entosis, in enclysis, intercellular adhesion molecule 1 (ICAM-1) is involved in T cell invasion and membrane lamellipodia or blebs by hepatocytes mediate T cell engulfment. Treg cells suppress immune effector function: therefore, enclysis, as a natural process in liver immune regulation, might be targeted therapeutically in combination with Treg therapeutic strategies [23]. Autoimmune hepatitis (AIH), as well as other autoimmune conditions such as transplantation, inhibits enclysis to increase the number of Tregs in the liver, which might be useful to dampen overactive immune responses. Conversely, the liver needs to mount active antiviral and antitumor immune responses, in which enhancing enclysis to delete Tregs might be effective for viral

clearance and tumor elimination. Considering that enclysis is a potentially specific target of immune regulation in the liver, it is important to elucidate the mechanisms by which “on/off switch” molecules regulate enclysis formation and which drugs could modulate enclysis in further research [30, 31].

#### 4. Cell-in-Cell Introduces Translational Medicine

As mentioned above, CIC formation is a natural process involved in various physiological and pathological processes, and research on CICs has provided some clues for translational medicine. Firstly, a large number of clinical studies indicate that the quantity or quality of CICs might be regarded as a marker of biological treatment prognosis. In breast cancer, homotypic CICs more often occurred in high-grade carcinomas, which generally exhibit rapid progression and decreased overall patient survival compared with low-grade carcinomas [32, 33]. Meanwhile, homotypic CICs were observed to be a favorable factor for the prognosis of breast cancer [33], which was consistent with entotic CIC formation contributing to tumor-suppressive function in breast cancer [7]. In contrast, homotypic CICs are common in malignant cases of bladder cancer, whereas a lack of CICs are observed in benign conditions; therefore, the presence of CICs is a dependable feature of malignancy in urine and effusions to distinguish malignant from benign lesions based on cytological examination [34]. Similar conclusions were obtained for CICs as a predictor of poor prognosis in different carcinomas, such as head and neck squamous cell carcinoma (HNSCC), lung cancer, and rectal cancer [20, 35, 36]. Therefore, homotypic CICs in different types of tumors can impact patient outcomes differently or even oppositely.

Meanwhile, several recent approaches were employed to improve heterotypic CICs as markers of poor prognosis in different types of carcinomas. In a multicenter retrospective study, researchers demonstrated that heterotypic CICs were valuable prognostic markers to predict the survival of patients with pancreatic ductal adenocarcinoma (PDAC). In particular, a heterotypic CIC pattern of lymphocytes/macrophages inside tumor cells (L/MiT) was identified as a potent adverse prognostic marker impacting young female patients with early-stage PDAC [37]. Alternatively, homotypic CICs correlate with aggressive biology and are regarded as an independent prognostic factor in PDAC [38]. These findings not only validated prior reports that CICs contribute to tumor progression but also suggested that CICs might be regarded as a feature of malignant cells for practical diagnostic pathology. Similarly, research on neutrophils and tumor cells forming CICs in buccal mucosa squamous cell carcinoma (BMSCC) suggested that CICs are negatively associated with both the recurrence-free survival (RFS) and disease-specific survival (DSS) of patients [39]. The roles of CIC subtypes in the diagnosis, treatment, and prognosis of many types of cancers are summarized in Table 1. These findings demonstrate a pathogenetic role for CICs in human pathology and indicate that this cellular characteristic is a novel pharmacological target in the clinical management of

TABLE 1: Cell-in-cell (CIC) in different clinical studies.

Disease	Target cell	Effector cell	Significance	Reference
Primary biliary cholangitis (PBC)	Biliary epithelial cell	CD8 <sup>+</sup> T cells	Emperipolesis aggravates the further injury of interlobular bile ducts.	[41]
Chronic hepatitis B (CHB)	Hepatocytes	CD8 <sup>+</sup> T cells	Emperipolesis is an indicator of active liver inflammation.	[42]
Autoimmune hepatitis (AIH)	Hepatocytes	CD8 <sup>+</sup> T cells	Emperipolesis a characteristic feature of AIH.	[44]
Pancreatic ductal adenocarcinoma (PDAC)	Pancreatic ductal cells	Lymphocytes/macrophages	Lymphocytes/macrophages inside tumor cells (L/MiT) as an adverse prognostic predictor for young patients with resectable PDAC.	[37]
PDAC	Pancreatic ductal cells	Pancreatic ductal cells	Entotic-CICs are an independent prognostic factor in PDAC.	[38]
Head and neck squamous cell carcinoma (HNSCC)	Head and neck squamous cells	Head and neck squamous cells	CICs associated with poor survival rates in HNSCC.	[35, 36]
Lung carcinoma	Lung cancer cells	Lung cancer cells	CICs is a poor prognostic facto in lung cancer.	[20]
Rectal cancer	Rectal cancer cells	Rectal cancer cells	CIC is a poor prognostic facto in rectal cancer.	[36]
Buccal mucosa squamous cell carcinoma	Buccal mucosa squamous cells	Neutrophils	Heterotypic neutrophil-in-tumor structure (FNiT) as a predictor is independently associated with relapse-free survival (RFS) and disease-specific survival (DSS).	[39]
Bladder cancer	Bladder cells	Bladder cells	Cannibalism is an important morphological feature to distinguish a benign from a malignant lesion.	[51]

tumors. Therefore, heterotypic CICs might serve as potential biomarkers to predict cancer therapy efficacy. Meanwhile, exploring CIC subtypes to predict the effect of treatment following surgery should be taken into account in future investigations.

Secondly, CICs are believed to be a potential histological hallmark associated with inflammation. It is well-established that inflammation is a key driver of hepatocellular carcinoma (HCC) tumorigenesis [40]. In primary biliary cholangitis (PBC), the attenuation of CICs formed by T cells and biliary epithelial cell leads to injury of the interlobular bile ducts [41]. In chronic hepatitis B, the presence of heterotypic CICs formed between CD8<sup>+</sup> T cell and hepatocytes is closely related with laboratory parameters such as HBV DNA load, accompanying the severity of liver injury [42, 43]. CD8<sup>+</sup> T cell invasion into hepatocytes was also increased in autoimmune hepatitis, which is associated with more severe necroinflammatory and fibrotic changes [44]. Thus, heterotypic CICs can serve as an indicator of active liver inflammation to mediate hepatocyte injury. There is also evidence for hepatic stellate cells (HSCs) engulfing and depleting natural killer (NK) cells by a CIC process, thus contributing to the progression of liver fibrogenesis [45]. Different stages of pathogenesis are linked to distinct signatures of cell-cell interactions, and the host cell could orchestrate highly complex immune responses via heterotypic CICs to regulate liver inflammation to fibrosis or even tumorigenesis.

Thirdly, CICs are regarded as a clinical feature of, and are involved in, the pathogenesis of infectious diseases. Recently, Zhang et al. discovered that CICs mediated lymphocyte elimination by severe acute respiratory syndrome coronavirus 2- (SARS-CoV-2-) induced syncytia, which contributes to lymphopenia and provides a potent target for COVID-19 therapy [46]. In addition to being involved

in lymphocyte clearance, CICs also play a certain role in virus infection of nonsusceptible epithelial cells, termed “in-cell infection.” In most cases, viruses infect tropic cells in a receptor-mediated manner [47]. However, Epstein-Barr virus (EBV) is well accepted to infect nonsusceptible epithelial cells by cell-to cell infection, by which EBV entries into epithelial cells through the conjugate formation between B cells and epithelial cells [48]. Of note, Ni et al. demonstrated that EBV could infect nonsusceptible nasopharyngeal epithelial cells (ECs) through the formation of CICs between epithelial cells and internalized B lymphocytes that are infected with EBV [49]. A similar method is also used for human immunodeficiency virus (HIV) transmission to nonsusceptible cells [50]. HIV is well known to specifically infect CD4<sup>+</sup> immune cells. However, CD4-negative cells such as colon epithelial cells were also found to contain HIV, suggesting the mechanism of the existence of CD4-independent virus spreading. The formation of heterotypic CICs leads to transmission of HIV from internalized CD4<sup>+</sup> T cells to the nonsusceptible epithelial cells. In these settings, CICs might be potential markers and targets for the prevention and treatment of virus infections in the clinic.

In summary, CICs could be a clinical target for the development of diagnostic, prognostic, and treatment strategies that could be used in clinical applications; however, several important issues need to be addressed in future investigations. Firstly, although previous studies shed light on the mechanisms and core elements of CIC formation, we lack information regarding “on/off switch” for CIC formation, the identification of which will help to develop methods for the accurate detection of CIC and their therapeutic target. Thus, the specific molecules to indicate CICs and related signaling pathways are worthy of further study and will provide measurable parameters for clinical evaluation. Secondly,

because of a lack of efficient and uniform standards, artificial counting is the main means of CIC detection in current research, which inhibits the further application of CICs as diagnosis markers in the clinic. It will be interesting to explore artificial intelligence (AI) for image recognition, which is an effective method used in high-throughput screening that might be considered for diagnostic strategies for CICs. Thirdly, it is necessary to explore new preparation methods of CICs from different clinical samples for diagnosis. Meanwhile, these methods, combined with high-throughput sequencing, might provide a new way to determine the pathogenesis of diseases associated with CICs.

## 5. Conclusion

For decades, CICs, referred to one or more intact cells internalized into another cell, have been overlooked. This stance has dramatically changed with the recognition of the involvement of CICs in physiological functions and malignant progression. In the present review, we outlined the mechanisms of homotypic/heterotypic CIC formation, their biological roles in the homeostasis and the development of diseases, and their potential utility in translational medicine, while recognizing yet unanswered questions. Three core machineries, including adherens junctions, contractile actomyosin, and the mechanical ring, have been identified in the formation of homotypic CICs. In addition, CICs play important roles under different physiological and pathological conditions, such as in embryonic development, homeostasis, tumor evolution, and tumor immune escape. Investigators have focused on identification of CICs as biomarkers and therapeutic targets for tumorigenesis, inflammation, and viral infection to explore their clinical implication. Specific detection markers, high-throughput detection methods, and standardized procedures for clinical samples should be studied in the future. Thus, further research on CICs might lead to a new branch of biotherapy and clinical prognosis research.

## Data Availability

The data supporting this review are from previously reported studies and datasets, which have been cited. The processed data are available from the corresponding author upon request.

## Conflicts of Interest

The authors declare that they have no conflicts of interest.

## Authors' Contributions

All authors made a significant contribution to the work reported, whether in the conception, design, execution, and interpretation, or in all these areas. All authors gave final approval of the version to be published, agreeing on the journal to which the article has been submitted, and confirmed their accountability for all aspects of the work.

## Acknowledgments

This work was supported by the National Natural Science Foundation of China (81972483), the Natural Science Foundation of Guangdong (2021A1515010127), and the Guangzhou Municipal Science and Technology Project (202102020028).

## References

- [1] J. Durgan and O. Florey, "Cancer cell cannibalism: multiple triggers emerge for entosis," *Biochimica et Biophysica Acta (BBA)-Molecular Cell Research*, vol. 1865, no. 6, pp. 831–841, 2018.
- [2] B. Ruan, Z. Niu, X. Jiang et al., "High frequency of cell-in-cell formation in heterogeneous human breast cancer tissue in a patient with poor prognosis: a case report and literature review," *Frontiers in Oncology*, vol. 9, pp. 1444–1444, 2019.
- [3] Z. Niu, M. He, and Q. Sun, "Molecular mechanisms underlying cell-in-cell formation: core machineries and beyond," *Journal of Molecular Cell Biology*, vol. 13, no. 5, pp. 329–334, 2021.
- [4] J. C. Hamann, A. Surcel, R. Chen et al., "Entosis is induced by glucose starvation," *Cell Reports*, vol. 20, no. 1, pp. 201–210, 2017.
- [5] J. Durgan, Y.-Y. Tseng, J. C. Hamann et al., "Mitosis can drive cell cannibalism through entosis," *eLife*, vol. 6, article e27134, 2017.
- [6] J. Liang, Z. Niu, B. Zhang et al., "p53-dependent elimination of aneuploid mitotic offspring by entosis," *Cell Death and Differentiation*, vol. 28, no. 2, pp. 799–813, 2021.
- [7] M. Overholtzer, A. A. Mailleux, G. Mouneimne et al., "A non-apoptotic cell death process, entosis, that occurs by cell-in-cell invasion," *Cell*, vol. 131, no. 5, pp. 966–979, 2007.
- [8] Q. Sun, E. S. Cibas, H. Huang, L. Hodgson, and M. Overholtzer, "Induction of entosis by epithelial cadherin expression," *Cell Research*, vol. 24, no. 11, pp. 1288–1298, 2014.
- [9] V. Purvanov, M. Holst, J. Khan, C. Baarlink, and R. Grosse, "G-protein-coupled receptor signaling and polarized actin dynamics drive cell-in-cell invasion," *Elife*, vol. 3, article e02786, 2014.
- [10] M. Wang, Z. Niu, H. Qin et al., "Mechanical ring interfaces between adherens junction and contractile actomyosin to coordinate entotic cell-in-cell formation," *Cell Reports*, vol. 32, no. 8, article 108071, 2020.
- [11] M. Wang, X. Ning, A. Chen et al., "Impaired formation of homotypic cell-in-cell structures in human tumor cells lacking alpha-catenin expression," *Scientific Reports*, vol. 5, no. 1, article 12223, 2015.
- [12] C. E. Cano, M. J. Sandi, T. Hamidi et al., "Homotypic cell cannibalism, a cell-death process regulated by the nuclear protein 1, opposes to metastasis in pancreatic cancer," *EMBO Molecular Medicine*, vol. 4, no. 9, pp. 964–979, 2012.
- [13] Y. Lee, J. C. Hamann, M. Pellegrino et al., "Entosis controls a developmental cell clearance in *C. elegans*," *Cell Reports*, vol. 26, no. 12, pp. 3212–3220.e4, 2019.
- [14] Y. Li, X. Sun, and S. K. Dey, "Entosis allows timely elimination of the luminal epithelial barrier for embryo implantation," *Cell Reports*, vol. 11, no. 3, pp. 358–365, 2015.
- [15] W. Li and N. E. Baker, "Engulfment is required for cell competition," *Cell*, vol. 129, no. 6, pp. 1215–1225, 2007.

- [16] Q. Sun, T. Luo, Y. Ren et al., "Competition between human cells by entosis," *Cell Research*, vol. 24, no. 11, pp. 1299–1310, 2014.
- [17] H. Huang, Z. Chen, and Q. Sun, "Mammalian cell competitions, cell-in-cell phenomena and their biomedical implications," *Current Molecular Medicine*, vol. 15, no. 9, pp. 852–860, 2015.
- [18] S. Krishna, W. Palm, Y. Lee et al., "PIKfyve regulates vacuole maturation and nutrient recovery following engulfment," *Developmental Cell*, vol. 38, no. 5, pp. 536–547, 2016.
- [19] M. Krajcovic, N. B. Johnson, Q. Sun et al., "A non-genetic route to aneuploidy in human cancers," *Nature Cell Biology*, vol. 13, no. 3, pp. 324–330, 2011.
- [20] H. L. Mackay, D. Moore, C. Hall et al., "Genomic instability in mutant p53 cancer cells upon entotic engulfment," *Nature Communications*, vol. 9, no. 1, pp. 3070–3070, 2018.
- [21] L. Lugini, P. Matarrese, A. Tinari et al., "Cannibalism of live lymphocytes by human metastatic but not primary melanoma cells," *Cancer Research*, vol. 66, no. 7, pp. 3629–3638, 2006.
- [22] S. Wang, M. F. He, Y. H. Chen et al., "Rapid reuptake of granzyme B leads to emperitosis: an apoptotic cell-in-cell death of immune killer cells inside tumor cells," *Cell Death & Disease*, vol. 4, no. 10, article e856, 2013.
- [23] S. P. Davies, G. M. Reynolds, A. L. Wilkinson et al., "Hepatocytes delete regulatory T cells by enclysis, a CD4<sup>+</sup> T cell engulfment process," *Cell Reports*, vol. 29, no. 6, article e4, pp. 1610–1620.e4, 2019.
- [24] L. Lugini, F. Lozupone, P. Matarrese et al., "Potent phagocytic activity discriminates metastatic and primary human malignant melanomas: a key role of ezrin," *Laboratory Investigation*, vol. 83, no. 11, pp. 1555–1567, 2003.
- [25] D. Sumi, H. Tsuyama, T. Ogawa, M. Ogawa, and S. Himeno, "Arsenite suppresses IL-2-dependent tumoricidal activities of natural killer cells," *Toxicology and Applied Pharmacology*, vol. 412, article 115353, 2021.
- [26] S. Wang, Z. Guo, P. Xia et al., "Internalization of NK cells into tumor cells requires ezrin and leads to programmed cell-in-cell death," *Cell Research*, vol. 19, no. 12, pp. 1350–1362, 2009.
- [27] Y. Su, H. Huang, T. Luo et al., "Cell-in-cell structure mediates in-cell killing suppressed by CD44," *Cell Discovery*, vol. 8, no. 1, pp. 1–18, 2022.
- [28] C. Chen, S. Zhao, A. Karnad, and J. W. Freeman, "The biology and role of CD44 in cancer progression: therapeutic implications," *Journal of Hematology & Oncology*, vol. 11, no. 1, pp. 1–23, 2018.
- [29] V. Benseler, A. Warren, M. Vo et al., "Hepatocyte entry leads to degradation of autoreactive CD8 T cells," *Proceedings of the National Academy of Sciences of the United States of America*, vol. 108, no. 40, pp. 16735–16740, 2011.
- [30] S. P. Davies, L. V. Terry, A. L. Wilkinson, and Z. Stamataki, "Cell-in-cell structures in the liver: a tale of four E's," *Frontiers in Immunology*, vol. 11, article 650, 2020.
- [31] Y. O. Aghabi, A. Yasin, J. I. Kennedy, S. P. Davies, A. E. Butler, and Z. Stamataki, "Targeting enclysis in liver autoimmunity, transplantation, viral infection and cancer," *Frontiers in Immunology*, vol. 12, article 662134, 2021.
- [32] W. T. Abodie, P. Dey, and O. Al-Hattab, "Cell cannibalism in ductal carcinoma of breast," *Cytopathology*, vol. 17, no. 5, pp. 304–305, 2006.
- [33] X. Zhang, Z. Niu, H. Qin et al., "Subtype-based prognostic analysis of cell-in-cell structures in early breast cancer," *Frontiers in Oncology*, vol. 9, pp. 895–895, 2019.
- [34] K. Gupta and P. Dey, "Cell cannibalism: diagnostic marker of malignancy," *Diagnostic Cytopathology*, vol. 28, no. 2, pp. 86–87, 2003.
- [35] H. Schenker, M. Büttner-Herold, R. Fietkau, and L. V. Distel, "Cell-in-cell structures are more potent predictors of outcome than senescence or apoptosis in head and neck squamous cell carcinomas," *Radiation Oncology*, vol. 12, no. 1, pp. 1–9, 2017.
- [36] M. Schwegler, A. M. Wirsing, H. M. Schenker et al., "Prognostic value of homotypic cell internalization by nonprofessional phagocytic cancer cells," *BioMed Research International*, vol. 2015, Article ID 359392, 14 pages, 2015.
- [37] H. Huang, M. He, Y. Zhang et al., "Identification and validation of heterotypic cell-in-cell structure as an adverse prognostic predictor for young patients of resectable pancreatic ductal adenocarcinoma," *Signal Transduction and Targeted Therapy*, vol. 5, no. 1, pp. 1–3, 2020.
- [38] A. Hayashi, A. Yavas, C. A. McIntyre et al., "Genetic and clinical correlates of entosis in pancreatic ductal adenocarcinoma," *Modern Pathology*, vol. 33, no. 9, pp. 1822–1831, 2020.
- [39] J. Fan, Q. Fang, Y. Yang et al., "Role of heterotypic neutrophil-in-tumor structure in the prognosis of patients with buccal mucosa squamous cell carcinoma," *Frontiers in Oncology*, vol. 10, article 541878, 2020.
- [40] K. Tarao, A. Nozaki, T. Ikeda et al., "Real impact of liver cirrhosis on the development of hepatocellular carcinoma in various liver diseases-meta-analytic assessment," *Cancer Medicine*, vol. 8, no. 3, pp. 1054–1065, 2019.
- [41] S.-X. Zhao, W.-C. Li, N. Fu et al., "Emperipolesis mediated by CD8(+) T cells correlates with biliary epithelia cell injury in primary biliary cholangitis," *Journal of Cellular and Molecular Medicine*, vol. 24, no. 2, pp. 1268–1275, 2020.
- [42] Y. Hu, L. Jiang, G. Zhou et al., "Emperipolesis is a potential histological hallmark associated with chronic hepatitis B," *Current Molecular Medicine*, vol. 15, no. 9, pp. 873–881, 2015.
- [43] H. P. Dienes, "Viral and autoimmune hepatitis. Morphologic and pathogenetic aspects of cell damage in hepatitis with potential chronicity," *Veröffentlichungen aus der Pathologie*, vol. 132, pp. 1–107, 1989.
- [44] Q. Miao, Z. Bian, R. Tang et al., "Emperipolesis mediated by CD8 T cells is a characteristic histopathologic feature of autoimmune hepatitis," *Clinical Reviews in Allergy and Immunology*, vol. 48, no. 2-3, pp. 226–235, 2015.
- [45] J. Shi, J. Zhao, X. Zhang et al., "Activated hepatic stellate cells impair NK cell anti-fibrosis capacity through a TGF- $\beta$ -dependent emperipolesis in HBV cirrhotic patients," *Scientific Reports*, vol. 7, no. 1, article 44544, 2017.
- [46] Z. Zhang, Y. Zheng, Z. Niu et al., "SARS-CoV-2 spike protein dictates syncytium-mediated lymphocyte elimination," *Cell Death and Differentiation*, vol. 28, no. 9, pp. 2765–2777, 2021.
- [47] G. R. Nemerow, R. A. Houghten, M. D. Moore, and N. R. Cooper, "Identification of an epitope in the major envelope protein of Epstein-Barr virus that mediates viral binding to the B lymphocyte EBV receptor (CR2)," *Cell*, vol. 56, no. 3, pp. 369–377, 1989.
- [48] C. Shannon-Lowe and M. Rowe, "Epstein-Barr virus infection of polarized epithelial cells via the basolateral surface by



## Retraction

# Retracted: A Novel Missense Mutation of Arginine Vasopressin Receptor 2 in a Chinese Family with Congenital Nephrogenic Diabetes Insipidus: X-Chromosome Inactivation in Female CNDI Patients with Heterozygote 814A>G Mutation

### BioMed Research International

Received 12 March 2024; Accepted 12 March 2024; Published 20 March 2024

Copyright © 2024 BioMed Research International. This is an open access article distributed under the Creative Commons Attribution License, which permits unrestricted use, distribution, and reproduction in any medium, provided the original work is properly cited.

This article has been retracted by Hindawi following an investigation undertaken by the publisher [1]. This investigation has uncovered evidence of one or more of the following indicators of systematic manipulation of the publication process:

- (1) Discrepancies in scope
- (2) Discrepancies in the description of the research reported
- (3) Discrepancies between the availability of data and the research described
- (4) Inappropriate citations
- (5) Incoherent, meaningless and/or irrelevant content included in the article
- (6) Manipulated or compromised peer review

The presence of these indicators undermines our confidence in the integrity of the article's content and we cannot, therefore, vouch for its reliability. Please note that this notice is intended solely to alert readers that the content of this article is unreliable. We have not investigated whether authors were aware of or involved in the systematic manipulation of the publication process.

Wiley and Hindawi regrets that the usual quality checks did not identify these issues before publication and have since put additional measures in place to safeguard research integrity.

We wish to credit our own Research Integrity and Research Publishing teams and anonymous and named external researchers and research integrity experts for contributing to this investigation.

The corresponding author, as the representative of all authors, has been given the opportunity to register their agreement or disagreement to this retraction. We have kept a record of any response received.

### References

- [1] L. Zang, Y. Gong, Y. Li et al., "A Novel Missense Mutation of Arginine Vasopressin Receptor 2 in a Chinese Family with Congenital Nephrogenic Diabetes Insipidus: X-Chromosome Inactivation in Female CNDI Patients with Heterozygote 814A>G Mutation," *BioMed Research International*, vol. 2022, Article ID 7073158, 7 pages, 2022.

## Research Article

# A Novel Missense Mutation of Arginine Vasopressin Receptor 2 in a Chinese Family with Congenital Nephrogenic Diabetes Insipidus: X-Chromosome Inactivation in Female CNDI Patients with Heterozygote 814A>G Mutation

Li Zang,<sup>1</sup> Yuping Gong,<sup>2</sup> Yijun Li,<sup>1</sup> Jingtao Dou,<sup>1</sup> Zhaohui Lyu,<sup>1</sup> Xiaoqing Su,<sup>2</sup> Yawei Zhang ,<sup>2</sup> and Yiming Mu <sup>1</sup>

<sup>1</sup>Department of Endocrinology, The First Medical Center of Chinese PLA General Hospital, Beijing 100853, China

<sup>2</sup>Department of Endocrinology, Jiangxi Pingxiang People's Hospital, Pingxiang 337055, China

Correspondence should be addressed to Yawei Zhang; 1178584337@qq.com and Yiming Mu; muyiming@301hospital.com.cn

Received 8 February 2022; Revised 10 April 2022; Accepted 2 June 2022; Published 12 July 2022

Academic Editor: Pengjun Shi

Copyright © 2022 Li Zang et al. This is an open access article distributed under the Creative Commons Attribution License, which permits unrestricted use, distribution, and reproduction in any medium, provided the original work is properly cited.

**Background.** To identify novel clinical phenotypic signatures of congenital nephrogenic diabetes insipidus (CNDI). **Methods.** A Chinese family with CNDI was recruited for participation in this study. The proband and one of his uncles suffered from polydipsia and polyuria since infancy. The results of clinical testing indicated the diagnosis of CNDI. 10 family members had similar symptoms but did not seek medical advice. Genetic testing of mutations in the coding region of the aquaporin 2 (AQP2) gene and the arginine vasopressin receptor 2 (AVPR2) gene were carried out in 11 family members. Somatic DNA from 5 female family members was used to test for methylation of polymorphic CAG repeats in the human androgen receptor (AR) gene, as an index for X-chromosome inactivation pattern (XCIP). **Results.** AQP2 gene mutations were not found in any family members, but a novel missense mutation (814th base A>G) in exon 2 of the AVPR2 gene was identified in 10 individuals. This mutation leads to a Met 272 Val (GAT-GGT) amino acid substitution. Skewed X-chromosome inactivation patterns of the normal X allele were observed in 4 females with the AVPR2 gene mutation and symptoms of diabetes insipidus, but not in an asymptomatic female with the AVPR2 gene mutation. **Conclusions.** Met 272 Val mutation of the AVPR2 gene was identified as a novel genetic risk factor for CNDI. The clinical NDI phenotype of female carriers with heterozygous AVPR2 mutation may be caused by X-chromosome inactivation induced by dominant methylation of the normal allele of AVPR2 gene.

## 1. Introduction

Congenital nephrogenic diabetes insipidus (CNDI) is a relatively rare genetic disorder which is characterized by renal resistance to the antidiuretic effects of arginine vasopressin (AVP), an antidiuretic hormone (ADH) that is produced in the posterior pituitary and functions as a regulator of the kidney's ability to reabsorb water. 90% of cases with CNDI are caused by mutations of arginine vasopressin type 2 receptor (AVPR2) gene, which encodes the vasopressin V2 receptor [1]. The remaining 10% of cases with CNDI are caused by mutations of aquaporin-2 (AQP2), a water channel gene located on chromosome 12q13.

In particular, mutations of AQP2 are linked to autosomal recessive or dominant forms of CNDI [2]. The AVPR2 gene is located on the long arm of the X-chromosome (Xq28), and mutations of AVPR2 gene can cause CNDI in an X-linked recessive manner. To date, approximately 250 AVPR2 mutations have been identified and the inheritance pattern is often used to distinguish various forms of CNDI [3]. Most of the female carriers with AVPR2 mutations are asymptomatic. However, some female carriers with AVPR2 mutations may experience symptoms of polydipsia and polyuria, due to their impaired ability to concentrate urine, as is observed in male patients with skewed X-chromosome inactivation.

In this study, we identify novel clinical phenotypic signatures of CNDI through genetic analysis of mutations in *AQP2* and *AVPR2* in a Chinese family with autosomal CNDI, which was confirmed by both clinical examination and the mode of inheritance. We found a novel mutation of the *AVPR2* gene, and this newly identified *AVPR2* mutation is considered the potential pathogeny of CNDI, because skewed X-chromosome inactivation was confirmed as the reason for symptoms in the female patients carrying this mutation.

## 2. Materials and Methods

This study was approved by the ethics committee of our institutions. Written informed consent was obtained from all participants in this study. The investigation was performed in adherence with the ethical principles of the Helsinki Declaration.

**2.1. Analysis of Clinical Data.** The pedigree of the Chinese family described in this study is presented in Figure 1. The proband (subject III-6) was a 31-year-old male, who was admitted to our department because of polydipsia, polyuria, and nocturia since infancy. His 24-hour urine volume was 5-6 L/24 h. The results of his urinary laboratory examination indicated marked hypernatremia (s-Na 155 mmol/L) along with hypoosmotic polyuria (urinometry 1.002-1.004). Serum urine nitrogen (9.6 mmol/L) and serum creatinine (140.2  $\mu$ mol/L) were mildly elevated. Pituitary magnetic resonance imaging (MRI) showed visible bright spots in the posterior pituitary. The pituitary was normal in appearance, without evidence of a hypothalamic mass (Figure 2). Computed tomography (CT) of the urinary system revealed bilateral ureterectasis and hydronephrosis combined with right kidney atrophy (Figure 2). Tests of the capacity for water deprivation and vasopressin loading revealed that dehydration and subcutaneous injection of 5 units of vasopressin did not increase the concentration of urine osmolality (Table 1). These findings supported the diagnosis of CNDI. The symptoms of polydipsia and polyuria were relieved, and the 24 h urine volume was controlled at 2000 mL after he was treated with hydrochlorothiazide and indomethacin. One of his uncles (subject II-2) suffered from the same symptoms, including bilateral ureterectasis and hydronephrosis. Measurements of urine osmolality obtained during water deprivation and vasopressin loading tests showed that the patient had lost the renal response to the injection of vasopressin. Hydrochlorothiazide treatment was proved effective. The other members of this pedigree, including his grandmother (subject I-1), another uncle (subject II-6), his mother and three aunts (subjects II-3, 4, 5, and 7), his brother and two cousins (subjects III-5, 3, and 4), and his 2-year-old nephew (subject IV-1), had developed varying degrees of diabetes insipidus, but they did not seek medical advice.

**2.2. Genomic DNA Extraction and Sequence Analysis.** 11 members of the family (including subjects II-1, 2, 3, 4, and 6; III-3, 4, 5, 6, and 7; and IV-1) provided written consent after being informed of the study's purpose. Five milliliters of peripheral blood samples was collected and placed into a tube with ethylenediaminetetraacetic acid (EDTA). Genomic DNA was extracted using a kit (Qiagen, Duesseldorf, Germany). To

amplify the *AVPR2* and *AQP2* genes, polymerase chain reaction (PCR) was performed using primers for *AVPR2* and *AQP2* genes as previously reported [4, 5]. After the purification of PCR products, automated DNA-sequencing was performed using an instrument (310 Genetic Analyzer; ABI Prism) and the BigDye kit (Applied Biosystems, USA).

**2.3. X-Chromosome Inactivation Pattern Analysis.** Among methylation sites on the inactive X-chromosome, the first exon of the human androgen receptor (AR) gene is typically used to analyze the X-chromosome inactivation pattern by counting the polymorphic CAG repeats in exon 1 of the AR gene [6]. Genomic DNA samples obtained from 5 female members (subjects II-3 and 4; III-3 and 4 with symptoms of diabetes insipidus; and subject III-7 without symptoms) were pretreated with bisulfite for DNA methylation detection using the EpiTect Bisulfite Kit (Qiagen) according to the manufacturer's instructions. Briefly, genomic DNA samples were digested by two methylation-sensitive restriction enzymes (HpaII and HhaI). Restriction enzyme (RE) digestion was designed to yield cleavage only at RE sites on the active X-chromosome, but not on the inactive methylated X-chromosomes. Then, RE-digested DNA samples were used for PCR amplification of the AR locus, including the HpaII and HhaI cleavage sites and the CAG repeat element. The primers for this study were designed as previously reported [7]. After 4% agarose gel electrophoresis, two bands of the PCR products were detected: 280 bp from one allele and 292 bp from another allele. The density of each band was quantified by scanning with Band scan software. The degree of X-chromosome inactivation for each allele was expressed as a percentage of the inactive X-chromosome. The value or percentage of relative X-chromosome inactivation for one allele was determined by calculations using the following equation:  $N_{280}/(N_{280} + N_{292}) \times 100$ . The pattern of X-chromosome inactivation was considered to be skewed if the percentage of X-chromosome inactivation was  $\geq 80\%$ . Values ranging from 50% to 80% were considered to indicate a random pattern of X-chromosome inactivation.

## 3. Results

**3.1. Mutations of the *AVPR2* and *AQP2* Genes.** Genomic DNA sequencing was performed for the precise diagnosis of CNDI using the samples obtained from 11 family members. Because of the initial suggested diagnosis of autosomal CNDI, the sequence of the entire coding region of the *AQP2* gene in each DNA sample was examined, but no variation was found in any of the family members recruited for this study. In the proband, two hemizygous mutations (814th base A>G and 927th base A>G) were found in the 2nd and 3rd exons of the *AVPR2* gene, respectively (Figures 3(a) and 3(c)). The A>G mutation in the 927th base of the 3rd exon suggested a silent Leu 309 Leu (TAG-TAC) mutation, while the A>G mutation at the 814th base of the 2nd exon resulted in an amino acid substitution (Met 272 Val, i.e., from GAT to GGT) in the *AVPR2*. A hemizygous Met 272 Val mutation was also found in some male family members with symptoms of diabetes insipidus, such as subjects II-2 and 6; III-5; and IV-1. Heterozygous Met 272 Val mutations were found in some female family members

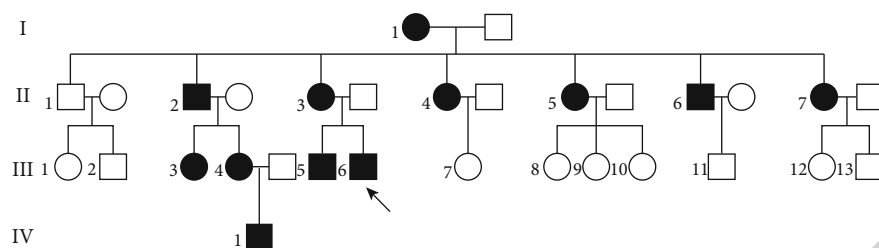


FIGURE 1: The pedigree of the Chinese family with congenital nephrogenic diabetes insipidus. Solid symbols denote the affected individuals. The arrow indicates the proband.

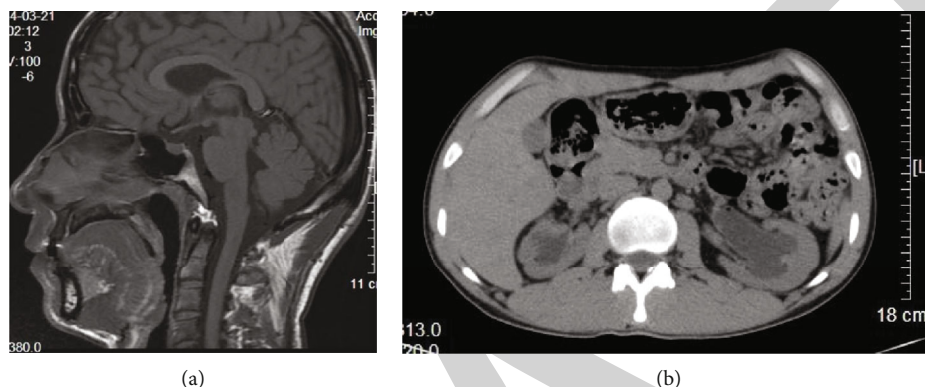


FIGURE 2: The imaging feature of the proband. (a) Pituitary MRI showed normal anterior and posterior pituitary. (b) Urinary system CT scan showed bilateral ureterectasis and hydronephrosis combined with right kidney atrophy.

TABLE 1: Results on the water deprivation and vasopressin test of proband.

Time (hours)	Urine volume (mL)	Urine specific gravity	Plasma osmolality (mOsm/L)	Body weight (kg)
1	150	1.002	307.1	51
2	190	1.003	306.9	51
3	150	1.003	312.2	51
4	100	1.002	305.5	50.5
5	70	1.002	306.9	51
6*	60	1.003	311.6	51
7	80	1.002	311.2	50.8

Note: 5U vasopressin was subcutaneously injected at the beginning of the 6th hour.

with symptoms of diabetes insipidus (subject II-3 and 4 and III-3 and 4) (Figures 3(b) and 3(d)), as well as one asymptomatic female member (subject III-7). No *AVPR2* gene mutation was detected in one asymptomatic male family member (subject II-1). The Met 272 Val mutation was considered responsible for the morbidity associated with CNDI, and it was not found in the 100 unrelated healthy individuals used as controls.

3.2. Assay for X-Chromosome Inactivation. Both 280-bp and 292-bp PCR products of the *AR* locus were examined for the analysis of X-chromosome inactivation. Digestion of the DNA samples with two methylation-sensitive REs prior to PCR resulted in a difference in density between the bands. Our study found that the percentages of relative X-chromosome inactivation for one allele were 90%, 83%, 87%, 85%, and 39% in subjects II-3 and 4, III-3 and 4, and subject III-7, respectively (Table 2). These findings indicated nonrandom X-

chromosome inactivation in subjects II-3 and 4 and III-3 and 4 but not in subject III-7. We explored the relationship between the age of the female subjects and the percentage of relative X-chromosome inactivation, and no correlation between two variables was found.

#### 4. Discussion

In this study, 12 members of a Chinese family suffered from polydipsia and polyuria from infancy were diagnosed with CNDI. An autosomal CNDI pedigree was considered because male as well as female members of the family were affected. Surprisingly, no mutations in the coding region of the *AQP2* gene, which was linked to autosomal recessive or dominant forms of CNDI, were detected in any of the family members, while genetic analysis of *AVPR2* gene revealed a novel mutation of 814th base A>G, which induced Met 272 Val amino

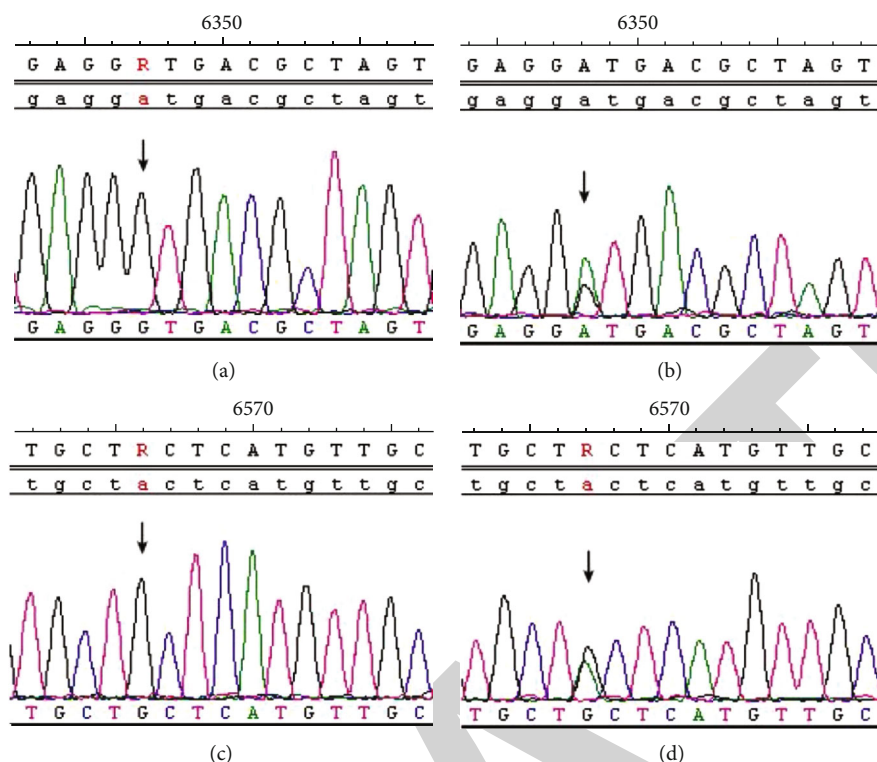


FIGURE 3: Sequence analysis of the 2nd and 3rd exons in AVPR2 gene. (a, b) sequencing in the 814th base of 2nd exon, A was substitute of G which resulted a Met 272 Val (GAT-GGT) amino acid substitution. A was hemizygous mutation in the male subjects, B was heterozygous mutation in the female subjects. (c, d) sequencing in the 927th base of 3rd exon, A was substitute of G which suggested a silent mutation Leu 309 Leu. C was hemizygous mutation in the male subjects; D was heterozygous mutation in the female subjects.

TABLE 2: Analysis of the X-chromosome inactivation pattern in the family.

	Subjects				
	II-3	II-4	III-3	III-4	III -7
Fragment length allele 1 (bp)	280	280	280	280	280
Fragment length allele 2 (bp)	292	292	292	292	292
Percentage of cells with allele 1 as inactive X-chromosome (%)	90	83	87	85	39
Percentage of cells with allele 2 as inactive X-chromosome (%)	10	17	13	15	61

acid substitution. The 814th base A>G mutation had not been reported previously and was suggested responsible for CNDI. The CNDI in this pedigree was considered to be an X-linked recessive inherited disease, with involvement in female patients caused by skewed inactivation of the X-chromosome.

CNDI was first described by McIlraith in 1892. Patients with CNDI mainly present with persistent polyuria, polyuria, dehydration, delayed growth, and intellectual disability. Laboratory examinations usually reveal hypernatremia and hyposthenuria that do not respond to exogenous AVP [2]. Because of persistent polyuria and delays in diagnosis, many of the patients have dysfunction of the kidney, such as urinary retention, hydronephrosis, and mild renal insufficiency. In this study, the 31-year-old proband and one of his uncles were diagnosed with CNDI based on their presentation of clinical symptoms, results of laboratory examinations, and positive

response to hydrochlorothiazide and indomethacin. Numerous other family members (males and females) also had symptoms of diabetes insipidus. So this pedigree was first considered as evidence of autosomal dominant CNDI caused by the AQP2 gene mutation. However, no variation in AQP2 was found in any family members.

Further analysis revealed two hemizygous mutations in the exons of AVPR2 in the proband, which indicated a diagnosis of X-linked recessive inherited disease in this family. van den Ouweland first reported that mutation of the AVPR2 gene was linked to X-linked recessive CNDI in 1992 [8]. Moreover, 50% of AVPR2 gene mutations are missense mutations [9]. There are three types of AVPR2 gene mutations, which are differentiated based on the function and subcellular localization of mutant proteins [10]. In Type 1, the mutant receptors are located on the cell surface, with

impaired ligand binding, leading decreased cAMP production. In Type 2, the mutant receptors are not transported to the cell surface, accumulating instead in a pre-Golgi compartment, due to defective intracellular transport. In Type 3, the mutant receptors are expressed at low levels because of the rapid degradation of unstable mRNA. The 927A>G *AVPR2* mutation harbored by the proband is a nonsense mutation reported in the literature as the most common polymorphism of this gene [11]. However, the 814A>G mutation found in our study is a novel missense mutation that causes a Met 272 Val substitution. In this family, hemizygous mutation of Met 272 Val was also found in some male family members with symptoms of diabetes insipidus, while heterozygous mutations of Met 272 Val were found only in female family members (with or without symptoms). However, the Met 272 Val mutation was not found in asymptomatic male members. These results suggested that the novel mutation identified in this study was responsible for V2 receptor dysfunction. The Met 272 Val mutation occurred in a transmembrane region of the V2 receptor, which may lead to improper assembly of the V2 receptor. Another study identified a different mutation (Met 272 Lys) at this residue in a patient with CNDI, resulting in insertion of a charged residue in the transmembrane domain, causing a failure to signal upon stimulation with AVP [12]. Other studies identified an *AVPR2* gene mutation at a residue next to position Thr273Met in Turkish and Spanish patients. The Thr273Met mutation is also located in the region that codes for the transmembrane domain, which affects proper assembly and function of the V2 receptor [13, 14]. The amino acid residue at positions 272 and 273 is vital for the structure of the V2 receptor, and the Met 272 Val mutation was not found in 100 unrelated healthy individuals used as controls. Therefore, based on previous reports, the novel mutation found in our study could be classified as a Type 1 mutation that was pathognomonic for CNDI. Further basic research is needed to investigate the potential effects of the 814A>G mutation on V2 receptor function.

In our study, there were 4 female patients with CNDI and *AVPR2* mutations. Female CNDI patients with the *AVPR2* mutations are usually diagnosed as a carrier of heterozygous mutation and asymptomatic. Therefore, it is necessary to test for other gene mutations related to CNDI for female patients, especially those affecting the *AQP2* gene, which have an autosomal dominant pattern of transmission. In our study, direct sequence analysis did not reveal any mutations in *AQP2* among all tested family members. *AQP2* mutations were not pathognomonic for CNDI among female members of this pedigree. The reason why female carriers of mutation of *AVPR2* gene showed NDI symptoms would be explain by skewed X-inactivation. As we know, X-chromosome inactivation occurs early in female embryogenesis at about the 32-to-64 cell stage, when there are few progenitor cells for a given tissue. X-chromosome inactivation is irreversible and affects all descendants of a given progenitor cell. Skewed inactivation of the X-chromosome bearing the normal *AVPR2* allele may suppress the expression of *AVPR2* protein with normal function, leading to female carriers with an NDI phenotype. In this study, we examined CAG repeat polymorphisms at the AR locus in DNA samples to measure X-chromosome inactivation in

female carriers. Female members of the pedigree with *AVPR2* mutation and symptoms of diabetes insipidus displayed X-chromosome inactivation, while this phenomenon did not appear in asymptomatic female members with *AVPR2* mutation, indicating that X-chromosome inactivation was responsible for the symptoms observed in female patients. There were 5 pedigrees with skewed X-inactivation in female carriers of *AVPR2* mutation had been reported [15–19]. Nomura et al. first reported 3 male members diagnosed with CNDI with *AVPR2* mutation (a G inserted at nucleotide 804 of the open reading frame). Three female individuals in the pedigree displayed different degrees of symptoms of NDI, and all of them possessed both the normal and abnormal genes. The X-inactivation patterns of the female members were investigated via the detection of methylated trinucleotide repeat in the human AR gene. The grandmother showed extremely skewed methylation of one X-chromosome, and the mother revealed moderately skewed methylation. The daughter of the grandmother's sister, who had no symptoms of NDI, showed random methylation. The highly skewed X-inactivation pattern of the grandmother suggested that her NDI phenotype was caused by dominant methylation of the normal allele of V2R gene [15]. Kinoshita et al. reported a pedigree of CNDI with a Japanese female proband (two-nucleotide deletion change at codon 30 (g.452-453delAC) in the V2R gene, resulting in a frameshift and premature termination in translation at codon 190). The X-chromosome inactivation pattern detection using methylation analysis of the polymorphic CAG repeat in the AR gene revealed that the value for relative X-chromosome inactivation of one allele was 70.2% [16]. Satoh et al. reported the value for relative X-chromosome inactivation was 71.6%-93% in female carriers with *AVPR2* mutation who showed clinical symptoms, while it was only 60.7%-61.9% in asymptomatic female carriers [17–19]. The results of our study are consistent with other previous observations of females with X-linked NDI. In previous reports, the ratios of X-chromosome inactivation for a given tissue were similar among individuals, but in a normal female, those ratios may vary depending on cell lineage [20]. Presumably, the X-chromosome inactivation pattern in leucocytes from blood samples may not precisely reflect that in renal tubular cells. Owing to difficulty in obtaining renal tubular tissue for this study, further research is needed to explore X-chromosome inactivation in the kidneys of females with NDI.

## 5. Conclusions

In conclusion, a novel *AVPR2* mutation (814A>G) in a Chinese family with CNDI has been identified in this study. This novel mutation may be involved in improper assembly of the V2 receptor. Female carriers with the heterozygous form of the 814A>G mutation had a clinical NDI phenotype, perhaps due to the pattern of X-chromosome inactivation. The clinical NDI phenotype in female carriers with the heterozygote 814A>G mutation may result from the methylation coded for by the normal allele of the *AVPR2* gene, which is dominant. It is necessary to perform functional studies in the future to investigate the effects of the Met272Val mutation on the V2 receptor on terms of intracellular localization, ligand binding, and adenylate cyclase activation.

## Abbreviations

CNDI: Congenital nephrogenic diabetes insipidus  
 AVP: Arginine vasopressin  
 ADH: Antidiuretic hormone  
 AVPR2: Vasopressin type 2 receptor  
 AQP2: Aquaporin-2  
 PCR: Polymerase chain reaction.

## Data Availability

The datasets generated during and/or analyzed during the current study are not publicly available but are available from the corresponding author on reasonable request. The sequencing data were deposited in the ClinVar database (<http://www.ncbi.nlm.nih.gov/clinvar>; accession number: SCV001469055).

## Ethical Approval

This study was approved by the ethics committee of the First Medical Center of Chinese PLA General Hospital. All procedures performed in studies involving human participants were in accordance with the ethical standards of the institutional and/or national research committee and with the 1964 Helsinki declaration and its later amendments or comparable ethical standards.

## Consent

Written informed consent was obtained from all participants or, if subjects are under 16, from a parent and/or legal guardian.

## Conflicts of Interest

The authors declare that they have no conflict of interest.

## Authors' Contributions

LZ, YG, YL, YZ, and YM conceived and designed research; LZ, YG, and YL collected data, conducted research, interpreted data, and wrote the initial paper; JD, ZL, and XS revised the paper; YZ and YM had primary responsibility for final content. All authors read and approved the final manuscript. Li Zang, Yuping Gong, and Yijun Li contributed equally to the work.

## References

- [1] T. H. Yoo, D. R. Ryu, Y. S. Song et al., "Congenital nephrogenic diabetes insipidus presented with bilateral hydronephrosis: genetic analysis of V2R gene mutations," *Yonsei Medical Journal*, vol. 47, no. 1, pp. 126–130, 2006.
- [2] J. P. Morello and D. G. Bichet, "Nephrogenic diabetes insipidus," *Annual Review of Physiology*, vol. 63, no. 1, pp. 607–630, 2001.
- [3] D. Bockenhauer and D. G. Bichet, "Nephrogenic diabetes insipidus," *Current Opinion in Pediatrics*, vol. 29, no. 2, pp. 199–205, 2017.
- [4] A. Çelebi Tayfur, T. Karaduman, M. Özcan Türkmen et al., "A novel mutation in the AVPR2 gene causing congenital nephrogenic diabetes insipidus," *Journal of Clinical Research in Pediatric Endocrinology*, vol. 10, no. 4, pp. 350–356, 2018.
- [5] R. Rugsolmuang, A. Deeb, Y. Hassan, T. Deekajorndech, V. Shotelersuk, and T. Sahakitrungruang, "Novel AQP2 mutation causing congenital nephrogenic diabetes insipidus: challenges in management during infancy," *Journal of Pediatric Endocrinology & Metabolism*, vol. 27, no. 1-2, pp. 193–197, 2014.
- [6] M. O. Lexner, A. Bardow, I. Juncker et al., "X-linked hypohidrotic ectodermal dysplasia. Genetic and dental findings in 67 Danish patients from 19 families," *Clinical Genetics*, vol. 74, no. 3, pp. 252–259, 2008.
- [7] R. C. Allen, H. Y. Zoghbi, A. B. Moseley, H. M. Rosenblatt, and J. W. Belmont, "Methylation of HpaII and HhaI sites near the polymorphic CAG repeat in the human androgen-receptor gene correlates with X chromosome inactivation," *American Journal of Human Genetics*, vol. 51, no. 6, pp. 1229–1239, 1992.
- [8] A. M. van den Ouweland, J. C. Dreesen, M. Verdijk et al., "Mutations in the vasopressin type 2 receptor gene (AVPR2) associated with nephrogenic diabetes insipidus," *Nature Genetics*, vol. 2, no. 2, pp. 99–102, 1992.
- [9] I. Bösel, D. Tramma, S. Kalamitsou et al., "Functional characterization of novel loss-of-function mutations in the vasopressin type 2 receptor gene causing nephrogenic diabetes insipidus," *Nephrology, Dialysis, Transplantation*, vol. 27, no. 4, pp. 1521–1528, 2012.
- [10] T. M. Fujiwara and D. G. Bichet, "Molecular biology of hereditary diabetes insipidus," *Journal of the American Society of Nephrology*, vol. 16, no. 10, pp. 2836–2846, 2005.
- [11] Y. Shen, X. Lai, X. Xiao et al., "Genetic analysis of a congenital nephrogenic diabetes insipidus pedigree," *Chinese Medical Journal*, vol. 127, no. 6, pp. 1089–1092, 2014.
- [12] R. S. Wildin, D. E. Cogdell, and V. Valadez, "AVPR2 variants and V2 vasopressin receptor function in nephrogenic diabetes insipidus," *Kidney International*, vol. 54, no. 6, pp. 1909–1922, 1998.
- [13] D. Duzenli, E. Saglar, F. Deniz, O. Azal, B. Erdem, and H. Mergen, "Mutations in the AVPR2, AVP-NPII, and AQP2 genes in Turkish patients with diabetes insipidus," *Endocrine*, vol. 42, no. 3, pp. 664–669, 2012.
- [14] A. García Castaño, G. Pérez de Nanclares, L. Madariaga et al., "Novel mutations associated with nephrogenic diabetes insipidus. A clinical-genetic study," *European Journal of Pediatrics*, vol. 174, no. 10, pp. 1373–1385, 2015.
- [15] Y. Nomura, K. Onigata, T. Nagashima et al., "Detection of skewed X-inactivation in two female carriers of vasopressin type 2 receptor gene mutation," *The Journal of Clinical Endocrinology and Metabolism*, vol. 82, no. 10, pp. 3434–3437, 1997.
- [16] K. Kinoshita, Y. Miura, H. Nagasaki, T. Murase, Y. Bando, and Y. Oiso, "A novel deletion mutation in the arginine vasopressin receptor 2 gene and skewed X chromosome inactivation in a female patient with congenital nephrogenic diabetes insipidus," *Journal of Endocrinological Investigation*, vol. 27, no. 2, pp. 167–170, 2004.
- [17] M. Satoh, S. Ogikubo, and A. Yoshizawa-Ogasawara, "Correlation between clinical phenotypes and X-inactivation patterns in six female carriers with heterozygote vasopressin type 2 receptor gene mutations," *Endocrine Journal*, vol. 55, no. 2, pp. 277–284, 2008.

## Review Article

# Association between Mesenchymal Stem Cells and COVID-19 Therapy: Systematic Review and Current Trends

Amaan Javed <sup>1</sup>, Saurab Karki <sup>2</sup>, Zeba Sami <sup>3</sup>, Zuha Khan <sup>4</sup>, Anagha Shree <sup>3</sup>,  
Biki Kumar Sah <sup>5</sup>, Shankhaneel Ghosh <sup>6</sup>, and Sara Saxena <sup>7</sup>

<sup>1</sup>University College of Medical Sciences (University of Delhi), Dilshad Garden, Delhi, India

<sup>2</sup>Nepalese Army Institute of Health Science, College of Medicine, Kathmandu, Nepal

<sup>3</sup>Shree Guru Gobind Singh Tricentenary Medical College and Research Institute, Gurugram, Haryana, India

<sup>4</sup>Public Health Consultant, Uttar Pradesh, India

<sup>5</sup>B.P. Koirala Institute of Health Sciences, Dharan, Nepal

<sup>6</sup>Institute of Medical Sciences and SUM Hospital, Bhubaneswar, India

<sup>7</sup>Dr. D. Y. Patil Medical College, Hospital and Research Centre, Pimpri-Chinchwad, Maharashtra, India

Correspondence should be addressed to Amaan Javed; [amaan09javed@gmail.com](mailto:amaan09javed@gmail.com)

Received 7 March 2022; Revised 20 May 2022; Accepted 2 June 2022; Published 22 June 2022

Academic Editor: Haixu Chen

Copyright © 2022 Amaan Javed et al. This is an open access article distributed under the Creative Commons Attribution License, which permits unrestricted use, distribution, and reproduction in any medium, provided the original work is properly cited.

**Background.** The novel coronavirus first emerged in Wuhan, China, and quickly spread across the globe, spanning various countries and resulting in a worldwide pandemic by the end of December 2019. Given the current advances in treatments available for COVID-19, mesenchymal stem cell (MSC) therapy seems to be a prospective option for management of ARDS observed in COVID-19 patients. This present study is aimed at exploring the therapeutic potential and safety of using MSC obtained by isolation from health cord tissues in the treatment of patients with COVID-19. **Methods.** A systematic search was done based on the guidelines of the PRISMA 2020 statement. A literature search was executed using controlled vocabulary and indexing of trials to evaluate all the relevant studies involving the use of medical subject headings (MeSH) in electronic databases like PubMed, Embase, Scopus, *Cochrane Central Register of Controlled Trials* (CENTRAL), and [clinicaltrials.gov](http://clinicaltrials.gov) up to 31 December 2021. The protocol was registered in the PROSPERO register with ID CRD42022301666. **Findings.** After screening finally, 22 remaining articles were included in this systematic review. The studies revealed that MSC exosomes are found to be superior to MSC alone in terms of safety owing to being smaller with a lesser immunological response which leads to free movement in blood capillaries without clumping and also cannot further divide, thus reducing the oncogenic potential of MSC-derived exosomes as compared to MSC only. The studies demonstrated that the lungs healed with the use of exosomes compared to how they presented initially at the hospital. MSCs are found to increase the angiogenesis process and alveolar reepithelization, reducing markers like TNF alpha, TGF beta, and COL I and III, reducing the growth of myofibroblasts and increasing survivability of endothelium leading to attenuated pulmonary fibrosis and even reversing them. **Interpretation.** We can conclude that the use of mesenchymal stem cells or their derived exosomes is safe and well-tolerated in patients with COVID-19. It improves different parameters of oxygenation and helps in the healing of the lungs. The viral load along with different inflammatory cells and biomarkers of inflammation tend to decrease. Chest X-ray, CT scan, and different radiological tools are used to show improvement and reduced ongoing destructive processes.

## 1. Introduction

The novel coronavirus first emerged in Wuhan, China, and quickly spread across the globe, spanning various countries and resulting in a worldwide pandemic by the end of Decem-

ber 2019. It followed a course of catastrophic global effects and resulted in more than 3.8 million deaths [1]. This highly contagious viral illness is caused by severe acute respiratory syndrome coronavirus 2 (SARS-CoV-2). The morphology of SARS-CoV-2 consists of a nucleocapsid with helical



symmetry surrounded by an envelope. The single-stranded viral RNA genome is responsible for causing enteric and respiratory diseases in humans and is mainly transmitted via respiratory droplets, aerosols, and contact routes. The virus enters the body by binding its spike glycoprotein antigen with the host cell receptor called angiotensin-converting enzyme 2 and thus gains entry inside host cells via endocytosis [2]. Typically, the patient can present with common symptoms such as fever, nonproductive cough, dyspnoea, fatigue, myalgia, rhinorrhoea, sore throat, and diarrhoea. The patients experiencing dyspnoea usually require intensive care as the body elicits an immune response to fight off the virus through antigen-presenting cells; they are presented to CD8 T cells and natural killer cells by incorporating into the major histocompatibility complex. Thus, both the innate and adaptive immune systems of defence are activated, releasing large numbers of cytokines which may manifest as cytokine storm in certain patients. Cytokine storm is largely responsible for the series of diverse local and remote signs associated with the infection. As the disease progresses acute respiratory distress syndrome (ARDS), acute cardiac injury, secondary infection resulting in generalized sepsis, and multisystem failure might ultimately result in high mortality rates [3]. Given the current advances in treatments available for COVID-19, mesenchymal stem cell (MSC) therapy seems to be a prospective option for the management of ARDS observed in COVID-19 patients. The cells exert potent modulatory effects on lungs and other tissue as they work by reducing and healing inflammation-induced injuries. Since ARDS is known to be one of the leading reasons for death in COVID-19 patients accompanied by hallmarks of cytokine storm, suppression of its aggravation might diminish the provocative cytokine production and subsequently decrease inflammation and lung injury. The immunological trademark comprises lymphopenia and a flurry of active molecules, largely dominated by interleukin IL-6 and tumour necrosis factor TNF- $\alpha$  [4]. As per a new declaration of the International Society for Stem Cell Research (ISSCR), at present, there are no endorsed stem cell-based methodologies for the counteraction of coronavirus disease. In any case, as of late, mesenchymal stem cells (MSCs) have presented one of the restorative methodologies for utilizing in the treatment of COVID-19 [5]. MSCs in general were first used as cellular therapy back in 1995 and have since been used in basic research and clinical applications [6] in cases of autoimmune disease, graft-versus-host disease (GVHD), and other diseases with very good safety rates. They assume a positive part in immunomodulatory effects through releasing many types of cytokines by paracrine secretion or making direct collaborations with immune cells. Among these, the human umbilical cord Wharton's jelly-derived MSCs (hWJCs) can be easily obtained and cultured. Inferable from their strong immunomodulatory capacity, hWJC transplantation might forestall or lessen the cytokine storm [4]. Thus, out of all the potential treatments, mesenchymal stem cell (MSC) therapy seems to be a promising option for the management of ARDS seen in COVID-19 patients. Therefore, this present study is aimed at exploring the therapeutic potential and safety of using MSC obtained by isolation from health cord tissues in the treatment of patients with COVID-19.

## 2. Methods

**2.1. Study Strategy.** In this study, a systematic search was done based on the guidelines of the Preferred Reporting Items for Systematic Reviews and Meta-Analyses (PRISMA 2020 statement) [7]. The data was collected and organised concerning synthesis without meta-analysis (SWiM) guidelines. A literature search was executed using controlled vocabulary and indexing of trials to evaluate all the relevant studies involving the use of medical subject headings (MeSH) in electronic databases like PubMed, Embase, Scopus, *Cochrane Central* Register of Controlled Trials (CENTRAL), and clinicaltrials.gov up to 31 December 2021. The protocol was registered in the PROSPERO register with ID CRD42022301666. The literature search was carried out using the following search keyword strategy:

**MEDLINE:** (COVID.mp. OR COVID-19.mp. OR coronavirus disease 2019.mp. OR 2019-nCoV.mp. OR severe acute respiratory syndrome coronavirus 2.mp. OR SARS-CoV-2.mp.) AND (mesenchymal stem cells.mp. OR exp mesenchymal stem cells/) OR [exp MSC/OR MSC.mp.] OR [stem cell.mp. OR exp stem cell/] OR [exosomes.mp. OR exp exosomes/]

**EMBASE:** (COVID OR COVID 19 OR coronavirus disease 2019.mp. OR 2019-nCoV.mp. OR SARS-CoV-2.mp. OR severe acute respiratory syndrome coronavirus 2.mp.) AND (mesenchymal stem cells.mp. OR exp mesenchymal stem cells/) OR [exp MSC/OR MSC.mp.] OR [stem cell.mp. OR exp stem cell/] OR [exosomes.mp. OR exp exosomes/]

**Scopus:** (TITLE-ABS-KEY (COVID OR COVID 19 OR [coronavirus AND disease 2019] OR 2019-nCoV OR SARS-CoV-2 OR [severe AND acute AND respiratory AND syndrome AND coronavirus 2]) AND TITLE-ABS-KEY (mesenchymal stem cells OR stem cells OR [cells AND exosomes])

**Cochrane Central:** COVID AND (neuro\* OR brain OR peripheral nerve OR cerebrospinal fluid)

**Clinicaltrials.gov:** Recruiting and not yet recruiting trials involving the use of mesenchymal stem cells in the treatment of COVID-19

**2.2. Study Selection.** The inclusion criteria considered in this systematic review were full-text articles with (a) English language, (b) the preceding search strategy, (c) requisite information, and (d) reported outcomes on the therapeutic efficacy of mesenchymal stem cells on COVID-19. The exclusion criteria were (a) duplicates, (b) poster, (c) not related to paper, (d) editorials, and (e) letter to the editor.

**2.3. Data Extraction.** Each eligible article will be reviewed, and the following data are extracted: (a) author name and relevant details; (b) outcomes of MSC stem cells and their derived exosomes on COVID-19; (c) study type; and (d) reported symptoms. The clinical trials included were analyzed for: identifier, study title, phase, subjects, cell therapy, route of administration, intervention, and efficacy.

## 3. Result

**3.1. Literature Review.** The process of study selection is illustrated in Figure 1.

909 articles were obtained by searching the aforementioned databases using the mentioned search keyword strategy. After the screening articles, 842 of them were excluded using the exclusion criteria by evaluation and abstracts, and 48 studies were qualified for assessment of their full-text. Thereafter, the studies still inconsistent with inclusion criteria were omitted. Finally, 22 remaining articles were included in this systematic review: Table 1 contains summary data extracted from these studies with the use of MSC therapy in cases of SARS-CoV-2 infection.

**3.2. Therapeutic Efficacy of MSC and MSC Exosomes.** MSC therapy has given hope for treating various autoimmune disease conditions. MSCs are nonhematopoietic cells that have immune-modulatory, regenerative, and differentiation properties [8, 9]. MSCs were first tested as cellular therapy in humans in 1995 and have since been used in basic research and clinical applications [10]. Due to the immunomodulatory properties possessed by mesenchymal stem cells, there has been growing evidence of its utility in offering a possible line of treatment for various diseases for which no reliable and efficacious treatment exists to date. The diseases for which MSC therapy holds a ray of hope are majorly autoimmune disorders. Hafsa Munir and Helen M McGettrick reviewed the clinical trials done on the effect of MSC therapy on Crohn's disease, systemic lupus erythematosus, and rheumatoid arthritis and revealed potent immunomodulatory effects in all the trials [11]. Although no adverse effects were reported, the mechanism of action of MSC needs more clarity. Chen et al. tested the effects of different treatments in a mouse model of experimental autoimmune hepatitis (EAH) and found that administration of culture-expanded bone marrow-derived MSCs can reduce EAH in a dose-dependent way, and the therapeutic effect observed in the group that received an intravenous (IV) injection three times was better than a single injection [12], whereas Wang et al. reported that both IL-35 gene-modified MSCs (IL-35-MSCs) and adipose-derived MSCs have a protecting effect in induced fulminant hepatitis in mice models. They reported that IL-35-MSCs exerted a therapeutic impact more powerful than adipose-derived MSCs [13]. Several experimental studies provide evidence that MSC derived from bone marrow has the potential for being effective in treating critically ill surgical patients who develop traumatic brain injury, acute renal failure, or acute respiratory distress syndrome. There is also preclinical evidence that MSC may be effective in treating sepsis-induced organ failure, including evidence that MSC has antimicrobial properties [14]. In humans, the most studied application for MSCs is graft-versus-host disease (GVHD). GVHD is a condition in which a genetically dissimilar, immunocompromised recipient gets attacked by the donor T cells after getting a hematopoietic stem cell transplantation [15]. Another clinical trial involving Crohn's disease (CD) resulted in the healing of fistulas with no adverse effects when treated with MSC injections [16, 17]. Perhaps the most remarkable results of human MSC therapy emerge now from clinical trials aimed at severe, treatment-refractory systemic lupus erythematosus (SLE) [18–21]. Thus, the number of preclinical and clinical

studies on patients and various experimental studies done on animal models support MSC therapy as the way forward. The properties of MSC are illustrated in Figure 2.

**3.3. Immunomodulation Mechanism of MSCs.** Mesenchymal stem cells can divide into various cell types, like  $\beta$  cells of islets of Langerhans in the pancreas, cardiac myocytes, fat cells, osteoblasts, and, conceivably, nerve cells. Apart from their differentiation ability, MSCs have been known to monitor the immune response in several conditions. It has been reported that adult MSCs can modify the T cell and B cell responses [22]. They improve tissue repair and regeneration by changing the immune response, and they work as modulators of inflammation instead of renewing the injured cells [23]. Immunomodulatory effects of both innate and adaptive immunity can be generated by MSCs. They suppress T cell production and cytokine release, including mediators such as IL-10, TGF  $\beta$ , indoleamine 2,3-dioxygenase, and PGE2, and they also limit the differentiation of dendritic cells, increasing the quantity of Tregs and suppressing the effector T cells via multiple growth factors, iNOS, heme oxygenase-1, prostaglandin E2 (PGE2), and indoleamine-2,3-dioxygenase (IDO) [24]. Cytokine storm leads to a rigorous inflammatory reaction due to the body's overactive immune system, which initiates focally and then spreads to the systemic circulation, causing damage to various organs in the body. Apart from COVID-19 infection, cytokine storm is also observed in infectious diseases due to SARS-CoV, influenza, Epstein-Barr virus, variola virus, and streptococci. It was originally seen in the graft-vs.-host disease during organ transplants [25]. MSCs can move to the damaged tissue. In the injured lung, acute respiratory distress syndrome, and sepsis, MSCs travel to and are confined in the lungs, leading to the release of growth factors, antimicrobial factors, and cytokines [26]. It even causes the reduction of apoptosis of various cells by the expression of TNF-alpha, IL-1, and IL-6 [27]. Disease caused by Th2-driven immune response has been decreased by the use of multipotent adipose-derived stem cells, a type of MSCs. It produces immunosuppressive effects by modulating both cellular and immune pathways. It inhibits Th2-dependent airway allergic diseases [28]. MSCs derived from bone marrow are found to inhibit Th2-mediated airway inflammation by causing CD4 cell differentiation which decreases lung inflammation mediated by Th2 through IFN-gamma dependent process [29]. In one of the study, gingivae-derived MSCs was able to reduce both clinical and histopathological severity of colonic inflammation and was able to reduce the inflammatory infiltration of T cells and expression of anti-inflammatory cytokine like IL-10 [30]. Suppression of antigen-specific cell Th1/Th17 decreases the production of inflammatory cytokines, and production of CD4+, CD25+, FoxP3+, and regulatory T cells suppresses self-reactive T cells which has been possible from the adipose-derived MSCs because it has been used in inflammatory conditions [31]. MSC activity has not only been limited to regeneration but the immunomodulatory and inflammatory property has heightened its importance in modern medicine. The use of MSC stem cells and their derived exosomes concerning other therapeutic roles has been discussed in the subsequent sections.

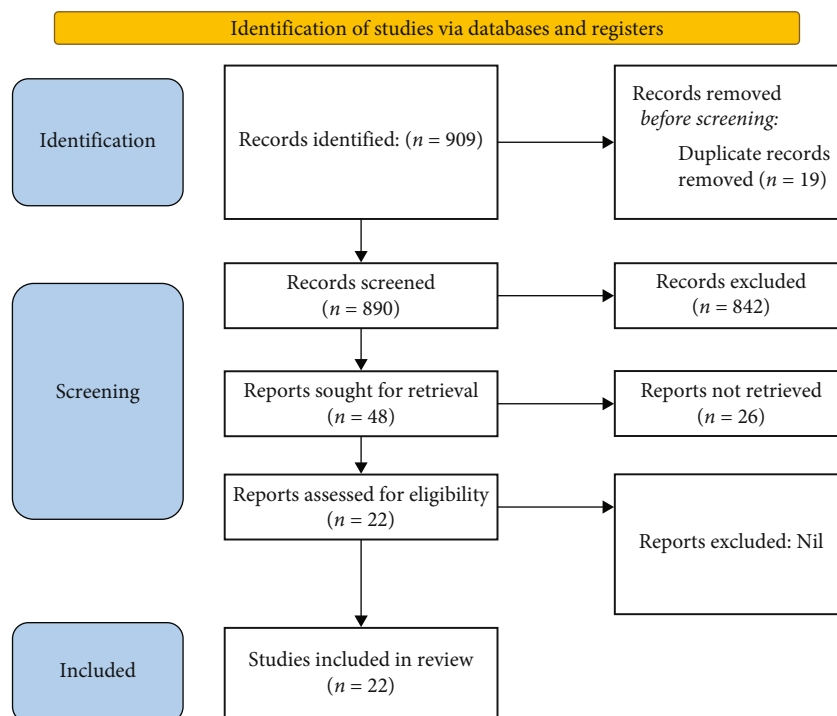


FIGURE 1: Process of study selection based on Preferred Reporting Items for Systematic Reviews and Meta-Analyses (PRISMA 2020 statement).

**3.3.1. Wound Healing and Soft Tissue Defects.** Optimal wound healing involves three overlapping phases: inflammation, proliferation, and resolution. The inflammatory phase is initiated by a microorganism or toxin that leads to the release of pathogen/damage-associated molecular patterns (PAMPs/DAMPs, respectively) that activate Toll-like receptors, NOD-like receptors (NLRs), and C-type lectin receptors (CLRs) on host cells. Interaction of these receptors causes the synthesis and release of GFs, cytokines, and chemokines that cause the migration of inflammatory cells, principally neutrophils, and monocytes. The monocytes reach the tissue and eventually develop into macrophages. Inflammatory macrophages and host cells generate reactive oxygen species that kill microorganisms [32]. Moreover, they promote the gene expression of numerous cytokines, inflammatory cells, and various proteases such as matrix metalloproteinases, serine, cysteine proteases, and elastases. These effects are caused by a variety of mechanisms, including changes in the balance of proinflammatory and anti-inflammatory cytokine release. Proinflammatory transcription factors necessary for neutrophil survival, such as NF- $\kappa$ B and IRF1, are downregulated [33], whereas the anti-inflammatory transcription factor IRF-4 is upregulated, eventually leading to the resolution of the inflammatory phase and initiation of the tissue repair phase. Fibrosis-promoting macrophages appear at this phase, either by the differentiation of newly recruited infiltrating monocytes or through the in situ transformation of previously differentiated infiltrating inflammatory macrophages to a profibrotic type. During this change, there is an activation of STAT6 which promotes IL-4/IL-13-mediated differentiation of pro-

fibrotic macrophages by upregulating the expression of arginase and other profibrotic phenotypic genes. Profibrotic macrophages elicit the activation of fibroblasts to increase extracellular matrix synthesis and secretion. The scar tissue is reformed in the last phase by replacing friable type III collagen with durable and long-lasting type I collagen by significant collagen cross-linking. These modifications are followed by the death of active myofibroblasts and decreased neovascularization. Adipose-derived stem cells (ASCs) are found in the stromal vascular fraction (SVF) of subcutaneous fat tissue. It contains a diverse group of mesenchymal cells. These cells can be separated further by using enzymatic digestion to remove most of the hematopoietic cells from the SVF cells or by combining the filtering and centrifugation procedures as mechanical digestion. ASCs-SVFs can enhance the fibrogenic activity of fibroblasts, which promotes vascularization by enhancing fat tissue survival and 3D organization/ASCs express proangiogenic factors like vascular endothelial growth factor (VEGF), interact with blood vessels perivascularly, and offer physical extracellular matrix guiding signals that lead to endothelial growth [33].

**3.3.2. Hair Regrowth.** To ameliorate the problem of alopecia and enhance hair growth, hair bioengineering has risen to the next level demonstrating new approaches for it. The mesenchymal stem cells are the solution to many problems and can be used even in the treatment of these problems too. Human intra and extradermal adipose tissue-derived hair follicle stem cells (HD-AFSCs) contain hair follicle mesenchymal stem cells (HF-MSCs), and hair follicle epithelial stem cells (HF-ESCs) can be used for the advancement of hair growth

TABLE 1: Summary of studies analysed for use of MSC and their derived exosomes for SARS-CoV-2 infection.

Reference	Therapy used	Intervention	Outcome
Ciccocioppo et al. [91] (n = 1)	Cell therapy	$1.1 \times 10^6$ cells/per kg body weight of MSCs	Improvement of the inflammatory, respiratory, thrombotic, and renal parameters was observed after 2 and 8 days after MSC infusion
Senegaglia et al. [92] (n = 1)	Tocilizumab and allogenic umbilical cord-derived mesenchymal stromal cells	Infusion of 400 mg of tocilizumab and three intravenous infusions of 500,000 Cells per kilogram in alternate days	The relative viral quantification decreased gradually from day zero and was undetectable in day 14 CRP and IL-6 levels were significantly lower from day 3 of infusion, the time for the lymphocyte count to return to the normal range was significantly faster, and lung inflammation absorption was significantly shorter on CT imaging in the hUC-MSC group than in the control group.
Shu et al. [75] (n = 41)	Standard treatment plus umbilical cord mesenchymal stem cell infusion vs. standard treatment	$2 \times 10^6$ cells/kg of MSCs suspended in 100 mL of normal saline	There was a significant improvement in dyspnea while undergoing MSC infusion on days 1, 3, and 5. Additionally, SpO2 was significantly improved following MSC infusion, and chest imaging results were improved in the experimental group in the first month after MSC infusion.
Xu et al. [93] (n = 44)	MSC transplantation along with comprehensive treatment vs. comprehensive treatment only	Three infusions totaling $9 \times 10^7$ MSCs every other day (day 1, day 3, and day 5). Each infusion contained $3 \times 10^7$ cells resuspended in 500 mL saline solution	Intravenous transplantation of hUC-MSCs accelerated partial pulmonary function recovery and improved HRQL, indicating relative safety and preliminary efficacy of this treatment for patients with severe COVID-19
Feng et al. [94] (n = 28)	Human umbilical cord mesenchymal stromal cells along with standard treatment vs. standard treatment	$2 \times 10^6$ cells/kg of MSCs suspended in 100 mL of normal saline	UC-MSC administration was safe and well tolerated and exerted a trend of improvement in whole lung lesion and significantly increased the resolution of lung solid component lesions compared with the placebo.
Shi et al. [95] (n = 100)	UC-MSC vs. placebo	UC-MSC at dose $4 \times 10^7$ cells per infusion on day, 0, 3 and 6 vs. placebo	Laboratory values revealed mean reduction by 32% in neutrophil count, average CD3+, CD4+, and CD8+ lymphocyte counts increasing by 46%, 45%, and 46%, respectively. Likewise, acute phase reactants declined, with mean C-reactive protein, ferritin, and D-dimer reduction of 77%, 43%, and 42%, respectively.
Sengupta et al. [96] (n = 27)	Exosomes (ExoFlo) derived from allogeneic bone marrow mesenchymal stem cells	15 mL of ExoFlo was added to 100 mL of normal saline	After these treatments, most of the laboratory indexes and CT images showed remission of the inflammation symptoms. The counts of CD3+ T cell, CD4+ T cell, and CD8+ T cell remarkably increased to the normal level, indicating the reversal of lymphopenia.
Liang et al. [97] (n = 1)	Human umbilical cord mesenchymal stem cells	Allogenic hUCMSCs given 3 times ( $5 \times 10^7$ cells each time) with a 3-day interval at days 13, 16, and 19, together with thymosin a1 and antibiotics daily injection	The MSC group had a significantly higher Horovitz score of healthy lungs on discharge than the control group.
Haberle et al. [98] (n = 23)	Mesenchymal stromal cells	One million MSCs/kg body weight was infused over 30 minutes, and the process was repeated in 3 patients twice and in 2 patients 3 times	Compared to controls, patients with MSC treatment showed a significantly lower Murray score of lung injury upon discharge than controls.

TABLE 1: Continued.

Reference	Therapy used	Intervention	Outcome
Yilmaz et al. [99] (n = 1)	Mesenchymal stem cells	MSC 1st application/day 1 $3 \times 10^6$ /kg IV 2nd application/day 3 $3 \times 10^6$ /kg IV 3rd application/day 6 $3 \times 10^6$ /kg IV 4th application/day 9 $2 \times 10^6$ /kg + $1 \times 10^6$ /kg intravenous + intrathecal	The application of MSCs has been found to have a healing effect on organs in this patient with severe COVID-19 infection.
Ping et al. [100] (n = 1)	Convalescent plasma and umbilical cord mesenchymal stem cells	$6.5 \times 10^7$ MSCs along with convalescent plasma	Intravenous infusion of CP and MSCs for the treatment of severe COVID-19 patients may have synergistic characteristics in inhibiting cytokine storm, promoting the repair of lung injury, and recovering pulmonary function
Lanzoni et al. [5] (n = 24)	Umbilical cord-mesenchymal stem cells	Subjects in the UC-MSc treatment group received two intravenous infusions of $100 \pm 20 \times 10^6$ UC-MSCs each, in 50 mL vehicle solution containing human serum albumin and heparin.	UC-MSc treatment was associated with a significant reduction in serious adverse events, mortality, and time to recovery, compared with controls. Treatment was associated with significantly improved patient survival (91% vs. 42%) The fraction of inspired O <sub>2</sub> (FiO <sub>2</sub> ) gradually decreased while the oxygen saturation (SaO <sub>2</sub> ) and partial pressure of oxygen (PO <sub>2</sub> ) improved. Additionally, the patients' chest computed tomography showed that bilateral lung exudate lesions were adsorbed after MSC infusion.
Tang et al. [101] (n = 2)	Mesenchymal stem cells	MSC infusion of 100 mL regardless of dose.	The percentage and counts of lymphocyte subsets (CD3+, CD4+, and CD8+ T cell) were increased, and the level of IL-6, TNF- $\alpha$ , and C-reactive protein is significantly decreased after hWJC treatment.
Zhang et al. [102] (n = 1)	Human umbilical cord Wharton's jelly-derived mesenchymal stem cells	$1 \times 10^6$ cells per kilogram of weight of MSC	Oxygenation index was improved, radiological presentations (ground glass opacity) were improved and the lymphocyte count and lymphocyte subsets (CD4+ T cells, CD8+ T cells, and NK cells) count showed recovery after transplantation.
Feng et al. [103] (n = 16)	Umbilical cord mesenchymal stem cells	UC-MSCs of $1 \times 10^8$ cells once. The patients would receive four rounds of transplantation in total, with one-day intervals in between.	Conventional treatment with add-on MSC transplantation brought the cytokine storm under control and attenuate disease progression. MSC mediated growth and differentiation decreased the harm too, and accelerated the recovery of damaged organs resulting in reduced mortality, decreased ICU stay, and a promising safety profile.
Adas et al. [104] (n = 25)	Mesenchymal stem cells	The conventional treatment: piperacillin-tazobactam, favipiravir, dexamethasone, hydroxychloroquine, enoxaparine. Experimental group were administered $3 \times 10^6$ cell/kg MSC by intravenous infusion.	The MSC-treated group demonstrated improved oxygenation index, reduction in the area of pulmonary inflammation, restoration of CT number in the inflamed area along with decreased IgM levels.
Wei et al. [105] (n = 25)	Umbilical cord mesenchymal stem cells	$1 \times 10^6$ cells/kg of MSCs along with conventional therapy vs. conventional therapy	
Meng et al. [74] (n = 18)	Human umbilical cord-derived mesenchymal stem cell	3 cycles of intravenous infusion of UC-MSCs ( $3 \times 10^7$ cells per infusion) on days 0, 3, and 6 for treatment group along with standard COVID treatment regimens vs. standard treatment regimens only	Intravenous UC-MSCs infusion in patients with moderate and severe COVID-19 was safe and well tolerated

TABLE 1: Continued.

Reference	Therapy used	Intervention	Outcome
Kouroupis et al. [106] ( $n = 24$ )	Mesenchymal stem cells	UC-MSC iv infusion	UC-MSC recipients develop significantly increased levels of plasma sTNFR2 and significantly decreased levels of TNF $\alpha$ and TNF $\beta$ , compared to controls indicating decrease of inflammation
Tao et al. [73] ( $n = 1$ )	Umbilical cord blood-derived mesenchymal stem cells	$1.5 \times 10^6$ USB-MSCs per kilogram of the patient's weight infused intravenously every 48 hours, with a total of five-time infusion.	USB-MSCs infusion, lymphocytes increased, and renal function improved, as well as pulmonary static compliance increased significantly and PaO $_2$ /FiO $_2$ ratio maintained stable.
Primorac et al. [72] ( $n = 1$ )	Compassionate mesenchymal stem cell	$10^6$ cells/kg of bone marrow-derived MSC on days 9, 12, and 16 days of hospitalization	MSC administration resulted in a reduction in leukocyte count, D-dimer levels, and CRP-levels, all of which are prognostic factors for COVID-19 severity.
Hashemian et al. [60] ( $n = 11$ )	Mesenchymal stem cells derived from perinatal tissues	3 intravenous infusions ( $200 \times 10^6$ cells) every other day for a total of $600 \times 10^6$ human umbilical cord MSCs (UC-MSCs; 6 cases) or placental MSCs (PL-MSCs; 5 cases).	Significant reductions in serum levels of tumor necrosis factor-alpha, IL-8, and C-reactive protein.

[34]. HF-MSCs show positive staining for CD44, CD73, CD90, and CD 105 which are the surface markers of bone marrow mesenchymal stem cells which has the potential to differentiate [35]. Gentile showed the HD-AFSCs show positivity for CD44, CD100, CD200, and S100A4 which represent the early progeny of stem cells and help in the expression with the growth of keratinocytes [34]. MSC cells express Wnt/ $\beta$ -catenin signalling molecules which have been shown as a fundamental factor that augments hair growth [36, 37]. There also occurs expression of VEGF, TGF- $\beta$ , IGF-1, IGFBP-1to-6, M-CSF, M-CSFR, PDGF, PDGFR- $\beta$ /- $\alpha$ 64, PGE2, and PGF2  $\alpha$  which all contributes in the hair regrowth [38]. Dermal papilla cells (DPCs), a part of autologous stem cells, also play role in the regulation of hair growth and regeneration [38]. DPCs secrete alkaline phosphate which is required in the early anagen period [39]. It expresses  $\alpha$ -smooth muscle actin and versican which are the marker of the dermal papilla and helps in the induction and maintenance of hair growth [40, 41]. It even expresses CD133 which is a stem cell marker and promotes hair follicle neogenesis. The application of MSCs in hair growth would lead to a breakthrough revolution in alopecia. More clinical trials and research are required in this field.

**3.4. COVID-19 Pathophysiology.** COVID-19 is a viral disease caused by SARS-Cov-2 which appeared in Wuhan of China around December 2019 [42]. The virus is an enveloped single-stranded RNA virus that enters the host cell through angiotensinogen converting receptor 2 [43]. The infection can affect the respiratory system, both the upper and lower, ranging from asymptomatic acute infection to subacute and chronic infection leading to fibrosis and scars as well as the dreadful acute respiratory distress syndrome along with multiple organ failure. Besides the respiratory system, it can affect multiple organs and tissues leading to complications like meningitis, encephalitis, myocarditis, acute renal failure, venous thromboembolism, and many more [44].

The virus primarily transmits through saliva, droplets, or respiratory secretions. It enters the cells through the ACE-2 receptor by binding to spike glycoprotein and thus gains entry inside the cells. The host immune system then identifies antigens of the virus, and through antigen-presenting cells, they are presented to CD8 T cells and natural killer cells by incorporating them into a major histocompatibility complex. Thus, both innate and adaptive immune systems of defence are activated. However, in some individuals, the production and secretion of cytokines are massive leading to cytokine storm which leads to coagulopathy and multiple organ failure resulting in death [45]. Another hypothesis that has been explained regarding the pathogenesis of COVID-19 is regarding inhibition of human heme metabolism. The RNA virus has been presumed to bind the beta chain of the porphyrin moiety of red blood cells and thus impairing heme metabolism as well as the release of iron which needs further study to confirm [46]. Multiple cytokines have been associated with COVID-19 infection like TNF alpha, IL-1 beta, and IL-8; however, there has been particular interest in IL 6. The cytokine has been associated with various types of tissue injury like burns, trauma as well as septic shock, and in the case of COVID-19, it has a vital role in the development of cytokine release syndrome [47]. This cytokine which normally plays a role to defend against tissue injuries and infections has also been found to be among the highest level among cytokines associated with severe and critical infection [48]. Thus, tocilizumab, a monoclonal antibody against IL-6, has a therapeutic role that decreases the chance of reducing the combined consequence of mechanical ventilation and demise [49, 50]. TNF alpha is another cytokine that also has been widely studied for its tissue-damaging role in cytokine release syndrome. It is produced by different inflammatory cells like macrophages, T cells, and epithelial cells, and it functions to recruit neutrophils at the site of inflammation-causing airway inflammation

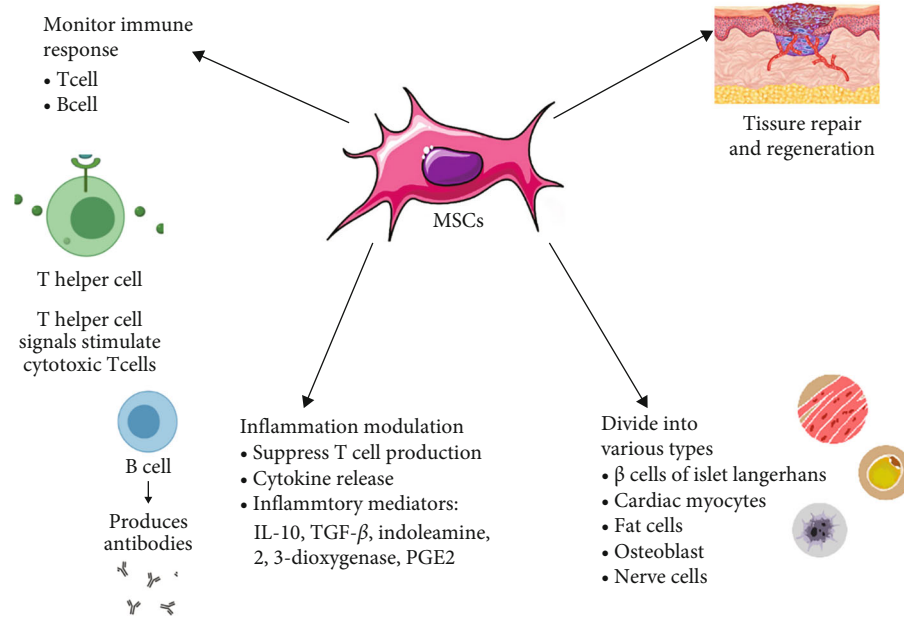


FIGURE 2: Summary of properties of MSC exosomes.

and hyperreactivity [51]. Another important context to discuss regarding the pathogenesis of COVID-19 is the role of the exosome. Exosomes, which are membrane vesicles, are released due to the fusion of the organelle following endocytosis with the plasma membrane [52]. It is believed that the protein of SARS CoV 2 protein interacts with the Rab proteins which is a component of the ESCRT (endosomal sorting complex required for transport) pathway which has a role in the synthesis of exosomes [53]. Similarly, with ganglioside (GM3) enrichment of the exosomes, it was found to be related to the disease severity and probable cause for lymphopenia, as the cells of the immune system would prefer exosomes with GM3 enrichment and thus leading to cellular cytotoxicity [54]. Most viruses are believed to enter the exosome during the synthesis of virion particles as well as spread to the naïve host cells which are not seen in SARS CoV 2, though the experimental studies are present to show that the virus exists in two-layered membrane vesicles. It is thus these extracellular vesicles and the exosomes which might be the potential mediators for infection, reinfection, and subsequent reactivation of the viral particles [55]. The first virus strain that appeared in the seafood market of Wuhan of China and the subsequent strains found in Italy differed in terms of mutation in the spike protein, precisely a missense mutation of aspartate for glycine at 614 (D614G) position and thus account for the difference in demographics factor as well as the viral lethal nature [56]. Similarly, the UK variant (201/501Y.Vq) had S: N501 mutation at RDB (receptor binding domain) which might result in higher binding of spike protein to ACE2. South African (20H/501Y.v2) strain and Brazilian (20J/501Y.V3) strain both had mutation S: E484 at the RDB location resulting in a similar role as the British variation [57]. Then, Delta variant with mutation such as E484Q, P614R, and L452R resulting in easier binding of spikes protein to the ACE-2

receptor, which emerged in India and replaced the existing variant of concerns, Alpha variant that was first reported in the UK, Beta variant of South Africa, and Gamma variant of Brazil, was associated with increased disease severity and rate of viral transmission and was also associated with infections among the vaccinated individual [58, 59]. It is thus important to know the viral pathogenesis and different mutations to ensure that a proper vaccination will work and prevent transmission among individuals to reduce the public health issue that the virus has imposed and the global burden of the ongoing pandemic. The process of action of MSC on patients suffering from SARS-CoV-2 is illustrated in Figure 3.

**3.5. COVID-19 concerning MSC and Their Derived Exosomes.** MSC cells present with multiple biological properties, which include high regenerative capacities and the ability to augment tissue repair [60], but most importantly the cell's ability to control and modulate immune responses is the reason why they are currently being investigated in several clinical diseases to establish them as cellular therapy tools in cases of inflammatory diseases [61]. These cells do not trigger any host responses that can lead to cell rejection thus making them the safer option of all the other kinds of stem cells available. Mesenchymal stem cells (MSCs) are already being used for the treatment of autoimmune disorders, type 2 diabetes, spinal cord injury, and other diseases [62, 63]. The cells are also the suggested potential treatment for H5N1 infection responsible for inducing acute lung injury, similar to what is observed in COVID-19 with inflammatory cytokines [64]. The presence of SARS-CoV2 in the lung induces an uncontrolled generalized immune response. Various immune cells like neutrophils, T-lymphocytes, and macrophages are recruited to the lungs. The leading cause of mortality in COVID-19 patients is hypoxemic

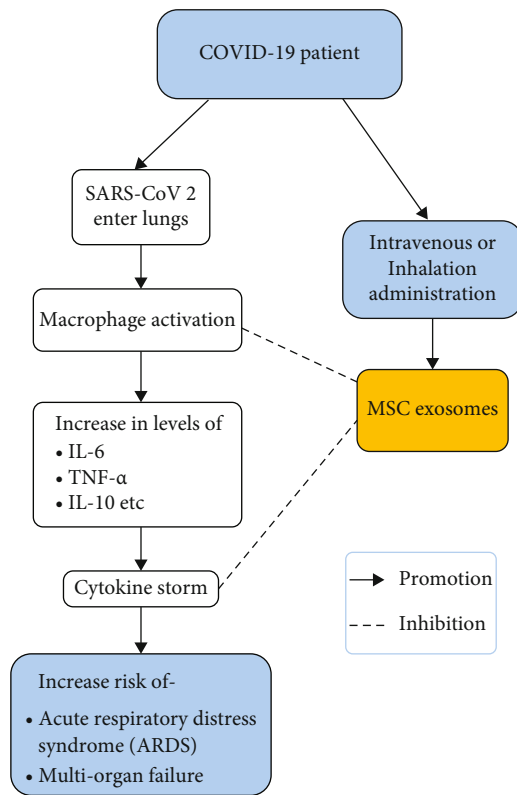


FIGURE 3: Summary of actions of MSC and their derived exosomes on patients with COVID-19.

respiratory failure, which results in acute respiratory distress syndrome (ARDS). When administered intravenously, the cells are trapped within the lung’s capillary beds in a short duration of action, allowing efficient delivery of MSC cells in the lungs making it beneficial in cases of ARDS involving COVID [65–67]. They mitigate the effect of viral disease due to the presence of specific cytokines. MSCs can decrease cytokine storm, replace injured alveolar epithelial cells, and facilitate tissue repair by secreting anti-inflammatory cytokines and antifibrotic growth factors, suppress and modulate immune responses, lower inflammatory effects, and protect the epithelial lining of alveoli during ILI and acute respiratory distress syndrome [68]. Therefore, the immunomodulatory functions of stem cells and MSC exosomes can potentially enable us to use them as a treatment for COVID-19 [69]. As the pandemic is pacing, it is essential to consider various therapeutic options to treat the population. Since the immune system is the main target of the infection, we need to maintain a balance to prevent the exaggerated immune responses that eventually lead to multi-organ failure. The cells stop pulmonary fibrosis, heal the pulmonary circuit and alveolar epithelial lining, treat lung collapse and SARS-CoV 2 associated pneumonia, and improve the overall lung function [70]. Several clinical trials reported the effectiveness and safety of MSCs sequestered from plenty of allogeneic sources. It was noticed that after one dose of stem cell infusion, there was considerable progress in the conditions of these patients without any damaging effects. After two days of stem cell transplantation,

there was marked progress in the respiratory functioning of these subjects [71]. During the clinical trials for the treatment of severely ill patients who had COVID-19-induced ARDS, the majority of the cases who recovered responded substantially in about 48 to 96 hours after the initial infusion of stem cells. The patients who survived were in good health throughout the follow-up evaluation for 60 days. The only adverse effect was temporary shivering and chills, which happened initially in two patients. The shivering was not linked with fever and COVID-19 infection, and it ceased in an hour with the help of supportive treatment [60]. Upon further investigation, the lab findings showed an elevated inflammatory response accompanied by severe thrombocytopenia, D-dimer levels were also found to be high. There were no known signs of pulmonary embolism in the CT pulmonary angiography but there was a progression of bilateral consolidations [72]. Overall, no improvement was observed in radiological findings, CT scan images, and histological findings after the administration of umbilical-cord blood-mesenchymal stem cells (UCB-MSCs), but there was significant consolidation of the lungs which progressed into diffuse lung fibrosis, which commonly occurs in critical COVID-19 patients. Pulmonary fibrosis comes under the category of increasing interstitial pneumonia that occurs due to an exaggerated response of chronic inflammation and healing wound. It is usually started by recurrent injury to the epithelium [73]. MSC cells use and safety profile also requires monitoring in patients with COVID-19 while undergoing treatment because of the multisystem nature of the disease associated with coagulopathy [74]. Another study conducted in Hubei Province where patients were divided into two groups found that of the 12 patients who were treated with hUC-MSC, there was no need for invasive ventilation. No patient progressed from severe to critical illness as the 28-day mortality rate was found to be zero but in the control group, the results were the opposite, in a total of four patients. They progressed to critical illness and, as a result, had to receive invasive ventilation out of which three patients died; hence, the 28-day mortality was calculated to be 10.34%. Although in comparison the differences were not very significant, the improvement trend could be easily traced. In light of this information, it is safe to believe that if the sample size is large, there could be significant differences [75]. Moreover, a noninvasive treatment, hUC-MSC therapy, is a very effective and promising method for clinical application. Table 2 contains a summary of clinical trials recruiting and not yet recruiting aiming to use MSC and their derived exosomes for COVID-19 therapy.

3.6. *Biomolecular Basis of AD-MSCs and Application in COVID-19.* Adipose-derived stem cells (ASCs) are a type of mesenchymal stem cells (MSCs) that can be easily obtained from adipose tissues. They possess regenerative properties similar to that of other MSCs. ASCs differentiate into multiple cell lineages, offering the potential to repair, maintain, or enhance various tissues. They contain various types of cells like preadipocytes, adipocytes, macrophages, endothelial cells, and smooth muscle cells supported by connective tissue and fine capillaries. ASCs have been shown to



TABLE 2: Summary of recruiting and not yet recruiting clinical trials involving use of mesenchymal stem cells in the treatment of COVID-19.

Identifier	Study title	Cell therapy	Intervention (intravenous infusion)	Primary outcome
1	Therapeutic Study to Evaluate the Safety and Efficacy of DW-MSC in COVID 19 Patients ( <i>n</i> = 9)	Allogenic MSC low dose, high dose, and placebo	Drug: allogenic mesenchymal stem cell	Incidence of treatment-emergent adverse event in treatment group
2	Treatment of COVID 19 Patients Using Wharton's Jelly-Mesenchymal Stem Cells ( <i>n</i> = 5)	3 IV doses of WJ-MSCs consisting of $1 * 10^6$ /kg	Wharton's jelly-MSCs	Clinical outcomes followed by CT scan and RT-PCR
3	Application of Umbilical Cord Mesenchymal Stem Cells as Adjuvant Therapy for Critically-Ill Patients ( <i>n</i> = 40)	Umbilical cord-derived MSC/kg body weight in addition to standardised drugs.	Drug: oseltamivir Drug: azithromycin Biological: umbilical cord MSCs	Clinical improvement: presence of dyspnoea, sputum, fever, and ventilation status, blood pressure, heart rate, respiratory rate and oxygen saturation
4	Mesenchymal Stromal Cell-based Therapy for COVID 19 associated Acute Respiratory Distress: a Pilot Clinical Study ( <i>n</i> = 20)	MSC in low dose, intermediate dose, and doses	Mesenchymal stromal cell-based therapy	Intrahospital mortality within 28 days
5	Clinical Research Regarding the Availability and Safety of UC-MSCs Treatment for Serious Pneumonia and Critical Pneumonia caused by 2019-nCoV Infection ( <i>n</i> = 16)	UC-MSCs $3.3 * 10^7$ cell number/50 mL/bag, on 1 <sup>st</sup> , 3 <sup>rd</sup> , 5 <sup>th</sup> , and 7 <sup>th</sup> days after enrolment	Biological: umbilical cord-derived mesenchymal stem cells	Oxygenation index on day 14 after enrolment
6	The Safety of Therapeutic Treatment with Immunomodulatory Mesenchymal Stem Cells in Adults with COVID 19 Infection Requiring Mechanical Ventilation ( <i>n</i> = 45)	BM-Allo. MSC derived from bone marrow (CD73+, CD90+, CD105+, CD14-, CD34-, CD45-, and HLA-DR-)	Biological: BM-Allo. MSC	Incidence of adverse effects, mortality within 30 days, cause of death within 30 days, number of ventilation free days within 60 days of randomisation
7	Treatment of COVID 19 Induced Acute Respiratory Distress: A Phase 2 Study of Intravenous Administration of Allogenic Adipose Derived Mesenchymal Stem Cells ( <i>n</i> = 100)	COVI-MSC 2 vials on day 0, day 2, and day 4	Biological: COVI-MSC	All-cause mortality rate at day 28
8	Safety and Feasibility of Allogenic Mesenchymal Stromal Cells in the Treatment of COVID 19 ( <i>n</i> = 10)	$1 * 10^6$ MSCs/kg body weight mesenchymal stromal cell infusions	Biological: mesenchymal stromal cells infusion	Overall survival [time frame: 60 days]
9	A Phase 1/2a Study of the Safety and Efficacy of BX-U001 for the Treatment of Severe COVID-19 Pneumonia with Moderate to Severe ARDS ( <i>n</i> = 39)	Single infusion of hUC-MCS product at dose of 0.5 million cells/kg	Biological: human umbilical cord mesenchymal stem cells+ supportive care	Incidence of infusion-related adverse events [time frame-day 3] and incidence of any treatment emergent adverse events and treatment emergent serious adverse events [time frame: day 28]
10	Prospective, Randomized Phase 2 Clinical Trial of MSCs for the Treatment of COVID-19 ( <i>n</i> = 20)	Experimental: MSCs at dose $2 * 10^6$ /kg MSCs on day 1 and day 7 in addition to standard of care	Drug: mesenchymal stem cells	Overall survival [time frame-30 days postintervention]
11	A Prospective Double-blind, Randomized, Parallel, Placebo controlled Pilot Clinical Trial for the Evaluation of the Efficacy and Safety of Two Doses of WJ-MSC in Patients with ARDS Secondary to Infection by COVID-19 ( <i>n</i> = 30)	Experimental-Wharton-jelly MSCs on day 1 and day 3	Drug: XCEL-UMC-BETA	All-cause mortality at day 28
12	Mesenchymal Stromal Cells for the Treatment of Moderate to Severe COVID-19 ARDS ( <i>n</i> = 223)	Experimental-infusion of remestemcel-L $2 * 10^6$ MSC/kg body weight plus standard of care	Biological: remestemcel-L Drug: placebo	Number of all-cause mortalities within 30 days of randomisation

TABLE 2: Continued.

Identifier	Study title	Cell therapy	Intervention (intravenous infusion)	Primary outcome
13 NCT04339660	Clinical Research of Human MSCs in the Treatment of COVID-19 Pneumonia (n = 30)	Experimental: $1 \times 10^6$ cells/kg of weight of MSCs	Biological: UC-MSCs	The immune function-improvement and evaluative of pneumonia change
14 NCT04798716	MSC Exosomes for the Treatment of COVID-19 Positive Patients with ARDS and/or Novel Coronavirus Pneumonia (n = 55)	MSC-exosomes escalating dose every other day for a period of 5 days. Conventional treatment plus 4 times of UC-MSCs ( $0.5 \times 10^6$ UC-MSCs/kg body weight IV on day 1, 3, 5, and 7)	Drug: MSC-exosomes delivered IV every other day on escalating day Biological: UC-MSCs Drug: placebo	Treatment-related adverse events as assessed by CTCAE v4; for patients receiving ARDOXSO™, perinatal MSC-derived exosome therapy [time frame 90 days]
15 NCT04273646	Clinical Study of Human Umbilical Cord MSCs in the Treatment of Severe COVID 19 (n = 48)			Pneumonia severity index (time frame- 0 to 12 weeks after treatment) and oxygenation index (PaO2/FiO2)
16 NCT04537351	A Pilot, Open-label, Randomised Controlled Clinical Trial to Investigate Early Efficacy of CYP-001 in Adults Admitted to Intensive Care with Respiratory Failure (n = 24)	Experimental: CYP-001 IV infusion of 2 million Cymerus MSCs/kg body weight	Biological- CYP-001	Trend in trajectory of PaO2/FiO2 ratio [time frame- 7 days]
17 NCT04445220	A Multicentre, Randomised, Case controlled, Double-Blind, Ascending-dose study of Extracorporeal MSC in COVID-19 Subjects with Acute Kidney Injury Receiving Renal Replacement Therapy (n = 22)	Experimental: low dose and high dose SBI-101 device containing MSCs	Biological- SBI-101	Safety and tolerability as measured by incidence of IP-related serious adverse events [time frame- adverse events through day 180]
18 NCT04798066	HBPCOV01: Intermediate Size Patient Population Expanded Access Protocol to Evaluate the Safety and Efficacy of HB-adMSCs for the Treatment of Patients with Post COVID-19 Syndrome.	Autologous adipose-derived MSCs with a treatment duration of 14 weeks	Biological: HB-adMSCs	Treatment outcomes and adverse effects
19 NCT04456439	Intermediate size Expanded Access of Remestemcel-L, Human Mesenchymal Stromal Cells, for Multisystem Inflammatory Syndrome in Children Associated with Coronavirus Disease (COVID 19) (n = )	Remestemcel-L – participants may receive upto 2 infusions of $2 \times 10^6$ L within a 5-day period Drug: hydrocortisone receiving and diphenhydramine receiving participants 30 minutes prior to the infusion of remestemcel-L	Biological: remestemcel-L Drug: hydrocortisone and diphenhydramine	Treatment outcomes and adverse effects

demonstrate the ability to proliferate in a culture medium greater than other MSCs. Various receptor pathways regulate ASC proliferation and differentiation. FGFRs and the ErbB tyrosine kinase receptor family are involved in the control of both the growth and differentiation of ASCs [76, 77]. Increased Akt activity plays a crucial role in this process, as well as through the parallel downregulation of EGFR and ErbB2 expression, and Erk-1 activity [78]. Also, it is known that the degree of tissue growth and regeneration is based on the level of formation of new blood vessels known as neoangiogenesis [79]. Studies suggest that neovascularization and adipogenesis interact through paracrine signalling and occur in a coupled manner throughout adult life. Recent studies indicate that ASCs and MSCs are capable to promote neoangiogenesis through the secretion of growth factors, in particular VEGF [79–81]. Since human adipose tissue is easily obtained in large quantities using a minimally invasive procedure, the use of autologous ASCs is promising for both regenerative medicine and organs damaged by injury and disease, leading to a rapidly increasing field of research.

The application of stem cells as potential therapeutic strategies has shown promising results in vitro experiments and pre-clinical studies. After bone marrow, adipose tissue is regarded as the most estimable source for the cultivation of MSCs, with a total estimate of 98–100% cell viability [82]. The large quantity and facile access to the cells via liposuction procedures prove to be of great advantage when combating COVID-19-induced pneumonia. Thirteen such severe cases of COVID-19 consisting of patients under invasive mechanical ventilation support were administered doses of allogenic adipose stem cells. These cases later presented favourable clinical and biological outcomes. Another study conducted by Zheng et al. to demonstrate the safety of intravenous administration of allogeneic ASCs in patients with ARDS resulted in a short-term improvement of oxygenation in the body [83]. In most clinical cases, no adverse events were reported concerning cell therapy. The treatment with AT-MSC showed a decrease in levels of inflammatory parameters (C-reactive protein, IL-6, ferritin, LDH, and d-dimer) along with an increase in lymphocytes, especially in the patients who showed clinical improvement [84]. These results comply with ASCs' ability to differentiate into multiple cell lineages along with the secretion of various cytokines, and other immunomodulatory properties [85]. These adipose tissue grafts typically involve a minimum of two cell type mature adipocytes and stromal vascular fraction (SVF). SVF incorporates endothelial cells, smooth muscle cells, leukocytes, mast cells, preadipocytes, pericytes, and multipotent adipose-derived stem cells (ASCs) coming together to form a heterogeneous cell population [86]. Other studies have highlighted the potential use of AD-MSCs in regeneration of damaged tissue through the use of exosomes and microRNAs. The excessive secretory action by SVFs and AD-MSCs makes them a fitting vehicle for the delivery of drug molecules in the cellular microenvironment [87]. The results of antimicrobial activity of mesenchymal stem cells carried out by Francisca A. Miranda provides credible insights into adipocyte-secreted exosomal microRNA (A-SE-miR) function and potential use as an antiviral [88]. On this basis, ASC treatments may reduce the demand for critical hospital resources in COVID-19 patients.

## 4. Discussion

From our studies which include 22 analyzed studies with the use of mesenchymal cells and their derived exosomes and 17 ongoing clinical trials involving the use of mesenchymal cells in the treatment of COVID-19, significant data involving therapeutic use of MSCs concerning COVID-19 was extracted. Out of those analyzed studies, four studies demonstrated that the use of mesenchymal cells and their exosomes are found to be safe and well-tolerated by patients with COVID-19. It is to be noted that MSC exosomes are found to be superior to MSC alone in terms of safety owing to being smaller with a lesser immunological response which leads to free movement in blood capillaries without clumping and also cannot further divide, thus reducing the oncogenic potential of MSC derived exosomes as compared to MSC only [89]. Improvement in oxygenation was shown in four studies. These oxygenation parameters are reported in terms of improved SpO<sub>2</sub> following infusion of MSC, decreasing FiO<sub>2</sub> with improved PaO<sub>2</sub> and SaO<sub>2</sub>, PaO<sub>2</sub>/FiO<sub>2</sub> ratio, and oxygenation index. Six studies demonstrated that the lungs healed with the use of exosomes compared to how they presented initially at the hospital. MSCs are found to increase the angiogenesis process and alveolar reepithelization, reducing markers like TNF alpha, TGF beta, and COL I and III, reducing the growth of myofibroblasts and increasing survivability of endothelium leading to attenuated pulmonary fibrosis and even reversing them [90]. Similarly, two studies focused on the improvement of renal function. As many as eleven studies showed that there was a significant reduction in inflammatory cells and inflammatory markers. A review by Shetty et al. demonstrated that the use of mesenchymal cells can increase the release of different factors leading to protection of epithelium of alveoli with decreased fibrosis and hence better lung physiology [60]. Such cells are responsible for decreasing inflammatory response, with regulated immunity ultimately leading to protection of respiratory cells at times of severity like ARDS and acute lung injury [71]. Improvement of radiological presentation as clearing of CT findings of bilateral lung exudate or ground-glass opacity or chest X-ray findings was demonstrated by six studies. Two studies demonstrated that the use of exosomes could reduce the deadly cytokine storm. With the combined efforts of the proliferation of the epithelium, modulated immune response, and removal of excess fluid from alveoli, this can reduce the damage induced by the virus in lung parenchyma as well as the body systems leading to a reduction in the cytokine storm. As many as 12 studies demonstrated that mesenchymal stem cells do have an important role to improve patients' survival and reduction of mortality. As for ongoing registered clinical trials, four of them will be focusing on oxygen saturation following the use of exosomes. Six of the clinical trials will look for treatment-emergent adverse effects during therapy.

## 5. Conclusion and Future Perspectives

From this review, we can conclude that the use of mesenchymal stem cells or their exosomes is safe and well-tolerated in

patients with COVID-19. It improves different parameters of oxygenation and helps in the healing of the lungs. The viral load along with different inflammatory cells and biomarkers of inflammation tends to decrease. Chest X-ray, CT scan, and different radiological tools are used to show improvement and reduced ongoing destructive processes. Similarly, the severe form of COVID-19 infection, ARDS, and different complications of a cytokine storm are attenuated following MSC therapy. Thus, it tends to reduce morbidity and mortality leading to improved inpatient survival and reducing the length of ICU stay. MSC and MSC like derivatives are found to have shown promising results in terms of safety and suitability in the early stage of initiation. Exosomes that are released from MSCs are currently a novel way to treat COVID-19 infection owing to their role in immune system modulation and regenerative characteristics. Our systemic review has several limitations like there is only a small number of studies that have been recruited in the review. Each study has its heterogeneity in the design of studies and demographics of the population included. Similarly, each included studies have its limitations. Further, cohorts and randomised controlled trials with a larger sample size in this particular field of interest should be done to uncover the reality of its effect in COVID-19. Larger cohorts and clinical trials with greater sample sizes are required to uncover the current findings like its efficacy, potency, and timing of dosing with even greater consistency and accuracy. Similarly, additional emphasis should be given to standardizing the treatment and building protocols to upgrade the standard of care in the ongoing pandemic. Ongoing clinical trials should be completed properly to add something to the existing literature as well as in patient care.

## Consent

Consent is not necessary.

## Conflicts of Interest

The authors declare no conflict of interest, financial, or otherwise.

## Acknowledgments

We would like to thank the Peer Research Mentorship Programme (PRMP) started by the International Society for Chronic Illnesses (ISCI) for their support (mentors: Amaan Javed, Mentee: Anagha Shree Kapil, Zeba Sami, Zuha Khan, Saurab Karki, Biki Kumar Sah, Sara Saxena, and Shankhaneel Ghosh. The International Society for Chronic Illnesses (ISCI) helped all the authors by providing research mentors to reviewers and other required support. This article was prepared by the International Society for Chronic Illnesses by Amaan Javed, Saurab Karki, Zeba Sami, Zuha Khan, Anagha Shree Kapil, Biki Kumar Sah, Shankhaneel Ghosh, and Sara Saxena.

## References

- [1] M. Cascella, M. Rajnik, A. Cuomo, S. C. Dulebohn, and R. di Napoli, *Features, Evaluation and Treatment Coronavirus (COVID-19)*, StatPearls. StatPearls Publishing, United States, 2020.
- [2] A. C. Walls, Y. J. Park, M. A. Tortorici, A. Wall, A. T. McGuire, and D. Veessler, "Structure, function, and antigenicity of the SARS-CoV-2 spike glycoprotein," *Cell*, vol. 181, no. 2, pp. 281–292.e6, 2020.
- [3] J. de Seze and C. Lebrun-Frenay, "Covid-19, the pandemic war: implication for neurologists," *Revue Neurologique*, vol. 176, no. 4, pp. 223–224, 2020.
- [4] J. Bartolucci, F. J. Verdugo, P. L. González et al., "Safety and efficacy of the intravenous infusion of umbilical cord mesenchymal stem cells in patients with heart failure: a phase 1/2 randomized controlled trial (RIMECARD trial [randomized clinical trial of intravenous infusion umbilical cord mesenchymal stem cells on cardiopathy])," *Circulation Research*, vol. 121, no. 10, pp. 1192–1204, 2017.
- [5] G. Lanzoni, E. Linetsky, D. Correa et al., "Umbilical cord mesenchymal stem cells for COVID-19 acute respiratory distress syndrome: a double-blind, phase 1/2a, randomized controlled trial," *Stem Cells Translational Medicine*, vol. 10, no. 5, pp. 660–673, 2021.
- [6] M. Wang, Q. Yuan, and L. Xie, "Mesenchymal stem cell-based immunomodulation: properties and clinical application," *Stem Cells International*, vol. 2018, Article ID 3057624, 12 pages, 2018.
- [7] M. J. Page, J. E. McKenzie, P. M. Bossuyt et al., "The PRISMA 2020 statement: an updated guideline for reporting systematic reviews," *BMJ*, vol. 372, 2021.
- [8] J. Galipeau and L. Sensébé, "Mesenchymal stromal cells: clinical challenges and therapeutic opportunities," *Cell Stem Cell*, vol. 22, no. 6, pp. 824–833, 2018.
- [9] J. Behnke, S. Kremer, T. Shahzad et al., "MSC based therapies-new perspectives for the injured lung," *Journal of Clinical Medicine*, vol. 9, no. 3, article 682, 2020.
- [10] H. M. Lazarus, S. E. Haynesworth, S. L. Gerson, and A. I. Caplan, "Human bone marrow-derived mesenchymal (stromal) progenitor cells (MPCs) cannot be recovered from peripheral blood progenitor cell collections," *Journal of Hematotherapy and Stem Cell Research*, vol. 6, no. 5, pp. 447–455, 1997.
- [11] M. Dauletova, H. Hafsan, N. Mahhengam, A. O. Zekiy, M. Ahmadi, and H. Siahmansouri, "Mesenchymal stem cell alongside exosomes as a novel cell-based therapy for COVID-19: a review study," *Clinical Immunology (Orlando, Fla.)*, vol. 226, p. 108712, 2021.
- [12] Y. Chen, S. Chen, L. Y. Liu et al., "Mesenchymal stem cells ameliorate experimental autoimmune hepatitis by activation of the programmed death 1 pathway," *Immunology Letters*, vol. 162, no. 2, Part B, pp. 222–228, 2014.
- [13] W. Wang, H. Guo, H. Li et al., "Interleukin-35 gene-modified mesenchymal stem cells protect concanavalin A-induced fulminant hepatitis by decreasing the interferon gamma level," *Human Gene Therapy*, vol. 29, no. 2, pp. 234–241, 2018.
- [14] F. E. Tögel and C. Westenfelder, "Mesenchymal stem cells: a new therapeutic tool for AKI," *Nature Reviews Nephrology*, vol. 6, no. 3, pp. 179–183, 2010.

- [15] K. English, A. French, and K. J. Wood, "Mesenchymal stromal cells: facilitators of successful transplantation?," *Stem Cell*, vol. 7, no. 4, pp. 431–442, 2010.
- [16] D. Garcia-Olmo, D. Herreros, I. Pascual et al., "Expanded adipose-derived stem cells for the treatment of complex perianal fistula: a phase II clinical trial," *Diseases of the Colon and Rectum*, vol. 52, no. 1, pp. 79–86, 2009.
- [17] D. García-Olmo, M. García-Arranz, D. Herreros, I. Pascual, C. Peiro, and J. A. Rodríguez-Montes, "A phase I clinical trial of the treatment of Crohn's fistula by adipose mesenchymal stem cell transplantation," *Diseases of the Colon and Rectum*, vol. 48, no. 7, pp. 1416–1423, 2005.
- [18] R. H. Liu, Y. Q. Li, W. J. Zhou, Y. J. Shi, L. Ni, and G. X. Liu, "Supplementing mesenchymal stem cells improves the therapeutic effect of hematopoietic stem cell transplantation in the treatment of murine systemic lupus erythematosus," *Transplantation Proceedings*, vol. 46, no. 5, pp. 1621–1627, 2014.
- [19] S. Ji, Q. Guo, Y. Han, G. Tan, Y. Luo, and F. Zeng, "Mesenchymal stem cell transplantation inhibits abnormal activation of Akt/GSK3 $\beta$  signaling pathway in T cells from systemic lupus erythematosus mice," *Cellular Physiology and Biochemistry: International Journal of Experimental Cellular Physiology, Biochemistry, and Pharmacology*, vol. 29, no. 5–6, pp. 705–712, 2012.
- [20] D. Wang, H. Zhang, J. Liang et al., "A long-term follow-up study of allogeneic mesenchymal stem/stromal cell transplantation in patients with drug-resistant systemic lupus erythematosus," *Stem Cell Reports*, vol. 10, no. 3, pp. 933–941, 2018.
- [21] E. W. Choi, I. S. Shin, S. Y. Park et al., "Reversal of serologic, immunologic, and histologic dysfunction in mice with systemic lupus erythematosus by long-term serial adipose tissue-derived mesenchymal stem cell transplantation," *Arthritis and Rheumatism*, vol. 64, no. 1, pp. 243–253, 2012.
- [22] T. Liu, X. Zhang, S. Gao et al., "Exosomal long noncoding RNA CRNDE-h as a novel serum-based biomarker for diagnosis and prognosis of colorectal cancer," *Oncotarget*, vol. 7, no. 51, pp. 85551–85563, 2016.
- [23] N. Joyce, G. Annett, L. Wirthlin, S. Olson, G. Bauer, and J. A. Nolta, "Mesenchymal stem cells for the treatment of neurodegenerative disease," *Regenerative Medicine*, vol. 5, no. 6, pp. 933–946, 2010.
- [24] A. R. R. Weiss and M. H. Dahlke, "Immunomodulation by mesenchymal stem cells (MSCs): mechanisms of action of living, apoptotic, and dead MSCs," *Frontiers in Immunology*, vol. 10, article 1191, 2019.
- [25] V. Karantalis, D. L. DiFede, G. Gerstenblith et al., "Autologous mesenchymal stem cells produce concordant improvements in regional function, tissue perfusion, and fibrotic burden when administered to patients undergoing coronary artery bypass grafting: the prospective randomized study of mesenchymal stem cell therapy in patients undergoing cardiac surgery (PROMETHEUS) trial," *Circulation Research*, vol. 114, no. 8, pp. 1302–1310, 2014.
- [26] M. A. Matthay, S. Pati, and J. W. Lee, "Concise review: mesenchymal stem (stromal) cells: biology and preclinical evidence for therapeutic potential for organ dysfunction following trauma or sepsis," *Stem Cells*, vol. 35, no. 2, pp. 316–324, 2017.
- [27] Y. Guo, Y. Yu, S. Hu, Y. Chen, and Z. Shen, "The therapeutic potential of mesenchymal stem cells for cardiovascular diseases," *Cell Death and Disease*, vol. 11, no. 5, pp. 1–10, 2020.
- [28] K.-S. Cho and H.-J. Roh, "Immunomodulatory effects of adipose-derived stem cells in airway allergic diseases," *Current Stem Cell Research & Therapy*, vol. 5, no. 2, pp. 111–115, 2010.
- [29] M. Goodwin, V. Sueblinwong, P. Eisenhauer et al., "Bone marrow-derived mesenchymal stromal cells inhibit Th2-mediated allergic airways inflammation in mice," *Stem Cells*, vol. 29, no. 7, pp. 1137–1148, 2011.
- [30] F. Wang, M. Yu, X. Yan et al., "Gingiva-derived mesenchymal stem cell-mediated therapeutic approach for bone tissue regeneration," *Stem Cells and Development*, vol. 20, no. 12, pp. 2093–2102, 2011.
- [31] M. A. González, E. González-Rey, L. Rico, D. Büscher, and M. Delgado, "Treatment of experimental arthritis by inducing immune tolerance with human adipose-derived mesenchymal stem cells," *Arthritis and Rheumatism*, vol. 60, no. 4, pp. 1006–1019, 2009.
- [32] M. G. Scioli, G. Storti, F. D'amico et al., "Adipose-derived stem cells in cancer progression: new perspectives and opportunities," *International Journal of Molecular Sciences*, vol. 20, no. 13, p. 3296, 2019.
- [33] P. Gentile and S. Garcovich, "Concise review: adipose-derived stem cells (ASCs) and adipocyte-secreted exosomal microRNA (A-SE-miR) modulate cancer growth and promote wound repair," *Journal of Clinical Medicine*, vol. 8, no. 6, article 855, 2019.
- [34] P. Gentile, "Autologous cellular method using micrografts of human adipose tissue derived follicle stem cells in androgenic alopecia," *International Journal of Molecular Sciences*, vol. 20, no. 14, article 3446, 2019.
- [35] T. L. Ramos, L. I. Sánchez-Abarca, S. Muntión et al., "MSC surface markers (CD44, CD73, and CD90) can identify human MSC-derived extracellular vesicles by conventional flow cytometry," *Cell Communication and Signaling: CCS*, vol. 14, no. 1, pp. 1–14, 2016.
- [36] D. Talavera-Adame, D. Newman, and N. Newman, "Conventional and novel stem cell based therapies for androgenic alopecia," *Stem Cells and Cloning: Advances and Applications*, vol. 10, pp. 11–19, 2017.
- [37] E. Taghiabadi, M. A. Nilforoushzadeh, and N. Aghdami, "Maintaining hair inductivity in human dermal papilla cells: a review of effective methods," *Skin Pharmacology and Physiology*, vol. 33, no. 5, pp. 280–292, 2020.
- [38] M. Rendl, L. Polak, and E. Fuchs, "BMP signaling in dermal papilla cells is required for their hair follicle-inductive properties," *Genes & Development*, vol. 22, no. 4, pp. 543–557, 2008.
- [39] S. R. Kim, S. Y. Cha, M. K. Kim, J. C. Kim, and Y. K. Sung, "Induction of versican by ascorbic acid 2-phosphate in dermal papilla cells," *Journal of Dermatological Science*, vol. 43, no. 1, pp. 60–62, 2006.
- [40] Y. Ito, T. S. Hamazaki, K. Ohnuma, K. Tamaki, M. Asashima, and H. Okochi, "Isolation of murine hair-inducing cells using the cell surface marker prominin-1/CD133," *The Journal of Investigative Dermatology*, vol. 127, no. 5, pp. 1052–1060, 2007.
- [41] C. A. B. Jahoda, A. J. Reynolds, C. Chaponnier, J. C. Forester, and G. Gabbiani, "Smooth muscle alpha-actin is a marker for hair follicle dermis in vivo and in vitro," *Journal of Cell Science*, vol. 99, no. 3, pp. 627–636, 1991.

- [42] C. Huang, Y. Wang, X. Li et al., "Clinical features of patients infected with 2019 novel coronavirus in Wuhan, China," *The Lancet*, vol. 395, no. 10223, pp. 497–506, 2020.
- [43] Y. Wan, J. Shang, R. Graham, R. S. Baric, and F. Li, "Receptor recognition by the novel coronavirus from Wuhan: an analysis based on decade-long structural studies of SARS coronavirus," *Journal of Virology*, vol. 94, no. 7, 2020.
- [44] A. Javed, "Neurological associations of SARS-CoV-2 infection: a systematic review," *CNS & Neurological Disorders Drug Targets*, vol. 21, no. 3, pp. 246–258, 2022.
- [45] M. Soy, G. Keser, P. Atagündüz, F. Tabak, I. Atagündüz, and S. Kayhan, "Cytokine storm in COVID-19: pathogenesis and overview of anti-inflammatory agents used in treatment," *Clinical Rheumatology*, vol. 39, no. 7, pp. 2085–2094, 2020.
- [46] R. J. Read, "Flawed methods in COVID-19: attacks the 1-beta chain of hemoglobin and captures the porphyrin to inhibit human heme metabolism," 2020.
- [47] D. Darif, I. Hammi, A. Kihel, I. el Idrissi Saik, F. Guessous, and K. Akarid, "The pro-inflammatory cytokines in COVID-19 pathogenesis: what goes wrong?," *Microbial Pathogenesis*, vol. 153, article 104799, 2021.
- [48] H. Han, Q. Ma, C. Li et al., "Profiling serum cytokines in COVID-19 patients reveals IL-6 and IL-10 are disease severity predictors," *Emerging Microbes & Infections*, vol. 9, no. 1, pp. 1123–1130, 2020.
- [49] C. Salama, J. Han, L. Yau et al., "Tocilizumab in patients hospitalized with Covid-19 pneumonia," *The New England Journal of Medicine*, vol. 384, no. 1, pp. 20–30, 2021.
- [50] X. Xu, M. Han, T. Li et al., "Effective treatment of severe COVID-19 patients with tocilizumab," *Proceedings of the National Academy of Sciences of the United States of America*, vol. 117, no. 20, pp. 10970–10975, 2020.
- [51] C. H. Yan, F. Faraji, D. P. Prajapati, C. E. Boone, and A. S. DeConde, "Association of chemosensory dysfunction and COVID-19 in patients presenting with influenza-like symptoms," *International Forum of Allergy & Rhinology*, vol. 10, no. 7, pp. 806–813, 2020.
- [52] M. Simons and G. Raposo, "Exosomes - vesicular carriers for intercellular communication," *Current Opinion in Cell Biology*, vol. 21, no. 4, pp. 575–581, 2009.
- [53] W. B. Kannel and T. Gordon, "Evaluation of cardiovascular risk in the elderly: the Framingham study," *Bulletin of the New York Academy of Medicine*, vol. 54, no. 6, pp. 573–591, 1978.
- [54] S. Kumar, A. Veldhuis, and T. Malhotra, "Neuropsychiatric and cognitive sequelae of COVID-19," *Frontiers in Psychology*, vol. 12, pp. 1–6, 2021.
- [55] A. V. Vlassov, S. Magdaleno, R. Setterquist, and R. Conrad, "Exosomes: current knowledge of their composition, biological functions, and diagnostic and therapeutic potentials," *Biochimica et Biophysica Acta (BBA)-General Subjects*, vol. 1820, no. 7, pp. 940–948, 2012.
- [56] S. Isabel, L. Graña-Miraglia, J. M. Gutierrez et al., "Evolutionary and structural analyses of SARS-CoV-2 D614G spike protein mutation now documented worldwide," *Scientific Reports*, vol. 10, no. 1, pp. 14031–14039, 2020.
- [57] B. J. Bosch, R. van der Zee, C. A. M. de Haan, and P. J. M. Rotter, "The coronavirus spike protein is a class I virus fusion protein: structural and functional characterization of the fusion core complex," *Journal of Virology*, vol. 77, no. 16, pp. 8801–8811, 2003.
- [58] S. Alexandar, M. Ravisankar, R. S. Kumar, and K. Jakkam, "A comprehensive review on Covid-19 Delta variant," *International Journal of Pharmacology and Clinical Research (IJPCR)*, vol. 7, no. 5, pp. 83–85, 2021.
- [59] Y. Liu, J. Liu, B. A. Johnson et al., "Delta spike P681R mutation enhances SARS-CoV-2 fitness over Alpha variant. bioRxiv: the preprint server for biology," *Cell Reports*, vol. 39, no. 7, article 110829, 2021.
- [60] S. M. R. Hashemian, R. Aliannejad, M. Zarrabi et al., "Mesenchymal stem cells derived from perinatal tissues for treatment of critically ill COVID-19-induced ARDS patients: a case series," *Stem Cell Research & Therapy*, vol. 12, no. 1, pp. 1–12, 2021.
- [61] K. le Blanc and D. Mougiakakos, "Multipotent mesenchymal stromal cells and the innate immune system," *Nature Reviews Immunology*, vol. 12, no. 5, pp. 383–396, 2012.
- [62] K. le Blanc, I. Rasmusson, B. Sundberg et al., "Treatment of severe acute graft-versus-host disease with third party haploidentical mesenchymal stem cells," *The Lancet*, vol. 363, no. 9419, pp. 1439–1441, 2004.
- [63] X.-L. Fan, Y. Zhang, X. Li, and Q.-L. Fu, "Mechanisms underlying the protective effects of mesenchymal stem cell-based therapy," *Cellular and Molecular Life Sciences*, vol. 77, no. 14, pp. 2771–2794, 2020.
- [64] I. Darwish, S. Mubareka, and W. C. Liles, "Immunomodulatory therapy for severe influenza," *Expert Review of Anti-Infective Therapy*, vol. 9, no. 7, pp. 807–822, 2011.
- [65] X. Fu, G. Liu, A. Halim, Y. Ju, Q. Luo, and G. Song, "Mesenchymal stem cell migration and tissue repair," *Cell*, vol. 8, no. 8, article 784, 2019.
- [66] A. Sohni and C. M. Verfaillie, "Mesenchymal stem cells migration homing and tracking," *Stem Cells International*, vol. 2013, 8 pages, 2013.
- [67] R. H. Lee, A. A. Pulin, M. J. Seo et al., "Intravenous hMSCs improve myocardial infarction in mice because cells embolized in lung are activated to secrete the anti-inflammatory protein TSG-6," *Cell Stem Cell*, vol. 5, no. 1, pp. 54–63, 2009.
- [68] L. Rezakhani, A. F. Kelishadrokh, A. Soleimanizadeh, and S. Rahmati, "Mesenchymal stem cell (MSC)-derived exosomes as a cell-free therapy for patients infected with COVID-19: real opportunities and range of promises," *Chemistry and Physics of Lipids*, vol. 234, article 105009, 2021.
- [69] K. M. Jayaramayya, "Immunomodulatory Effect of Mesenchymal Stem Cells and Mesenchymal Stem-Cell-Derived Exosomes for COVID-19 Treatment," *BMB Reports*, vol. 53, no. 8, article 400, 2020.
- [70] A. Golchin, E. Seyedjafari, and A. Ardeshirylajimi, "Mesenchymal Stem Cell Therapy for COVID-19: Present or Future," *Stem Cell Reviews And Reports*, vol. 16, no. 3, pp. 427–433, 2020.
- [71] S. Gupta, V. Krishnakumar, Y. Sharma, A. K. Dinda, and S. Mohanty, "Mesenchymal stem cell derived exosomes: a nano platform for therapeutics and drug delivery in combating COVID-19," *Stem Cell Reviews and Reports*, vol. 17, no. 1, pp. 33–43, 2021.
- [72] D. Primorac, S. Stojanović, M. S. Stipić et al., "Compassionate mesenchymal stem cell treatment in a severe COVID-19 patient: a case report," *Croatian Medical Journal*, vol. 62, no. 3, pp. 288–296, 2021.
- [73] J. Tao, Y. Nie, H. Wu et al., "Umbilical cord blood-derived mesenchymal stem cells in treating a critically ill COVID-

- 19 patient,” *The Journal of Infection in Developing Countries*, vol. 14, no. 10, pp. 1138–1145, 2020.
- [74] F. Meng, R. Xu, S. Wang et al., “Human umbilical cord-derived mesenchymal stem cell therapy in patients with COVID-19: a phase 1 clinical trial,” *Signal Transduction and Targeted Therapy*, vol. 5, no. 1, pp. 1–7, 2020.
- [75] L. Shu, C. Niu, R. Li et al., “Treatment of severe COVID-19 with human umbilical cord mesenchymal stem cells,” *Stem Cell Research & Therapy*, vol. 11, no. 1, pp. 1–11, 2020.
- [76] M. G. Scioli, A. Bielli, P. Gentile, D. Mazzaglia, V. Cervelli, and A. Orlandi, “The biomolecular basis of adipogenic differentiation of adipose-derived stem cells,” *International Journal of Molecular Sciences*, vol. 15, no. 4, pp. 6517–6526, 2014.
- [77] M. H. Flågå, S. Knappskog, B. P. Haynes, P. E. Lønning, and G. Mellgren, “Inverse regulation of EGFR/HER1 and HER2-4 in normal and malignant human breast tissue,” *PLoS One*, vol. 8, no. 8, article e74618, 2013.
- [78] F. Bost, M. Aouadi, L. Caron, and B. Binétruy, “The role of MAPKs in adipocyte differentiation and obesity,” *Biochimie*, vol. 87, no. 1, pp. 51–56, 2005.
- [79] Y. Cao, “Angiogenesis modulates adipogenesis and obesity,” *The Journal of Clinical Investigation*, vol. 117, no. 9, pp. 2362–2368, 2007.
- [80] T. Kinnaird, E. Stabile, M. S. Burnett et al., “Marrow-derived stromal cells express genes encoding a broad spectrum of arteriogenic cytokines and promote in vitro and in vivo arteriogenesis through paracrine mechanisms,” *Circulation Research*, vol. 94, no. 5, pp. 678–685, 2004.
- [81] J. A. Salgado, L. R. Reis, N. Sousa, and M. J. Gimble, “Adipose tissue derived stem cells secretome: soluble factors and their roles in regenerative medicine,” *Current Stem Cell Research & Therapy*, vol. 5, no. 2, pp. 103–110, 2010.
- [82] M. S. Choudhery, M. Badowski, A. Muike, J. Pierce, and D. T. Harris, “Donor age negatively impacts adipose tissue-derived mesenchymal stem cell expansion and differentiation,” *Journal of Translational Medicine*, vol. 12, no. 1, pp. 1–14, 2014.
- [83] G. Zheng, L. Huang, H. Tong et al., “Treatment of acute respiratory distress syndrome with allogeneic adipose-derived mesenchymal stem cells: a randomized, placebo-controlled pilot study,” *Respiratory Research*, vol. 15, no. 1, pp. 1–10, 2014.
- [84] F. Sánchez-Guijo, M. García-Arranz, M. López-Parra et al., “Adipose-derived mesenchymal stromal cells for the treatment of patients with severe SARS-CoV-2 pneumonia requiring mechanical ventilation. A proof of concept study,” *EClinicalMedicine*, vol. 25, article 100454, 2020.
- [85] W. Tsuji, J. P. Rubin, and K. G. Marra, “Adipose-derived stem cells: implications in tissue regeneration,” *World Journal Of Stem Cells*, vol. 6, no. 3, article 312, 2014.
- [86] H. T. Liao, K. G. Marra, and J. P. Rubin, “Application of platelet-rich plasma and platelet-rich fibrin in fat grafting: basic science and literature review,” *Tissue Engineering Part B: Reviews*, vol. 20, no. 4, pp. 267–276, 2013.
- [87] P. Gentile and A. Sterodimas, “Adipose stem cells (ASCs) and stromal vascular fraction (SVF) as a potential therapy in combating (COVID-19)-disease,” *Aging and Disease*, vol. 11, no. 3, pp. 465–469, 2020.
- [88] C. J. Rogers, R. J. Harman, B. A. Bunnell et al., “Rationale for the clinical use of adipose-derived mesenchymal stem cells for COVID-19 patients,” *Journal of Translational Medicine*, vol. 18, no. 1, pp. 203–219, 2020.
- [89] X. Cheng, M. Jiang, L. Long, and J. Meng, “Potential roles of mesenchymal stem cells and their exosomes in the treatment of COVID-19,” *Frontiers in Bioscience-Landmark*, vol. 26, no. 10, pp. 948–961, 2021.
- [90] A. K. Shetty, “Mesenchymal stem cell infusion shows promise for combating coronavirus (COVID-19)- induced pneumonia,” *Aging and Disease*, vol. 11, no. 2, pp. 462–464, 2020.
- [91] R. Ciccocioppo, D. Gibellini, G. Astori et al., “The immune modulatory effects of umbilical cord-derived mesenchymal stromal cells in severe COVID-19 pneumonia,” *Stem Cell Research and Therapy*, vol. 12, no. 1, pp. 1–10, 2021.
- [92] P. Gourmelon, M. Benderitter, J. M. Bertho, C. Huet, N. C. Gorin, and P. de Revel, “European consensus on the medical management of acute radiation syndrome and analysis of the radiation accidents in Belgium and Senegal,” *Health Physics*, vol. 98, no. 6, pp. 825–832, 2010.
- [93] X. Xu, W. Jiang, L. Chen et al., “Evaluation of the safety and efficacy of using human menstrual blood-derived mesenchymal stromal cells in treating severe and critically ill COVID-19 patients: an exploratory clinical trial,” *Clinical and Translational Medicine*, vol. 11, no. 2, article e297, 2021.
- [94] H. Arien-Zakay, S. Lecht, A. Nagler, and P. Lazarovici, “Human umbilical cord blood stem cells: rational for use as a neuroprotectant in ischemic brain disease,” *International Journal of Molecular Sciences*, vol. 11, no. 9, pp. 3513–3528, 2010.
- [95] L. Shi, H. Huang, X. Lu et al., “Effect of human umbilical cord-derived mesenchymal stem cells on lung damage in severe COVID-19 patients: a randomized, double-blind, placebo-controlled phase 2 trial,” *Signal Transduction and Targeted Therapy*, vol. 6, no. 1, p. 58, 2021.
- [96] P. Sengupta, A. I. Benjamin, Y. Singh, and A. Grover, “Prevalence and correlates of cognitive impairment in a north Indian elderly population,” *WHO South-East Asia Journal of Public Health*, vol. 3, no. 2, pp. 135–143, 2014.
- [97] B. Liang, J. Chen, T. Li et al., “Clinical remission of a critically ill COVID-19 patient treated by human umbilical cord mesenchymal stem cells: a case report,” *Medicine*, vol. 99, no. 31, article e21429, 2020.
- [98] H. Häberle, H. Magunia, P. Lang et al., “Mesenchymal stem cell therapy for severe COVID-19 ARDS,” *Journal of Intensive Care Medicine*, vol. 36, no. 6, pp. 681–688, 2021.
- [99] R. Yilmaz, G. Adas, Z. Cukurova et al., “Mesenchymal stem cells treatment in COVID-19 patient with multi-organ involvement,” *Bratislavske Lekarske Listy*, vol. 121, no. 12, pp. 847–852, 2020.
- [100] L. Madhavan and T. J. Collier, “A synergistic approach for neural repair: cell transplantation and induction of endogenous precursor cell activity,” *Neuropharmacology*, vol. 58, no. 6, pp. 835–844, 2010.
- [101] L. Tang, Y. Jiang, M. Zhu et al., “Clinical study using mesenchymal stem cells for the treatment of patients with severe COVID-19,” *Frontiers of Medicine*, vol. 14, no. 5, pp. 664–673, 2020.
- [102] Y. Zhang, J. Ding, S. Ren et al., “Intravenous infusion of human umbilical cord Wharton’s jelly-derived mesenchymal stem cells as a potential treatment for patients with COVID-19 pneumonia,” *Stem Cell Research and Therapy*, vol. 11, no. 1, pp. 1–6, 2020.
- [103] Y. Feng, J. Huang, J. Wu et al., “Safety and feasibility of umbilical cord mesenchymal stem cells in patients with COVID-19 pneumonia: a pilot study,” *Cell Proliferation*, vol. 53, no. 12, p. e12947, 2020.

- [104] G. Adas, Z. Cukurova, K. K. Yasar et al., “The systematic effect of mesenchymal stem cell therapy in critical COVID-19 patients: a prospective double controlled trial,” *Cell Transplantation*, vol. 30, pp. 1–14, 2021.
- [105] F. Wei, D. Kong, T. Li et al., “Efficacy and safety of umbilical cord mesenchymal stem cells for the treatment of patients with COVID-19,” *Clinics*, vol. 76, 2021.
- [106] D. Kouroupis, G. Lanzoni, E. Linetsky, S. Messinger Cayetano, S. Wishnek Metalonis, and C. Leñero, “Umbilical cord-derived mesenchymal stem cells modulate TNF and soluble TNF receptor 2 (sTNFR2) in COVID-19 ARDS patients,” *European Review for Medical and Pharmacological Sciences*, vol. 25, no. 12, pp. 4435–4438, 2021.



## Retraction

# Retracted: Using Haemocoagulase Agkistrodon in Patients Undergoing Transurethral Plasmakinetic Resection of the Prostate: A Pilot, Real-World, and Propensity Score-Matched Study

### BioMed Research International

Received 12 March 2024; Accepted 12 March 2024; Published 20 March 2024

Copyright © 2024 BioMed Research International. This is an open access article distributed under the Creative Commons Attribution License, which permits unrestricted use, distribution, and reproduction in any medium, provided the original work is properly cited.

This article has been retracted by Hindawi following an investigation undertaken by the publisher [1]. This investigation has uncovered evidence of one or more of the following indicators of systematic manipulation of the publication process:

- (1) Discrepancies in scope
- (2) Discrepancies in the description of the research reported
- (3) Discrepancies between the availability of data and the research described
- (4) Inappropriate citations
- (5) Incoherent, meaningless and/or irrelevant content included in the article
- (6) Manipulated or compromised peer review

The presence of these indicators undermines our confidence in the integrity of the article's content and we cannot, therefore, vouch for its reliability. Please note that this notice is intended solely to alert readers that the content of this article is unreliable. We have not investigated whether authors were aware of or involved in the systematic manipulation of the publication process.

Wiley and Hindawi regrets that the usual quality checks did not identify these issues before publication and have since put additional measures in place to safeguard research integrity.

We wish to credit our own Research Integrity and Research Publishing teams and anonymous and named external researchers and research integrity experts for contributing to this investigation.

The corresponding author, as the representative of all authors, has been given the opportunity to register their agreement or disagreement to this retraction. We have kept a record of any response received.

### References

- [1] C. Zhu, L. Yang, H. Zi et al., "Using Haemocoagulase Agkistrodon in Patients Undergoing Transurethral Plasmakinetic Resection of the Prostate: A Pilot, Real-World, and Propensity Score-Matched Study," *BioMed Research International*, vol. 2022, Article ID 9200854, 9 pages, 2022.

## Research Article

# Using Haemocoagulase Agkistrodon in Patients Undergoing Transurethral Plasmakinetic Resection of the Prostate: A Pilot, Real-World, and Propensity Score-Matched Study

Cong Zhu,<sup>1,2</sup> Lan Yang,<sup>3</sup> Hao Zi,<sup>1,2</sup> Bing-Hui Li,<sup>1</sup> Qiao Huang<sup>1,2</sup>, Meng-Xin Lu,<sup>1</sup> Xiao-Dong Li,<sup>4</sup> Xuan-Yi Ren,<sup>5</sup> Hua Tao<sup>1,6</sup>, Hankun Hu<sup>1,7</sup>, and Xian-Tao Zeng<sup>1,2</sup>

<sup>1</sup>Department of Urology, Zhongnan Hospital of Wuhan University, Wuhan 430071, China

<sup>2</sup>Center for Evidence-Based and Translational Medicine, Zhongnan Hospital of Wuhan University, Wuhan 430071, China

<sup>3</sup>Division of Medical Affairs, Zhongnan Hospital of Wuhan University, Wuhan 430071, China

<sup>4</sup>Department of Urology, Huaihe Hospital of Henan University, Kaifeng 475000, China

<sup>5</sup>Department of Urology, Kaifeng Central Hospital, Kaifeng 475000, China

<sup>6</sup>Department of Pharmacy, Zhengzhou Second Hospital, Zhengzhou 450006, China

<sup>7</sup>Department of Pharmacy, Zhongnan Hospital of Wuhan University, Wuhan 430071, China

Correspondence should be addressed to Hua Tao; [zztaohua@126.com](mailto:zztaohua@126.com), Hankun Hu; [huhankun@whu.edu.cn](mailto:huhankun@whu.edu.cn), and Xian-Tao Zeng; [zengxiantao1128@163.com](mailto:zengxiantao1128@163.com)

Received 23 March 2022; Accepted 1 June 2022; Published 22 June 2022

Academic Editor: Haixu Chen

Copyright © 2022 Cong Zhu et al. This is an open access article distributed under the Creative Commons Attribution License, which permits unrestricted use, distribution, and reproduction in any medium, provided the original work is properly cited.

**Objectives.** To compare the clinical outcomes of using different hemostatic agents after transurethral plasmakinetic resection of the prostate (TUPKP) in benign prostatic hyperplasia (BPH) patients. **Methods.** The patients were divided into 5 groups according to the hemostatic agents used after TUPKP, including the haemocoagulase agkistrodon for injection (HCA), hemocoagulase for injection (HC), hemocoagulase bothrops atrox for injection (HCB), ethylenediamine diacetate injection (EDD), and tranexamic acid (TXA). Propensity score matching was performed based on age, body mass index, prostate volume, hypertension status, fasting blood glucose, smoking, and drinking history. The hospitalization time, bladder irrigation time, indwelling catheterization time, the patency of urine flow, and blood transfusion records were used as outcome indicators to compare the clinical effects of these five agents. **Results.** We finally matched 65 pairs receiving HCA or HC, 71 pairs receiving HCA or HCB, 38 pairs receiving HCA or TXA, and 29 pairs receiving HCA or EDD. Compared with HC, HCA given during the perioperative period significantly reduced the median hospitalization time [7.00 days (5.00, 8.00) vs. 9.00 days (8.00, 10.00);  $p < 0.001$ ] and median catheterization time (109.00 hours [88.00, 129.00] vs. 164.00 hours [114.00, 189.00],  $p < 0.001$ ). Compared with EDD, the median hospitalization time (7.00 days [6.00, 8.00] vs. 10.00 days [8.00, 11.00];  $p < 0.001$ ) and median catheterization time (113.00 hours [95.00, 143.00] vs. 160.00 hours [139.00, 168.00];  $p < 0.001$ ) were also significant shorter in HCA group. Compared with HCB, median bladder irrigation time (45.00 hours [27.00, 71.00] vs. 49.00 hours [45.00, 72.00];  $p = 0.04$ ) was shorter in the HCA group. However, there were no statistical differences in outcomes between HCA and TXA. **Conclusions.** HCA probably has an advantage over HC, HCB, and EDD in reducing the hospitalization time, catheterization time, and bladder irrigation time among BPH patients undergoing TUPKP.

## 1. Introduction

Benign prostatic hyperplasia (BPH) is a common urinary system disease in elderly men, often leading to lower urinary tract symptoms (LUTS), which seriously affect the patients'

quality of life. In 2019, it was estimated that the incidence of BPH was as high as 2298.45/100,000 in the age group of 65-70 years [1]. The burden of BPH will further increase as global population ageing accelerates [2]. When conservative and pharmacological treatments are not effective, surgery is

often unavoidable. Transurethral resection of the prostate (TURP) is the preferred surgical paradigm for the treatment of BPH. However, traditional monopolar TURP has two main limitations [3, 4], one is water toxicity which can lead to negative outcomes and the other is poor hemostasis. In 2011, the European Association of Urology included transurethral plasmakinetic resection of the prostate (TUPKP) in its guidelines and recommended it for the first time, because of the benefits of less intraoperative bleeding and fluid absorption and fewer postoperative complications [5–7]. Even though various devices and techniques have been developed, perioperative bleeding is still a challenge for urologists, given that it may lead to prolonged bladder irrigation time and hospitalization time [8].

The use of hemocoagulase, tranexamic acid, and ethylenediamine diacetate in hemostasis in TURP patients have been reported in previous studies [9–11]. However, there were few studies comparing the clinical prognostic effects among these different hemostatic agents on patients undergoing TUPKP. Haemocoagulase agkistrodon for injection (HCA) is a national first-class drug in China with a good hemostatic efficiency and is safe when used in capillary bleeding from abdominal incisions having few side effects [12, 13]. Therefore, we compared the clinical prognostic effects of HAC with other hemocoagulase drugs, tranexamic acid (TXA), and ethylenediamine diacetate (EDD) on patients undergoing TUPKP.

## 2. Methods

**2.1. Study Design and Subjects.** This was a preliminary, multicenter, real-world, and propensity score-matched study. The subjects were selected from a prospective study, the Bladder Cancer and Benign Prostatic Hyperplasia Study in Chinese Populations, which ran from September 2016 to November 2018 [10, 14–19]. This study was reviewed and approved by the Committee for Ethical Affairs of the Zhongnan Hospital of Wuhan University. All participants signed written informed consent before enrollment.

Patients with confirmed BPH who had undergone TUPKP were included, while patients with urinary malignancies, urinary tract infections, and abnormal coagulation disorders were excluded. The included patients were divided into five groups according to the real-world data of hemostatic agents: HCA (brand name: Suling), hemocoagulase for injection (HC, brand name: Bangting), hemocoagulase bothrops atrox for injection (HCB, brand name: Baquting), TXA, and EDD; all of them were intravenously administered after TUPKP. Each patient may have been given more than one coagulant. When comparing two specific hemostatic agents, patients who had been given only one specific hemostatic agent were included in treatment groups.

**2.2. Measurements and Data.** Detailed demographic characteristics and medical history were collected, including age (years), body mass index (BMI,  $\text{kg}/\text{m}^2$ ), hypertension status, smoking, and drinking history. Physical examination data were recorded, including prostate volume (PV, mL), systolic pressure (SBP, mmHg), diastolic pressure (DBP, mmHg),

and fasting blood glucose (FBG,  $\text{ng}/\text{mL}$ ). These data served as baseline characteristics of each enrolled patient. Moreover, details of hemostatic agents received by each patient after operation were recorded. The hospitalization time (days), bladder irrigation time (hours), catheterization time (hours), patency of urine flow, and blood transfusion records served as outcome indicators to compare the clinical effects of these hemostatic agents.

BMI ( $\text{kg}/\text{m}^2$ ) was calculated by dividing weight in kilograms by the square of height in meters. SBP and DBP were measured according to the standard method recommended by the American Heart Association guidelines [20]. Prostate ultrasound was used to measure the largest anteroposterior height ( $H$ , cm), transverse width ( $W$ , cm), and cephalocaudal length ( $L$ , cm) of prostate, and prostate volume (mL) was calculated using the ellipsoid formula [21]  $PV = (\pi/6) \times H \times W \times L$ .

**2.3. Statistical Analysis.** Propensity score matching (PSM) was used to reduce the bias and imbalance of confounding variables that is present in observational studies [22]. In this study, age, BMI, PV, hypertension status, FBG, and history of smoking and drinking were used to estimate the propensity score. A 1 : 1 greedy match was performed based on a caliper width of 0.2 for the propensity score. Categorical variables were expressed as frequencies (percentage), and continuous variables were described using mean  $\pm$  standard deviation or median (the first quantile, the third quantile) based on normality test. Before and after PSM, patients' characteristics and outcomes were compared between HCA and the other four groups, using chi-squared tests for categorical variables and Student's  $t$ -test (or Wilcoxon rank-sum test) for continuous variables, as appropriate. All analyses were carried out using the SAS software, version 9.4 TS1M6 (SAS Institute Inc., Cary, NC).

## 3. Results

**3.1. Patients' Characteristics before PSM.** Overall, 113 patients received HCA after TUPKP, while 86 patients received HC, 99 patients received HCB, 49 patients received TXA, and 37 patients received EDD. Compared with patients who received only HCA or HC, the median age of the two groups were 73 (66.00, 79.00) and 71 (66.00, 76.00) years old ( $p = 0.14$ ), respectively. The median BMI of two groups were 23.36 (20.62, 25.53)  $\text{kg}/\text{m}^2$  and 23.05 (20.76, 24.57)  $\text{kg}/\text{m}^2$  ( $p = 0.49$ ), the mean prostate volume were 51.65 mL (32.46, 81.68) and 50.31 (38.73, 71.42) for the two groups ( $p = 0.96$ ). Likewise, there were no statistically significant differences between the two groups in the SBP, DBP, FBG, hypertension status, and history of smoking and drinking (all  $p > 0.05$ ) (Table 1).

There were no significant statistical differences in baseline characteristics between the patients receiving HCA and those receiving HCB. There were no differences in baseline characteristics between patients receiving HCA and patients receiving TXA (Tables 2 and 3). However, the SBP was significantly higher ( $p = 0.4$ ) in patients who had received HCA (132.00 mmHg [121.00, 142.00]) than in

TABLE 1: Baseline characteristics of patients used haemocoagulase agkistrodon for injection or hemocoagulase for injection before and after propensity score matching.

Baseline	Before propensity score matching			After propensity score matching		
	Haemocoagulase agkistrodon (N = 111)	Hemocoagulase (N = 86)	<i>p</i>	Haemocoagulase agkistrodon (N = 65)	Hemocoagulase (N = 65)	<i>p</i>
Age (years)	73.00 (66.00, 79.00)	71.00 (66.00, 76.00)	0.14	70.00 (65.00, 77.00)	69.00 (66.00, 76.00)	0.86
Body mass index (kg/m <sup>2</sup> )	23.36 (20.62, 25.53)	23.05 (20.76, 24.57)	0.49	23.42 ± 3.82	23.01 ± 3.06	0.51
Prostate volume (mL)	51.65 (32.46, 81.68)	50.31 (38.73, 71.24)	0.96	54.05 (35.94, 70.01)	49.69 (37.35, 69.89)	0.67
Systolic pressure (mmHg)	132.00 (120.00, 142.00)	130.00 (120.00, 135.50)	0.21	130.00 (120.00, 140.00)	130.00 (120.00, 134.00)	0.54
Diastolic pressure (mmHg)	77.89 ± 11.23	77.79 ± 9.75	0.95	78.20 ± 11.22	77.75 ± 9.23	0.81
Fasting blood glucose (ng/mL)	5.11 (4.80, 5.60)	4.93 (4.40, 5.50)	0.05	5.06 (4.75, 5.57)	4.86 (4.40, 5.45)	0.09
Hypertension status (n [%])			0.38			0.21
Yes	12 (10.81%)	6 (7.14%)		8 (12.31%)	4 (6.15%)	
No	99 (89.19%)	80 (92.86%)		57 (87.69%)	61 (93.85%)	
History of smoking (n [%])			0.34			0.51
Yes	28 (25.23%)	27 (31.40%)		18 (27.69%)	15 (23.08%)	
No	83 (74.77%)	59 (68.60%)		47 (72.31%)	50 (76.92%)	
History of drinking (n [%])			0.57			0.55
Yes	29 (26.13%)	25 (29.76%)		19 (29.23%)	16 (24.62%)	
No	82 (73.87%)	61 (70.24%)		46 (70.77%)	49 (75.38%)	

patients who had received EDD (126.00 mmHg [116.00, 130.00]). In addition, the proportion of patients with smoking history in the EDD group was higher than that in the HCA group (56.76% vs. 25.66%) ( $p < 0.001$ ) (Table 4).

**3.2. Patients' Characteristics after PSM.** After PSM, we matched 65 pairs who had received HCA or HC, 71 pairs received HCA or HCB, 38 pairs received HCA or TXA, and 29 pairs received HCA or EDD according to the propensity score. Overall, there was no significant statistical difference in the baseline characteristics of the four matched treatment groups (all  $p > 0.05$ ) (Tables 1–4).

**3.3. Outcome Difference of Each Matching Group.** The median time of hospitalization of the HCA group was 7.00 days (5.00, 8.00), which was significantly shorter than the 9.00 days (8.00, 10.00) of the HC group ( $p < 0.001$ ). The median catheterization time was also shorter in the HCA group (109.00 hours [88.00, 129.00]) than in the HC group (164.00 hours [114.00, 189.00]) ( $p < 0.001$ ). Nevertheless, the median bladder irrigation time ( $p = 0.06$ ), patency of urine flow ( $p = 0.68$ ), and blood transfusion records ( $p = 1.000$ ) showed no statistical differences between the two groups. The median hospitalization time (7.00 days [6.00, 8.00] vs. 8.00 days [7.00, 10.00]) ( $p < 0.001$ ), median bladder irrigation time (45.00 hours [27.00, 71.00] vs. 49.00

hours [45.00, 72.00]) ( $p = 0.04$ ), and median catheterization time (114.00 hours [88.00, 143.00] vs. 141.00 hours [120.00, 166.00]) ( $p < 0.001$ ) were significantly shorter in the HCA group compared with the HCB group (Table 5).

No significant difference was recorded when comparing the outcome indicators of patients receiving HCA and patients receiving TXA (all  $p > 0.05$ ). The median hospitalization time (7.00 days [6.00, 8.00] vs. 10.00 days [8.00, 11.00]) ( $p < 0.001$ ) and median catheterization time (113.00 hours [95.00, 143.00] vs. 160.00 hours [139.00, 168.00]) ( $p < 0.001$ ) of patients who had received HCA were significantly shorter than that of patients who had received EDD. The median bladder irrigation time, patency of urine flow, and blood transfusion records showed no significant differences between the two groups ( $p > 0.05$ ) (Table 6).

## 4. Discussion

In this propensity score matching study, we compared the clinical effects of HCA with 4 clinically commonly used hemostatic agents in BPH patients receiving TUPKP. Overall, the use of HCA for patients during the perioperative period significantly reduced the hospitalization time and catheterization time compared with HC and EDD. Bladder irrigation time was also shortened when compared with HCB. However, there were no statistical difference in all

TABLE 2: Baseline characteristics of patients used haemocoagulase agkistrodon for injection or hemocoagulase bothrops atrox for injection before and after propensity score matching.

Baseline	Before propensity score matching			After propensity score matching		
	Haemocoagulase agkistrodon (N = 109)	Hemocoagulase Bothrops Atrox (N = 99)	<i>P</i>	Haemocoagulase agkistrodon (N = 71)	Hemocoagulase Bothrops Atrox (N = 71)	<i>P</i>
Age (years)	72.87 ± 7.31	72.81 ± 7.40	0.95	73.45 ± 7.64	73.13 ± 7.46	0.81
Body mass index (kg/m <sup>2</sup> )	23.36 (20.76, 25.35)	23.02 (20.86, 25.34)	0.63	23.47 ± 3.65	22.81 ± 3.27	0.26
Prostate volume (mL)	51.46 (32.46, 79.88)	57.38 (37.01, 76.99)	0.47	51.65 (32.46, 77.62)	58.07 (37.52, 76.66)	0.46
Systolic pressure (mmHg)	132.00 (120.00, 140.00)	130.00 (120.00, 143.00)	0.83	132.73 ± 18.83	130.83 ± 16.93	0.53
Diastolic pressure (mmHg)	78.00 (70.00, 85.00)	80.00 (74.00, 88.00)	0.06	78.00 (69.00, 85.00)	80.00 (73.00, 84.00)	0.38
Fasting blood glucose (ng/mL)	5.11 (4.82, 5.59)	5.14 (4.71, 6.04)	0.87	5.10 (4.75, 5.55)	5.05 (4.59, 5.56)	0.48
Hypertension status ( <i>n</i> [%])			0.20			0.44
Yes	13 (11.93%)	18 (18.37%)		10 (14.08%)	7 (9.86%)	
No	96 (88.07%)	81 (81.63%)		61 (85.92%)	64 (90.14%)	
History of smoking ( <i>n</i> [%])			0.23			0.47
Yes	29 (26.61%)	34 (34.34%)		21 (29.58%)	25 (35.21%)	
No	80 (73.39%)	65 (65.66%)		50 (70.42%)	46 (64.79%)	
History of drinking ( <i>n</i> [%])			0.76			0.85
Yes	27 (24.77%)	22 (22.92%)		19 (26.76%)	20 (28.17%)	
No	82 (75.23%)	77 (77.08%)		52 (73.24%)	51 (71.83%)	

outcome indicators between HCA and TXA. Our results suggest that postoperative use of HCA and TAX in patients with BPH undergoing TUPKP can effectively reduce the patient and medical burden compared with HC, HCB, and EDD.

TUPKP has advantages in reducing TURP syndrome, clot retention, irrigation, and catheterization duration [23]. Nonetheless, perioperative bleeding management remains a priority for BPH patients [8], for which increases the operation time, irrigation fluids, the risk of TURP syndrome and sepsis, hospitalization time, catheter obstruction, and transfusion [8]. Our results indicated that BPH patients using HCA had the significantly shorter hospitalization time than those using HC, HCB, and EDD. Reducing hospitalization time means reducing the financial burden and improving patient comfort, as well as facilitating the efficient use of medical resources [24]. Previous clinical research found that HCB can significantly shorten the hospitalization time and prothrombin time among BPH patients undergoing TUPKP, but this study did not compare HCB with other hemostatic agents [10]. These results affirm the positive effect of hemocoagulase in BPH patients receiving TUPKP; however, HCA significantly shortened the hospitalization time of patients compared with HCB. We speculate that it may be related to the single component, high purity, and high active potency of HCA, which can significantly reduce the bleeding time and volume without causing thrombosis [25–27].

We further compared the bladder irrigation time and catheterization time among BPH patients using different hemostatic agents after TUPKP. We found that HCA significantly shortened bladder irrigation time and catheterization time than HC, HCB, and EDD, suggesting better hemostasis effect. Although studies of HCA in patients with TUPKP are lacking, phase II and III clinical trials of HCA have demonstrated its effectiveness in reducing hemostatic time, bleeding volume, and bleeding volume per unit area during abdominal surgery [26, 28]. Perioperative intravenous HCA was also found to significantly reduce blood loss and blood transfusion in elderly fracture-related hip arthroplasty without increasing short-term adverse event rates and increase postoperative subacute hemoglobin and coagulation factor levels [29]. This also demonstrates the safety of HCA in the elderly, since patients with BPH requiring surgical treatment are generally elderly.

The antifibrinolytics TXA was also used to reduce perioperative bleeding in TURP patients [30, 31]. In our study, HCA and TXA showed no significant differences in postoperative indicators of concern. A meta-analysis indicated that TXA effectively reduced perioperative blood loss compared with placebo in patients undergoing TURP; however, there was no significant improvement in preventing transfusions and increasing hemoglobin [32]. The hemostatic effects of EDD and TXA have been compared, and EDD was found to be more effective than TXA in reducing blood loss in open

TABLE 3: Baseline characteristics of patients used haemocoagulase agkistrodon for injection or tranexamic acid before and after propensity score matching.

Baseline	Before propensity score matching			After propensity score matching		
	Haemocoagulase agkistrodon (N = 111)	Tranexamic acid (N = 49)	<i>P</i>	Haemocoagulase agkistrodon (N = 38)	Tranexamic acid (N = 38)	<i>P</i>
Age (years)	72.72 ± 7.34	72.82 ± 5.75	0.93	72.61 ± 6.97	72.11 ± 5.87	0.74
Body mass index (kg/m <sup>2</sup> )	23.38 (20.62, 25.53)	22.96 (21.40, 24.42)	0.46	23.24 (21.72, 26.61)	23.10 (21.11, 24.77)	0.39
Prostate volume (mL)	51.65 (32.46, 82.32)	43.60 (30.66, 71.24)	0.43	52.38 (34.68, 79.88)	44.61 (32.65, 68.43)	0.81
Systolic pressure (mmHg)	132.00 (121.00, 143.00)	133.00 (120.00, 140.00)	0.98	133.55 ± 15.77	130.92 ± 15.63	0.47
Diastolic pressure (mmHg)	79.00 (70.00, 85.00)	80.00 (70.00, 90.00)	0.40	79.50 ± 12.24	79.63 ± 11.16	0.96
Fasting blood glucose (ng/mL)	5.12 (4.80, 5.60)	5.17 (4.42, 5.60)	0.61	5.12 (4.83, 5.59)	5.07 (4.51, 5.50)	0.36
Hypertension status ( <i>n</i> [%])			0.08			0.53
Yes	13 (11.71%)	11 (22.45%)		5 (13.16%)	7 (18.42%)	
No	98 (88.29%)	38 (77.55%)		33 (86.84%)	31 (81.58%)	
History of smoking ( <i>n</i> [%])			0.75			0.60
Yes	28 (25.23%)	13 (27.66%)		9 (23.68%)	11 (28.95%)	
No	83 (74.77%)	36 (72.34%)		29 (67.32%)	27 (71.05%)	
History of drinking ( <i>n</i> [%])			0.69			0.61
Yes	30 (27.03%)	11 (23.91%)		12 (31.58%)	10 (26.32%)	
No	81 (72.97%)	38 (76.09%)		26 (68.42%)	28 (73.68%)	

prostatectomy patients [11]. Our results showed that HCA was more effective than EDD in reducing the hospitalization time and catheterization time among patients undergoing TUPKP, which may suggest that HCA is more suitable for minimally invasive surgery than EDD. It is known that prostate tissue contains a large amount of tissue plasminogen activator, and urine flow contains high concentrations of urokinase, which are released in large quantities during prostatectomy to activate the fibrinolytic system [33, 34]. The HCA can antagonize this effect by promoting the synthesis of fibrin, and TXA reduces the degradation of fibrin by inhibiting the binding of fibrinolytic enzyme to fibrin. However, EDD inhibits the fibrinolytic system by inhibiting the synthesis of fibrinolytic enzyme, it does not directly protect fibrin from degradation or promote fibrin aggregation as the two former drugs do. Therefore, we inferred that this may be the reason that why HCA and TXA were more effective in reducing hospitalization time and catheterization time than EDD in patients after TUPKP.

In addition, some urologists selectively use 5 $\alpha$ -reductase inhibitors (5-ARIs) before surgery to reduce intraoperative and postoperative bleeding in patients with large prostate volumes, hematuria, or high risk of bleeding [35]. Some studies showed that 5-ARIs can reduce blood loss or transfusion requirements in BPH patients undergoing TURP [36–38]. However, other studies did not find significant differences between 5-ARIs and placebo in blood loss during

surgery, excessive or severe bleeding, or retention of clots [39, 40]. No studies compared the role of 5-ARIs and HCA in perioperative prophylaxis or hemostasis in patients with BPH, but the different mechanisms and ways of use determine the scope of their use. Compared with HCA, 5-ARIs reduces prostate blood flow by downregulating vascular endothelial growth factor, which is typically administered before surgery for 2-4 weeks [37, 38]. On the other hand, side effects of 5-ARIs should also be considered such as hypophrodisia, erectile dysfunction, ejaculatory dysfunction, and potential depression [41].

Although the efficacy of the hemostatic agents mentioned above has been proved in related studies, their safety is still a concern of urologists. Several studies have reported that HCA did not show significant complications [25, 28, 29, 42, 43]. Moreover, it was reported that 36% to 44% of patients undergoing TURP used anticoagulant or antiplatelet drugs [44]. Although the safety of TUPKP for patients receiving anticoagulant and antiplatelet drugs has been explored, there is still an increased risk of perioperative bleeding among these patients [45, 46]. A study found that HCA exerted hemostatic effect without causing thrombosis [25]; however, more clinical trials are still needed to support the safety and effectiveness of perioperative use of hemocoagulase in TUPKP patients needing oral anticoagulant drugs or antiplatelet drugs. Recent studies have shown that topical administration of hemocoagulase was effective in reducing

TABLE 4: Baseline characteristics of patients given haemocoagulase agkistrodon for injection or ethylenediamine diacetate injection before and after propensity score matching.

Baseline	Before propensity score matching			After propensity score matching		
	Haemocoagulase agkistrodon (N = 113)	Ethylenediamine Diacetate (N = 37)	P	Haemocoagulase agkistrodon (N = 29)	Ethylenediamine Diacetate (N = 29)	P
Age (years)	72.73 ± 7.31	71.14 ± 7.28	0.25	71.59 ± 7.41	71.69 ± 6.97	0.96
Body mass index (kg/m <sup>2</sup> )	23.47 ± 3.83	22.51 ± 2.68	0.11	23.54 ± 3.85	22.36 ± 2.79	0.19
Prostate volume (mL)	51.65 (33.89, 81.68)	48.35 (39.77, 73.58)	0.73	57.29 (34.80, 74.40)	46.31 (39.30, 73.89)	0.65
Systolic pressure (mmHg)	132.00 (121.00, 142.00)	126.00 (116.00, 130.00)	0.04	133.00 (125.00, 140.00)	130.00 (116.00, 135.00)	0.08
Diastolic pressure (mmHg)	79.00 (70.00, 85.00)	80.00 (72.00, 86.00)	0.18	77.45 ± 9.50	80.93 ± 9.93	0.18
Fasting blood glucose (ng/mL)	5.12 (4.82, 5.60)	4.97 (4.69, 5.40)	0.17	5.06 (4.75, 5.50)	4.86 (4.40, 5.32)	0.22
Hypertension status (n [%])			1			1
Yes	13 (11.50%)	4 (10.81%)		3 (10.34%)	4 (13.79%)	
No	100 (88.50%)	33 (89.19%)		26 (89.66%)	25 (86.21%)	
History of smoking (n [%])			<0.001			1
Yes	29 (25.66%)	21 (56.76%)		16 (55.17%)	16 (55.17%)	
No	84 (74.34%)	16 (43.24%)		13 (44.83%)	13 (44.83%)	
History of drinking (n [%])			0.71			0.77
Yes	30 (26.55%)	11 (29.73%)		9 (31.03%)	8 (27.59%)	
No	83 (73.45%)	26 (70.27%)		20 (68.97%)	21 (72.41%)	

TABLE 5: Effects of haemocoagulase agkistrodon for injection, hemocoagulase for injection, or hemocoagulase bothrops atrox for injection on patients after transurethral bipolar plasmakinetic prostatectomy.

Outcomes	Haemocoagulase agkistrodon (N = 65)	Hemocoagulase (N = 65)	P	Haemocoagulase agkistrodon (N = 71)	Hemocoagulase Bothrops Atrox (N = 71)	P
Hospitalization time (days)	7.00 (5.00, 8.00)	9.00 (8.00, 10.00)	<0.001	7.00 (6.00, 8.00)	8.00 (7.00, 10.00)	<0.001
Bladder irrigation time (hours)	41.00 (21.00, 64.00)	45.00 (23.00, 71.00)	0.06	45.00 (27.00, 71.00)	49.00 (45.00, 72.00)	0.04
Catheterization time (hours)	109.00 (88.00, 129.00)	164.00 (114.00, 189.00)	<0.001	114.00 (88.00, 143.00)	141.00 (120.00, 166.00)	<0.001
Urination unobstructed			0.68			0.36
Yes	63 (96.92%)	61 (93.85%)		70 (98.59%)	67 (94.37%)	
No	2 (3.08%)	4 (6.15%)				
Blood transfusion			1			1
Yes	1 (1.54%)	2 (3.08%)		1 (1.41%)	0 (0.00%)	
No	64 (98.46%)	63 (96.92%)		70 (98.59%)	75 (100%)	

bleeding, pain, and swelling after tooth extraction and accelerating the wound healing process [47, 48]. Obviously, the drug potential of hemocoagulase remains to be developed, and its application prospect in urology still needs more exploration. Overall, we still need to pay attention to the scope of application of hemocoagulases, monitor the coagu-

lation function of patients, and adjust the dosage according to the specific conditions of patients.

Our research also had some limitations. Firstly, we chose the hospitalization time, catheterization time, and bladder perfusion time as outcome variables rather than the more intuitive indicators of hemostatic effect, such as volume of

TABLE 6: Effects of haemocoagulase agkistrodon for injection, tranexamic acid, or ethylenediamine diacetate injection on patients after transurethral bipolar plasmakinetic prostatectomy.

Outcomes	Haemocoagulase agkistrodon (N = 38)	Tranexamic acid (N = 38)	p	Haemocoagulase agkistrodon (N = 29)	Ethylenediamine Diacetate (N = 29)	p
Hospitalization time (days)	7.00 (6.00, 8.00)	7.00 (6.00, 9.00)	1	7.00 (6.00, 8.00)	10.00 (8.00, 11.00)	<0.001
Bladder irrigation time (hours)	44.00 (31.00, 80.00)	44.75 (39.00, 67.40)	0.99	46.00 (37.00, 71.00)	70.00 (45.00, 93.00)	0.10
Catheterization time (hours)	128.16 ± 55.94	123.57 ± 47.92	0.70	113.00 (95.00, 143.00)	160.00 (139.00, 168.00)	<0.001
Urination unobstructed			0.26			0.47
Yes	36 (94.74%)	32 (84.21%)		29 (100.00%)	27 (93.10%)	
No	2 (5.26%)	6 (15.79%)				
Blood transfusion			—			1
Yes	0 (0.00%)	0 (0.00%)		1 (3.45%)	0 (0.00%)	
No	38 (100%)	38 (100%)		28 (96.55%)	29 (100%)	

blood loss and hemoglobin reduction ratio, because we considered the heterogeneity between patients and the influence of confounding factors. Hospitalization time and catheterization time are also more in line with the current concept of enhanced recovery after surgery. Moreover, administration period of hemostatic agents is a factor needed to be taken into account in future studies. Second, propensity matching was used to make baseline characteristics more balanced between treatment groups, but it also reduced the sample size of each group. Thirdly, due to the limitation of the available data, the study did not compare the health economics outcomes of these drugs. In addition, this study was only based on the Chinese population, and its universality needs to be verified in other regions of the world.

## 5. Conclusion

In conclusion, our results indicated that HCA had an advantage over other types of hemocoagulase and EDD in reducing the hospitalization time, catheterization time, and bladder irrigation time among BPH patients undergoing TUPKP, but such differences were not found between the HCA and TXA. We also recommend performing more randomized controlled trials with large sample sizes to confirm these results.

## Data Availability

The data used to support the findings of this study are included within the article and are available from the corresponding author upon request.

## Conflicts of Interest

The authors declare that the research was conducted in the absence of any commercial or financial relationships that could be construed as a potential conflict of interest.

## Authors' Contributions

ZC collected and analyzed the data and was a major contributor in the writing of the manuscript. HQ was in charge of data analyzing and proofreading. YL, ZH, LBH, and LMX participated in data collecting and revised literature. TX, HHK, and ZXT contributed to the study design and revised the manuscript. All authors read and approved the final manuscript.

## Acknowledgments

We greatly thank the patients and workers for completing our study. This work was supported by the National Key Research and Development Plan of China (Technology helps Economy 2020; 2016YFC0106302) and Technical Innovation Major Program of Hubei Province (2016ACA152), without any financial interest or benefit.

## References

- [1] C. Zhu, D. Q. Wang, H. Zi et al., "Epidemiological trends of urinary tract infections, urolithiasis and benign prostatic hyperplasia in 203 countries and territories from 1990 to 2019," *Military Medical Research*, vol. 8, no. 1, p. 64, 2021.
- [2] X. F. Xu, G. X. Liu, Y. S. Guo et al., "Global, regional, and national incidence and year lived with disability for benign prostatic hyperplasia from 1990 to 2019," *American Journal of Men's Health*, vol. 15, no. 4, p. 15579883211036786, 2021.
- [3] V. Poulakis, S. Haramoglis, M. J. Manyak, U. Witzsch, E. Becht, and A. Giannopoulos, "Transurethral prostate resection: immediate and postoperative complications. A cooperative study of three participating institutions in three different countries," *The Journal of Urology*, vol. 165, p. 365, 2001.
- [4] W. K. Mebust, H. L. Holtgrewe, A. T. K. Cockett, and P. C. Peters, "Transurethral prostatectomy: immediate and postoperative complications. A cooperative study of 13 participating institutions evaluating 3, 885 patients," *The Journal of Urology*, vol. 141, no. 2, pp. 243–247, 1989.



- [5] S. Li, J. S. W. Kwong, X. T. Zeng et al., "Plasmakinetic resection technology for the treatment of benign prostatic hyperplasia: evidence from a systematic review and meta-analysis," *Scientific Reports*, vol. 5, no. 1, article 12002, 2015.
- [6] L. Qu, X. Wang, X. Huang, Y. Zhang, and X. Zeng, "The hemostatic properties of transurethral plasmakinetic resection of the prostate: comparison with conventional resectoscope in an ex vivo study," *Urologia Internationalis*, vol. 80, no. 3, pp. 292–295, 2008.
- [7] C. E. Alexander, M. M. F. Scullion, M. I. Omar et al., "Bipolar versus monopolar transurethral resection of the prostate for lower urinary tract symptoms secondary to benign prostatic obstruction," *Cochrane Database of Systematic Reviews*, vol. 12, no. 12, article Cd009629, 2019.
- [8] L. E. Kavanagh, G. S. Jack, and N. Lawrentschuk, "Prevention and management of TURP-related hemorrhage," *Nature Reviews Urology*, vol. 8, no. 9, pp. 504–514, 2011.
- [9] M. A. Longo, B. T. Cavalheiro, and G. R. de Oliveira Filho, "Systematic review and meta-analyses of tranexamic acid use for bleeding reduction in prostate surgery," *Journal of Clinical Anesthesia*, vol. 48, pp. 32–38, 2018.
- [10] B. H. Li, Z. J. Yu, C. Y. Wang et al., "A preliminary, multicenter, prospective and real world study on the hemostasis, coagulation, and safety of hemocoagulase bothrops atrox in patients undergoing transurethral bipolar plasmakinetic prostatectomy," *Frontiers in Pharmacology*, vol. 10, p. 1426, 2019.
- [11] H. Y. Chen and L. Li, "Application of diacetoacetic acid ethylenediamine in prostatectomy," *National Medical Frontiers of China*, vol. 5, no. 14, 2010.
- [12] H. Waheed, S. F. Moin, and M. I. Choudhary, "Snake venom: from deadly toxins to life-saving therapeutics," *Current Medicinal Chemistry*, vol. 24, no. 17, pp. 1874–1891, 2017.
- [13] Y. Y. Xu, X. H. Ma, and S. J. Zhang, "Hemocoagulase agkistrodon-induced anaphylactic shock: a case report and literature review," *International Journal of Clinical Pharmacology and Therapeutics*, vol. 54, no. 2, pp. 129–134, 2016.
- [14] X. T. Zeng, T. Z. Liu, K. Gong, D. L. He, X. H. Wang, and on behalf of BPSC Investigators, "The BPSC: a prospective study investigating the clinical effect of interventional therapy and the risk factors for bladder cancer and benign prostatic hyperplasia in Chinese population," *Journal of Evidence-Based Medicine*, vol. 11, no. 1, pp. 64–67, 2018.
- [15] X. T. Zeng, H. Weng, Y. H. Jin et al., "Association between diabetes mellitus and hypertension in benign prostatic hyperplasia patients," *Chinese Medical Journal*, vol. 131, no. 9, pp. 1120–1121, 2018.
- [16] X. T. Zeng, H. Weng, J. Xiong et al., "Comparison of clinical and physiological parameters for benign prostatic hyperplasia in hypertensive and normotensive patients," *Frontiers in Physiology*, vol. 9, p. 1330, 2018.
- [17] M. J. Zhao, Q. Huang, X. H. Wang, X. Y. Ren, Y. H. Jin, and X. T. Zeng, "Comparing clinical parameters of abnormal and normal fasting blood glucose in benign prostatic hyperplasia patients," *The Aging Male*, vol. 23, no. 5, pp. 655–662, 2020.
- [18] H. Zi, X. J. Wang, M. J. Zhao, Q. Huang, X. H. Wang, and X. T. Zeng, "Fasting blood glucose level and hypertension risk in aging benign prostatic hyperplasia patients," *Aging*, vol. 11, no. 13, pp. 4438–4445, 2019.
- [19] L. Wu, B. H. Li, Y. Y. Wang et al., "Periodontal disease and risk of benign prostate hyperplasia: a cross-sectional study," *Military Medical Research*, vol. 6, no. 1, p. 34, 2019.
- [20] T. G. Pickering, J. E. Hall, L. J. Appel et al., "Recommendations for blood pressure measurement in humans and experimental animals: part 1: blood pressure measurement in humans: a statement for professionals from the Subcommittee of Professional and Public Education of the American Heart Association Council on High Blood Pressure Research," *Circulation*, vol. 111, no. 5, pp. 697–716, 2005.
- [21] L. M. Eri, H. Thomassen, B. Brennhovd, and L. L. Håheim, "Accuracy and repeatability of prostate volume measurements by transrectal ultrasound," *Prostate Cancer and Prostatic Diseases*, vol. 5, no. 4, pp. 273–278, 2002.
- [22] C. Andrade, "Propensity score matching in nonrandomized studies: a concept simply explained using antidepressant treatment during pregnancy as an example," *The Journal of Clinical Psychiatry*, vol. 78, no. 2, pp. e162–e165, 2017.
- [23] C. Mamoulakis, D. T. Ubbink, and J. J. de la Rosette, "Bipolar versus monopolar transurethral resection of the prostate: a systematic review and meta-analysis of randomized controlled trials," *European Urology*, vol. 56, no. 5, pp. 798–809, 2009.
- [24] M. Xu, C. Sun, Y. Zang, J. Zhu, B. Xue, and W. Tao, "The feasibility and safety of photoselective vaporization for prostate using a 180-W XPS Greenlight laser in day-surgery pattern in China," *Lasers in Medical Science*, vol. 36, no. 7, pp. 1421–1426, 2021.
- [25] H. Li, Y. Huang, X. Wu et al., "Effects of hemocoagulase agkistrodon on the coagulation factors and its procoagulant activities," *Drug Design, Development and Therapy*, vol. Volume 12, pp. 1385–1398, 2018.
- [26] D. Weisz, J. A. Seabrook, and R. K. Lim, "The presence of urinary nitrites is a significant predictor of pediatric urinary tract infection susceptibility to first- and third-generation cephalosporins," *The Journal of Emergency Medicine*, vol. 39, no. 1, pp. 6–12, 2010.
- [27] J.-M. Wei, M. W. Zhu, Z. T. Zhang, Z. G. Jia, H. E. Xiao-Dong, and Y. L. Wan, "The effects of hemocoagulase agkistrodon on its hemostatic and hemoagglutinant function, on abdominal incision and safety in surgical patients, a multicenter clinical study," *Chinese New Drugs Journal*, vol. 16, no. 14, p. 1126, 2007.
- [28] J. J. Zhou, Z. H. Huang, J. L. Yu, Z. Li, and G. J. Zhou, "Phase IIa clinical trial of hemocoagulase acutus for injection," *Nan Fang Yi Ke Da Xue Xue Bao*, vol. 27, no. 5, pp. 644–646, 2007.
- [29] M. Qiu, X. Zhang, H. Cai, Z. Xu, and H. Lin, "The impact of hemocoagulase for improvement of coagulation and reduction of bleeding in fracture-related hip hemiarthroplasty geriatric patients: a prospective, single-blinded, randomized, controlled study," *Injury*, vol. 48, no. 4, pp. 914–919, 2017.
- [30] A. Rannikko, A. Pétas, and K. Taari, "Tranexamic acid in control of primary hemorrhage during transurethral prostatectomy," *Urology*, vol. 64, no. 5, pp. 955–958, 2004.
- [31] R. A. Miller, M. W. May, W. F. Hendry, H. N. Whitfield, and J. E. Wickham, "The prevention of secondary haemorrhage after prostatectomy: the value of antifibrinolytic therapy," *British Journal of Urology*, vol. 52, no. 1, pp. 26–28, 1980.
- [32] S. H. Mina and H. A. Garcia-Perdomo, "Effectiveness of tranexamic acid for decreasing bleeding in prostate surgery: a systematic review and meta-analysis," *Central European Journal of Urology*, vol. 71, no. 1, pp. 72–77, 2018.
- [33] S. Ziegler, A. Ortu, C. Reale et al., "Fibrinolysis or hypercoagulation during radical prostatectomy? An evaluation of thrombelastographic parameters and standard laboratory tests,"